U.PORTO

FEUP FACULDADE DE ENGENHARIA
UNIVERSIDADE DO PORTO

Classification of knee arthropathy with accelerometer-based vibroarthrography

Dinis Benjamim Ferreira Moreira

Supervisor at Feup: Miguel Velhote Correia, PhD

Supervisor at Fraunhofer: Joana Silva, MSc

Mestrado Integrado em Bioengenharia

September, 2015

Faculdade de Engenharia da Universidade do Porto

Classification of knee arthropathy with accelerometer-based vibroarthrography

Dinis Benjamim Ferreira Moreira

Dissertation submitted to Faculdade de Engenharia da Universidade do Porto
to obtain the degree of

Master in Bioengineering

September, 2015

Abstract

The knee is one of the most important and injured sites in the human body, playing an essential role in the human musculoskeletal system. The complex dynamics of its constituents make accurate diagnosis challenging. In addition to the obvious traumatic causes, progressive cartilage degeneration, also known as osteoarthritis, is one of the most common knee joint disorders that affects essentially elderly adults. Current evaluation of the knee joint status are based on imaging techniques or semi-invasive procedures. Image-based techniques are either complex, expensive or fails into detection of small and progressive changes in the knee joint until they are noticeable, either anatomically or symptomatically while arthoscopy, which remains the gold standard tool in the medical practice, carries risks associated with the procedure itself, such as its invasiveness, required anaesthesia and surgically related risks. Thus, none of them are considered as a practical diagnostic tool, revealing the need of a new and innovative approach.

Vibroarthrography appear as an innovative approach to solve this problem. Mechanical vibratory signals arising from the defected knee joint can be recorded recurring to a tiny accelerometer. Healthy cartilage is smooth and slippery, producing minimum vibration while deteriorated cartilage is more irregular, producing additional vibrations. Vibrations generated by the friction of deteriorated articular surfaces are different in terms of frequency and amplitude originating distinct and representative vibroarthrographic signals which allows the differentiation of a healthy and a pathological knee. With the purpose of creating a knee joint vibration-based classification system, a dataset was created, that is composed of 92 healthy and 120 pathological knee joint signals segments collected from 19 healthy (mean: 46.6 years old) and 20 volunteers with arthritic knee (mean: 62.5 years old) which were evaluated with several types of classifiers, respectively. The classification process was performed using k-nearest neighbor, support vector machine and decision tree algorithms. The best classification was obtained using the k-nearest neighbor classifier with 6 selected time-frequency features with an overall accuracy of 89.77% and with a precision, recall and f-measure of 88.27 %, 92.44% and 90.13%, respectively.

Preliminary results showed that vibroarthrography can be a promising, non-invasive and low cost technique that could be used for screening and maybe even for rehabilitation purposes on the medical field. This novel technique revealed the potentiality to be suitable for an efficient classification of the knee joint status recurring only to a miniature accelerometer during a knee joint extension/flexion test. Despite the promising results, several upgrades as the sampling frequency, segmentation process and leg swing velocity during the trials can be implemented in order to improve the overall data gathering process and analysis.

Keywords: Knee joint sounds; Osteoarthritis; Accelerometer; Stethoscope; Vibroarthrographic signals;k-NN; SVM; Decision Tree

Resumo

A articulação do joelho é dos sítios mais importantes e mais lesados do corpo humano, desempenhando um papel fundamental para o sistema musculo-esquelético. A complexidade da sua dinâmica e dos seus próprios constituintes, faz com que o seu diagnóstico seja difícil e impreciso. Para além das causas de foro traumático, a degeneração progressiva da cartilagem do joelho, denominada de osteoartrite, é umas das maiores causas de problemas articulares podendo afectar toda a população, maioritariamente os idosos. Actualmente, os meios de diagnóstico são baseados em imagiologia médica ou em procedimentos semi-invasivos, como a artroscopia. Os meios de diagnóstico baseados em imagem são complexos, caros ou então falham na deteção de pequenas mudanças estruturais que passam despercebidas até serem perceptíveis, quer a nível anatómico ou sintomático. Por outro lado, a artroscopia, que permanece como gold standard é invasiva, requer cuidados pré e pós operatórios, não podendo ser considerada um meio de diagnóstico prático e simples. Assim sendo, nenhuma das técnicas actulmente usadas oferece um rápido, simples e preciso diagnóstico, evidenciando a necessidade de um novo método de deteção.

A vibroartrografia aparece como uma inovadora abordagem e solução para este tipo de problemas. As vibrações mecânicas emitidas pelo joelho são gravadas, recorrendo ao uso de um acelerómetro durante um teste de extensão/flexão do joelho, e posteriormente analisadas, permitindo a diferenciação entre um joelho saudável e um artrítico. A cartilagem saudável é lisa e escorregadia, produzindo mínimas vibrações, enquanto que a cartilagem lesada é mais irregular, produzindo vibrações adicionais. Estas vibrações são diferentes em termos de amplitude e frequência, originando sinais distintos. Para criação de um sistema de classificação da articulação do joelho, baseado nas vibrações emitidas por estes, foi recolhido um dataset composto por 92 sinais provenientes de joelhos saudáveis e 120 sinais de joelhos artríticos recolhidos de entre 19 voluntários sem qualquer tipo de artrose (idade média: 46.6 anos) e 20 voluntários com artrose no joelho (idade média: 46.6 anos). Estes sinais foram avaliados com vários tipos de classificadores, nomeadamente *k-nearest neighbor*, *support vector machines* e árvores de decisão, respectivamente. A melhor classificação foi obtida com o classificador *k-nearest neighbor*, usando apenas 6 características baseadas numa análise tempo-frequência, com uma eficácia global de 89.77% (*precision* 88.27 % , *recall* 92.44% e *f-measure* 90.13%, respectivamente).

Resultados preliminares demonstraram que a vibroartrografia pode ser uma técnica bastante promissora, totalmente não-invasiva e de baixo custo, que poderá ser usada para o rastreio e até no processo de reabilitação. Apesar destes resultados, várias melhorias podem ser implementadas como aumentar a frequência de amostragem, melhorar o processo de segmentação e manter a velocidade durante todos os testes constantes com vista a melhorar todo o processo de classificação.

Keywords: Vibracoes do Joelho. Osteoartrite. Vibroartrografia. *k-NN*; *SVM*; Árvores de Decisão.

Acknowledgments

I would like to thank to:

Professor Miguel Velhote Correia, my supervisor at FEUP, for all the provided support, experience and guidance during this project.

Joana Silva, my supervisor at Fraunhofer AICOS, for all the suggestions, discussions, patient, shared information and knowledge exchange during this project.

To Dr. Marta Massada, Dr. Daniel Soares, Dr. Paulo Pereira and Dr. Adélio Vilaça to all the kindness, sympathy and essentially, because without them, all the data gathering process would be compromised.

To all my family and friends for never giving up on me and for all the provided supported, specially during the though times.

Dinis Moreira

"Do or do not. There is no try."

Yoda, Star Wars

Contents

List of Figures

List of Tables

List of Abbreviations

2D	Two Dimensional
3D	Three Dimensional
ACC	Accelerometer
AUC	Area Under the Receiver Operating Characteristics Curve
BPNN	Back-Propagation Neural Network
CH	Chair Rise
CMA	Cascade Moving Average
CT	Computerized Tomography
dB2	Daubechies 2
DFA	Detrended Fluctuation Analysis
DKB	Deep Knee Bend
DTW	Dynamic Time Warping
EEMD	Ensemble Empirical Mode Decomposition
EMG	Electromyography
EMU	Environment Measurement Unit
ES	Electro-Stethoscope
EP	Energy Parameter
ESP	Energy Spread Parameter
f	Frequency
F0	Fundamental Frequency
FE	Flexion-Extension
FEUP	Faculdade de Engenharia da Universidade do Porto
FF	Form Factor
FFT	Fast Fourier Transform
FhP	Fraunhofer
fn	False Negatives
FP	Frequency Parameter
fp	False Positives
FSP	Frequency Spread Parameter
FT	Fourier Transform
g	G-force
IMU	Inertial Measurement Unit

k-NN	k-Nearest Neighbors
LFC	Lateral Femoral Condyle
LM	Lateral Meniscus
LMS	Least-Mean Square
LTP	Lateral Tibial Plateau
MFC	Medial Femoral Condyle
MM	Medial Meniscus
MP	Matching Pursuit
MRI	Magnetic Resonance Imaging
OA	Osteoarthritis
pc	Principal Components
PCA	Principal Component Analysis
PDF	Probability Density Function
QMF	Quadrature Miniature Filters
R	Ratio Index
RA	Rheumatoid Arthritis
RLS	Recursive Least Square
SBS	Sequential Backward Selection
SC	Stair Climb
SD	Stair Descent
Sd	Secure Digital
SFS	Sequential Forward Selection
SS	Sample Statistics
std	Standard Deviation
STFT	Short-Time Fourier Transform
SVM	Support Vector Machine
t	Time
TC	Turns Count
TF	Time-Frequency
TFD	Time-Frequency Distribution
Th	Threshold
TIP	Tetra-Polar Impedance Plethysmography;
tn	True Negatives
tp	True Positives
VAG	Vibroarthrography
VMS	Variance of the Mean-Squared
WPD	Wavelet Packet Decomposition
WT	Wavelet Transform
WVD	Wigner-Ville Distribution

Chapter 1

Introduction

The knee is one of the most frequent injured sites in the human body making this joint particularly interesting for research because without its well-functioning human motion could be compromised along with the capability to perform simple daily tasks. The knee joint is the largest and one of the strongest joints in the human body making this one of the most important joints in the human body. This joint is considered to be the most complex in the human body because of its remarkable its ability to withstand all the person weight while executing a movement.

Osteoarthritis (OA) is the most common joint disease and one of the most common diseases diagnosed in clinical practice resulting from the progressive degeneration of joint constituents including articular cartilage and subchondral bone [1, 2]. The causes of this phenomenon can be quite different in terms of nature however the most common ones are trauma, sports-related injuries and overuse. OA causes inflammation, swelling, pain and subsequently reduced motion in joints. As a progressive disease, it gradually worsens with time being highly prevalent among obese and elderly people substantially decreasing their quality of life. It is reported that 10% of total world population and more than 50% of people over the age of 50, suffers from OA [1, 2]. In respect to non-traumatic causes, overuse is the major cause. Highly demanding rotation movements and improper body balance usually associated with sports practice as football, gymnastics, cycling, ballet, jogging, snowboarding, skateboarding and swimming may result in cartilage degradation over time. The latter one is also known as chondromalacia patella in which the cartilage softens, fibrillates and sheds off the undersurface of the patella. Healthy cartilage, that covers the ends of the bones in a joint, is a natural shock absorber during movement and its degradation leads to the bones rubbing together causing knee pain. A more accurate term for chondromalacia patella is patellofemoral pain syndrome [1].

1.1 Motivation

In terms of diagnosis there are currently several diagnostic tools available to assess knee joint condition. Image-based techniques as X-rays, computerized tomography (CT) and magnetic resonance imaging (MRI) are the most currently used non-invasive techniques while arthroscopy is

used as semi-invasive. Nowadays, arthroscopy is considered to be the gold standard diagnostic tool for the evaluation of cartilage condition. However such technique is not suitable for all patients due to its invasive nature, required anaesthesia and surgery related risks. Moreover, it is not appropriate for long term or periodic follow-up evaluations of cartilage status. Despite the availability of such techniques, small and progressive changes at cartilage level remains undetected until they are noticeable, either anatomically or symptomatically [1, 2]. Therefore a novel diagnostic method is indeed needed to fully characterize functional integrity of cartilage over time and to assess knee joint status prematurely.

1.2 Goals

The ultimate goal of this experiment is to create a new, accurate and non-invasive knee joint screening test in order to replace any of the current used methods and/or to provided additional information of the knee joint status that could be used either for diagnostic or to rehabilitation purposes.

Chapter 2

Contextualization

In order to evaluate knee joint disorders, there is a primary necessity to understand the anatomo-physiological mechanisms behind the well functioning of this specific joint. The knee joint is the most complex joint in the human body and it is of crucial importance knowing the general functioning of all its constituents [3]. There are several types of joints and each one of those with different characteristics intimately related to its function on the human body. A general background of the types of existing joints, its constituents and function are presented in this chapter. Moreover, an overview of the most common knee joint disorders along with the explanation of current used techniques advantages and drawbacks are also presented in this chapter.

2.1 Types of joints in the human body

Muscles, bones and movement are intimately related but movement does not actually exist without considering the joints between the bones. By definition a joint is the place where two or more bones come together being extremely crucial for movement articulation. Not all human joints are movable, therefore there are several and different types of joints allowing is some cases, only limited movement or no movement at all. The structure of a given joint is intimately related with its degree of movement. Movable joints are placed where the motion between bones is needed, allowing considerable movement between articulating surfaces. Joints can be defined and classified in several ways according to its structure or degree of motion. Structurally, joints can be classified as fibrous, cartilaginous or synovial according to the type of major connective tissue that connects the bones together. Joints can also be classified according to their degree of motion as synarthroses (non movable joints), amphiarthroses (allowing movement is some extent) or diarthroses (freely movable joints) [3].

In the human body there are different types of joints being one of the most important the synovial joints (diarthroses class joint) (see Figure 2.1). This type of joint is more complex than fibrous and cartilaginous joints due to the existence of capsules (synovial cavities) surrounding the articulating surfaces that contains within a lubricating and shock absorbing fluid, called synovial

fluid [3]. Moreover, this articular capsule is constituted by two layers: the outer fibrous membrane and the inner synovial membrane.

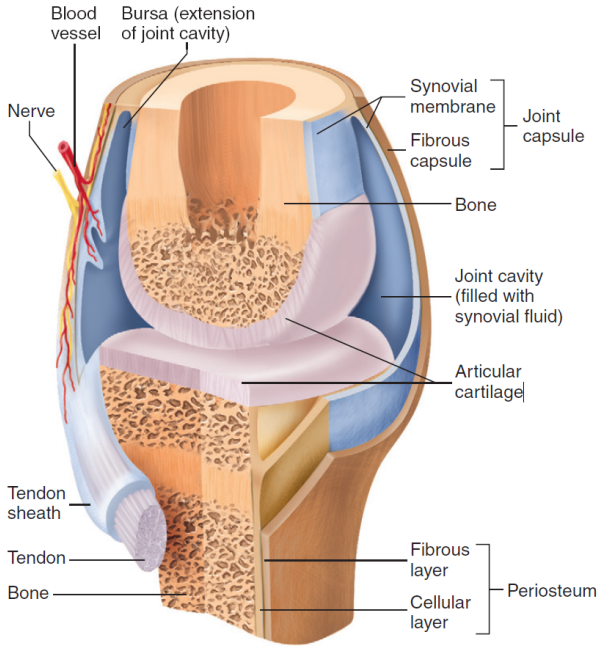

Figure 2.1: Schematics of the general structure of a synovial joint [3].

The outer fibrous capsule consists of dense irregular connective tissue adjacent to the fibrous layer of the periosteum that covers bones. Existing collagen fibers can be regularly re-arranged to form ligaments that in addition to the presence of tendons (in some cases) may contribute to the joint strength and stability. The inner synovial membrane lines the joint cavity and is filled with a lubricating film that is a complex mixture of cells, proteins, lipids and polysaccharides. The presence of the latter ones, especially hyaluronic acid, is the major responsible for the slippery consistency and lubricating characteristics that characterizes the synovial fluid.

The articular surfaces of bones present within this capsule are covered with a thin layer of hyaline cartilage called articular cartilage providing a smooth surface where the bones meet. In some synovial joints a flat plate or pad of fibrocartilage, called articular disk, lies between the articular cartilages of bones providing a cushion like effect when they move.

2.2 Knee Joint

The knee joint (see Figure 2.2) is a particularly complex and important joint in human motion. The knee joint is one of the strongest and most important joints in the human body since it allows lower leg movement relative to the thigh while supporting the body weight [3]. Movement at the knee joint level is crucial in simple daily tasks as walking, running, sitting or standing. Injuries or diseases that have an effect on knee joint integrity or functionality may compromise the ability to perform simple tasks as well as the locomotion itself. Therefore, it could result into a substantial

decrease in terms of quality of life along with several limitations at professional, social and even at an aesthetic level.

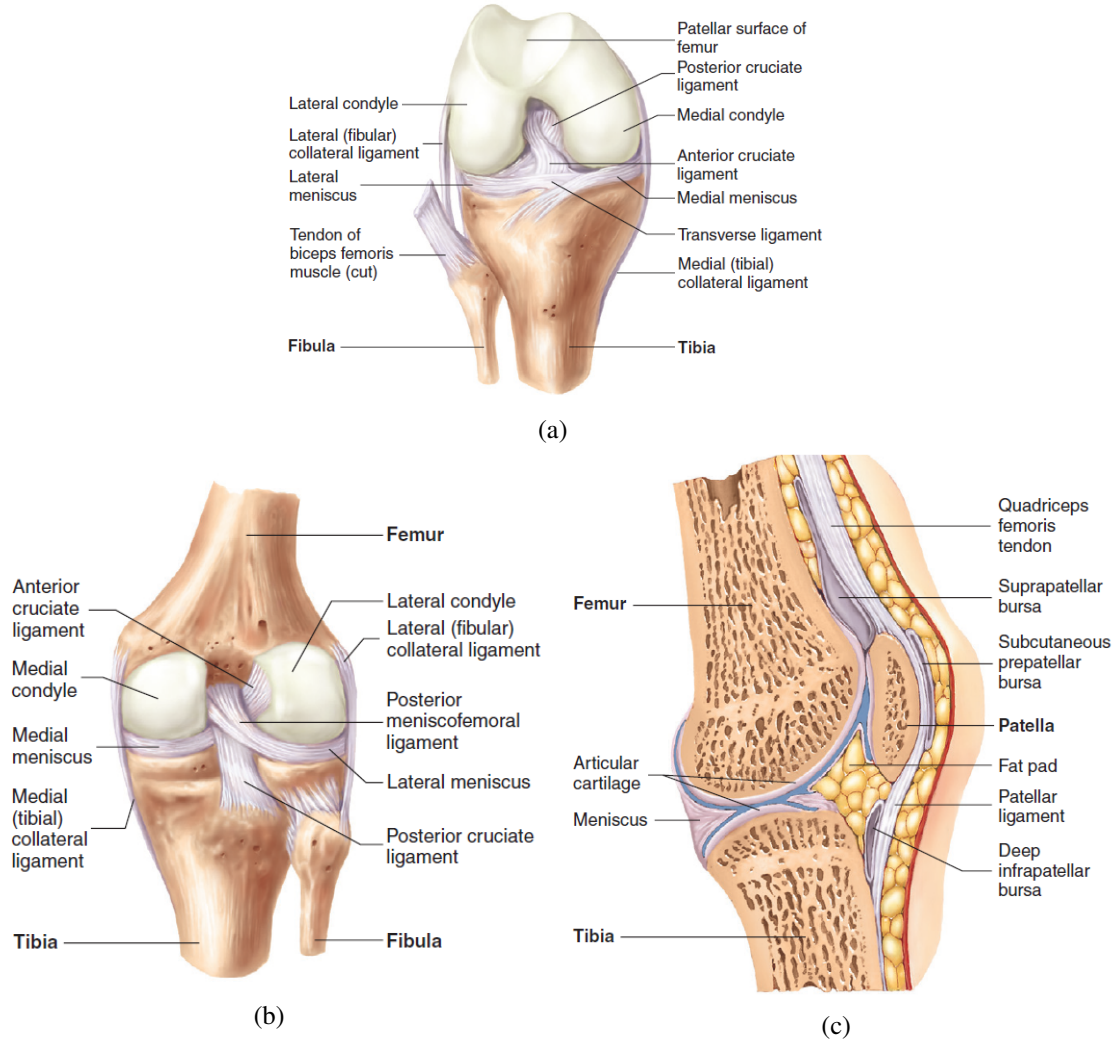

Figure 2.2: Representation of knee joint and its major constituents. (a)- Anterior, (b)- Posterior and (c)-Sagital View [3].

2.2.1 Articulating bodies

The knee joint is an ellipse-like joint located between the femur and the tibia constituted by two articulations: the tibiofemoral joint that connects tibia to the femur and the patellofemoral joint which joins the kneecap to the femur. This joint acts as a modified hinge joint (uniaxial) that allows flexion, extension and a small amount of rotation of the leg being the largest and most complex joint in the human body [3].

The articular bodies of this joint are the distal end of the femur (by its lateral and medial condyles) and the proximal end of the tibia (by the pair of tibial condyles separated by the intercondylar eminence). The patella connects posteriorly with the two femoral condyles of the

anterior side of the femur. As a typical synovial joint, the articulating surfaces of the femur and tibia are covered by a thin film of articular cartilage that provides a smooth, well lubricated surface for knee articulation and facilitates transmissions of loads (e.g. pressure and forces arising from the person own weight).

2.2.2 Menisci and ligaments

The knee joint is also constituted by two menisci, the medial and lateral meniscus. These C-shaped articulated disks keep the knee steady by balancing the person weight across the knee [4]. The functional integrity of the articular cartilage and menisci displays a major role for good articulation and to facilitate the transmission of loads. Additionally, the knee is also constituted by a set of ligaments that provides joint stability: two cruciate ligaments, the anterior and posterior cruciate ligament, and the collateral ligaments. The first one prevents anterior displacement of the tibia relative to the femur while the second one prevents posterior displacement of the tibia. Collateral ligaments by its turn stabilize the medial and lateral sides, respectively, of the knee.

2.2.3 Muscle and tendons

In order to move the knee joint several muscles belonging to either the anterior, medial or posterior compartment of the thigh are solicited according to the nature of the movement [3]. A list with all the responsible muscles for the movement of the knee joint is provided in the Table 2.1. Generally, muscles related to extension movements belong to the anterior compartment while muscles related to the flexion movements belong to the posterior compartment [5]. However there are two exceptions: the gracilis and the sartorius which belongs to the medial and anterior compartment, respectively.

In addition to the muscle, tendons are very important to the knee joint structure since they are an elastic tissue, technically making part of the muscle itself, which connect the muscles to the bones. Tendons are capable of withstanding tension and are very important for knee stabilization. There are two major tendons in the knee: the quadriceps and the patellar tendon. The first one establishes the connection of the quadriceps muscles (rectus femoris, vastus lateralis, vastus medialis and vastus intermedius) of the thigh to the kneecap, holding the patella in the femur's patellofemoral groove providing the necessary power for straightening the knee. The patellar tendon connects the bottom of the kneecap to the top of the shinbone (tibia) and it is actually a ligament, since it connects to two different bones, the patella and the tibia.

2.2.4 Bursae

The knee has also a number of bursae surrounding the knee that contain synovial fluid and provide a cushion between structures that would otherwise rub against each other. The most important ones are the suprapatellar (the largest one), subcutaneous prepatellar and deep infrapatellar bursa. These sacs filled with synovial fluid cushion the joint and reduce friction between bones, muscles,

tendons and ligaments. Inflammation of these bursae, also known as bursitis, causes pain and decrease mobility being one of the most common problems in clinical practice.

Table 2.1: Muscles involved in the extension and flexion mechanism of the knee joint [5]

Muscle	Category	Origin	Insertion	Action
Articularis genus	Extensor	Distal end of anterior femoral shaft	Proximal extension of the joint capsule of the knee	Pull suprapatellar bursa
Sartorius	Extensor	Superior relatively to the anterior superior iliac spine	Medial side of the upper tibia in the pesanserinus	Knee flexion and medial rotation: Flexion, lateral rotation and abduction of the thigh
Quadriceps femoris	Extensor	Combination of rectus femoris and vastus muscles	Patella and Tibial tuberosity	Knee extension Hip flexion
Biceps femoris	Flexors	Long head: tuberosity of ischium; Short head: linea aspera on the femur	Head of the fibula	Knee flexion and lateral rotation; Hip extension
Semitendinosus	Flexors	Tuberosity of the ischium	Pes abserinus	Knee flexion; Hip extension; Leg medial rotation at knee level
Semimembranosus	Flexors	Tuberosity of the ischium	Medial surface of tibia	Knee flexion; Hip extension; Leg medial rotation at knee level
Gastrocnemius	Flexors	Medial and lateral condyle of the femur	Calcaneus	Minor knee flexion; Plantar flexion
Plantaris	Flexors	Lateral supracondylar ridge of the femur	Tendo calcaneus	Knee flexion; Plantar flexion
Popliteus	Flexors	Middle of the lateral surface of the lateral femoral condyle	Posterior tibia	Knee flexion and medial rotation
Gracilis	Flexors	Inferior pubic ramus	Pes anserinus	Knee flexion and medial rotation; Hip adduction; Hip flexion

2.3 Knee Joint Disorders

The knee is the most common injured part of the human body [6, 7]. The causes behind the knee joint injuries can be quite different in terms of nature being predominantly divided into three subgroups: trauma-related injuries, over time cartilage degeneration (OA) and autoimmune diseases (rheumatoid arthritis) [8, 9].

2.3.1 Trauma

Trauma is one of the most responsible causes to knee injuries. Highly demanding physical activity involving rotation movements and improper body balance usually associated to sports practice as football, gymnastics, cycling, ballet, jogging, snowboarding, skateboarding or swimming are the major responsible by the appearing of these injuries [10]. Fractures, dislocations, tendon tears, meniscal tears and ligament injuries are the main causes for knee joint injuries [8, 10].

2.3.2 Rheumatoid Arthritis

Rheumatoid arthritis (RA) is a chronic, systemic inflammatory condition that causes inflammation of the synovial membrane (synovitis) and progressive bone erosion resulting into the knee joint destruction (see Figure 2.3). RA is the most common inflammatory arthritis [8, 11]. RA causes pain, increase in temperature, swelling and joint tenderness due to the presence of excess synovial fluid and the development of fibrous tissue (arthrofibrosis) [8]. This condition can be very painful and disabilitating leading to premature mortality [9, 12]. Although its etiology remains unknown, genetics was found to contribute in about 70% of cases to the development of this condition. Environmental triggers such as smoking and obesity are also thought to be related to its development. Moreover, female hormonal levels are also thought to be related to its development. Over time, the continuous inflammatory activity leads to tendon tethering and degradation, destroying the joint surface leading to joint deformity and movement impairment [9].

2.3.3 Osteoarthritis

OA, also known as degenerative arthritis or degenerative joint disease, is a condition characterized by the local and progressive loss of articular cartilage along with simultaneous changes in the bone underneath the cartilage (see Figure 2.4). OA is the most common form of arthritis [14]. It causes joint pain, tenderness, crepitus, movement limitation and variable degrees of local inflammation [9, 14]. Due to its irreversible character, it increases indefinitely with age becoming even more prevalent in the future. It is considered to be a chronic and disabilitating disease causing a considerable burden in lost time at work and early retirement [14].

OA is the most common reason for total knee replacement. It is estimated to be more prevalent among older adults despite it can affect people of all ages. Trauma and physical demanding activities like sports are thought to contribute to the development of this condition although systemic factors like a person's age, sex, inherited susceptibility to OA are not discarded for this matter.

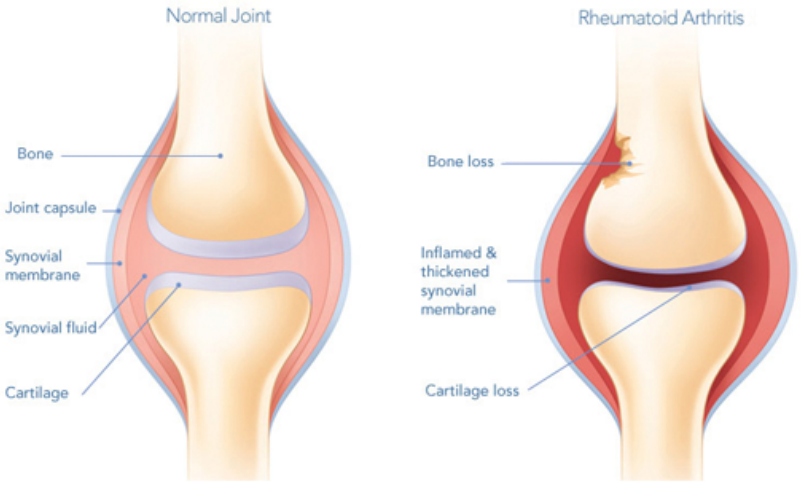

Figure 2.3: Schematic comparison between a healthy and a RA knee joint [13].

Systemic factors makes cartilage more vulnerable to daily injuries and diminish its natural ability to repair by its own [15]. Obesity, trauma and overuse are the main causes to its development resulting in impaired mobility and severe limitations in everyday life. Moreover, OA is no longer thought as an exclusively degenerative joint disease but rather a result of an abnormal remodelling of joint tissues driven by the host excessive inflammatory reaction [16, 17]. Despite the variety nature of OA, osteoarthritic joints share common features regarding the entire joint structure resulting in pain, deformity and ultimately, loss of function [17].

Current studies are now focusing more on the tibiofemoral joint OA assessment although patellofemoral joint OA has been proven to have bigger impact on performing daily activities as climbing stairs, walking, standing and sitting [9, 14, 18]. Currently, no immediate cure is available, being only possible to alleviate symptoms.

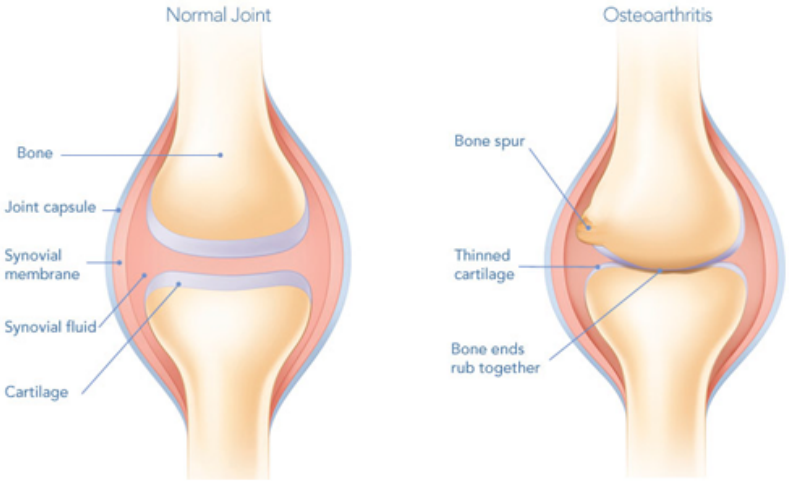

Figure 2.4: Schematic comparison between a healthy and a OA knee joint [13].

2.4 Current diagnostic tools

OA due to its tremendous complexity is not easy to assess. Structural tissue changes in OA are of slow progression and in most of the cases, changes cannot be seen macroscopically until they are gross resulting into an added challenge for this disease study as well as for the choice of adequate treatment. Current diagnostics techniques are sub-divided into two major groups, classified as: invasive and non-invasive techniques [19].

The non-invasive techniques generally are image-based techniques such as radiography, CT, ultrasound and MRI. Additionally, biochemical biomarkers of joint metabolism are nowadays under studies although more insight about them is needed. As for invasive techniques, arthroscopy remains the top choice of physicians [19].

2.4.1 Radiography

Conventional radiography is the gold standard imaging technique for the evaluation of known or suspected OA in clinical practice [19, 20]. This technique is the most simple, inexpensive, fast and easy to obtain being the most widely know and applied technique in OA diagnosis. It enables the detection of OA-associated bony features and estimation of the joint space width, cartilage thickness and meniscal integrity [19, 20]. Despite this, no precise measurements can be obtained through this method due to its lack of sensitivity and specificity regarding OA-related articular tissue damages. Moreover, knee joint movement during image acquisition may affect quantitative measurements and variations on knee position across follow up care may affect its feasibility [20, 21]. Also, clinically significant changes in radiographic images (see Figure 2.5) take a large amount of time to be noted (approximately at least 1 or even 2 years) [19].

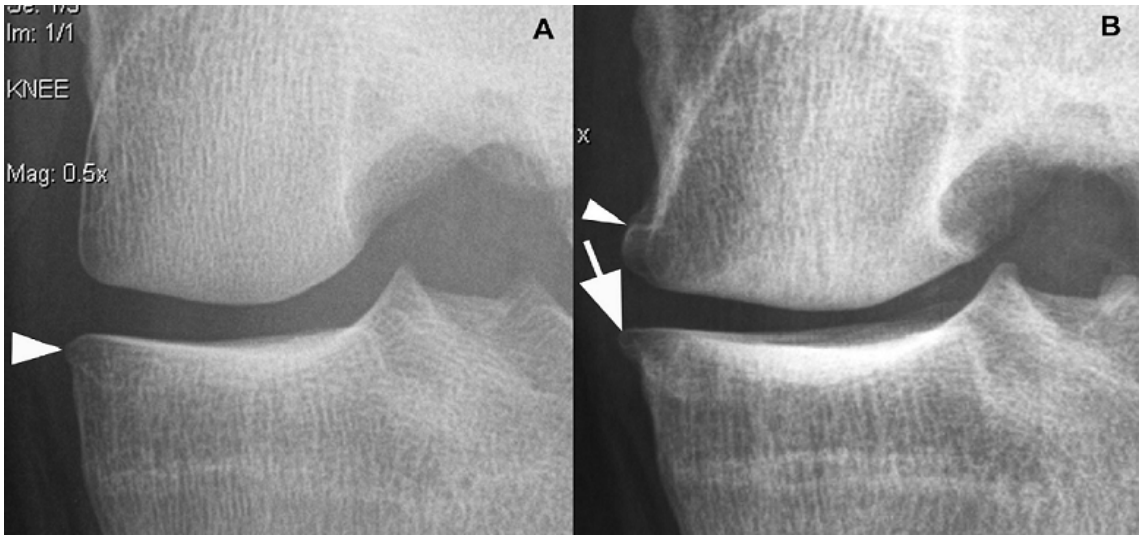

Figure 2.5: Radiographic diagnosis of OA. Follow-up case of a patient with anterior cruciate ligament disruption. (A) Knee joint radiography at the beginning and (B) three years after OA diagnosis. Clinically significant anatomical differences only noticeable in radiographic images after three years pasted (notice the arrow and arrowheads) [20].

2.4.2 Computerized Tomography

CT is more or less equivalent to the plain radiography. Regular CT has similar limitations compared to the conventional radiography but in addition, it requires a higher exposure period to ionizing radiation. Despite this, CT provides a multiplanar three-dimensional image that enables the evaluation of articular cartilage damage with high anatomical resolution (see Figure 2.6) since it allows the use of contrast agents (contrast enhanced CT) for cartilage visualization in addition to the bone [19, 20, 21].

2.4.3 Magnetic Resonance Imaging

MRI is the major imaging tool for OA evaluation, specially used for research. It provides not only accurate quantitative measurements of articular cartilage morphology such as the volume, area and thickness but also good indication of its integrity (see Figure 2.7) [19, 20]. Using MRI, several limitations of radiographies can be overcome since it enables the detection of structures that do not appear before such as articular cartilage, menisci, ligaments, synovium, capsular structures, fluids and bone marrow lesions [20]. The joint can be evaluate as a whole organ and multiple tissue changes can be monitored simultaneously overtime allowing a better and earlier diagnostic [20]. However, MRI its not generally used in clinical practice for OA detection or follow up of OA patients due to its high cost, complexity, long acquisition times (an average of 45 minutes) and analytical time restrictions [19, 21]. Despite these current limitations, MRI assessments are predicted to become standard in clinical practice in a near future [19].

2.4.4 Ultrasound

Ultrasound properties enable real time and multiplanar imaging of joint structures providing a reliable source for the assessment of OA-associated features as joint inflammation and structural abnormalities [20]. Ultrasound dismisses the use of contrast agent as well as ionizing radiation exposure. Moreover, it allows visualization of movement. Ultrasound imaging (see Figure 2.8) is relatively low cost and provides good soft tissue structures images such as synovial tissue in several planes that can be fundamental for a deeper OA analysis. The limitations of this method are intrinsically related to the physical properties of the sound that limits the deep penetration of the signal restraining it to the more superficial structures. Also, the proper execution of this technique is dependent on the experience and skills of the technician [19, 20, 21]. Currently, ultrasound is majoritarily used for assessment of hand OA despite knee OA studies have also been performed [20].

A summarized comparison of the currently image-based techniques major advantages and limitations is provided in the Table 2.2.

Figure 2.6: CT scans evidencing synovial chondromatosis of the knee joint in a 50-year-old woman. CT scan shows osteophytes and narrowing of joint spaces, consistent with OA. Several ossified intra-articular loose bodies (arrows) can be seen in the sagittal view (B) of the knee joint with the CT scan [22].

Figure 2.7: Longitudinal evaluation of focal cartilage lesion using MRI over a 2-year time period visualized by intermediate-weighted MRI. At baseline (A), very discrete surface indentation of cartilaginous surface is observed (white arrow). 2-year later (B), a more pronounced fissure-like full thickness defect is noticeable [20].

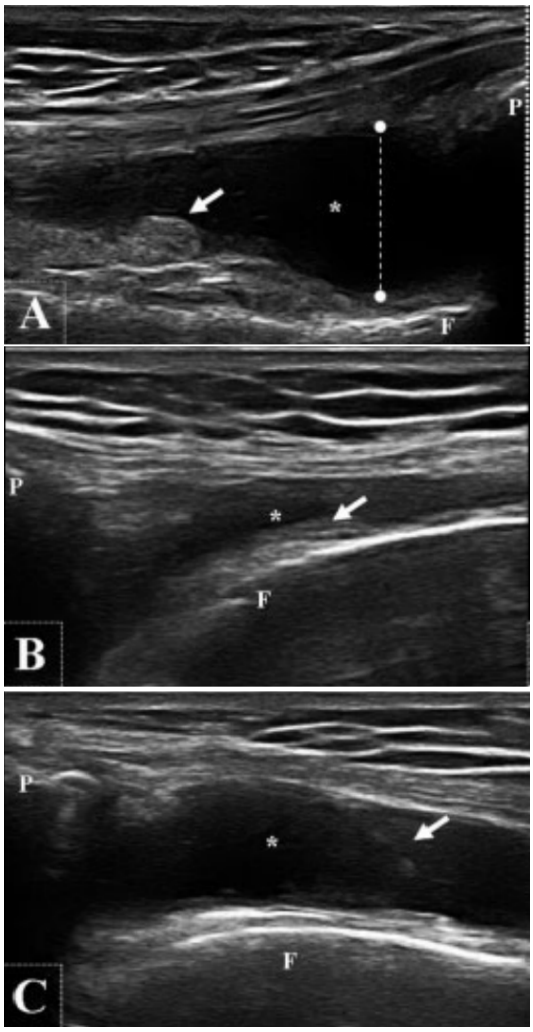

Figure 2.8: Ultrasound assessment of synovial fluid in the three major recesses of the knee: (A) sagittal plane - suprapatellar recess, (B) midpatellar tranverse plane - medial parapatellar recess and (C) midpatellar transverse plane - lateral parapatellar recess [23]. * - effusion; F - femur; P - patella; arrow - synovial hypertrophy; dotted line - measurement of greatest diameter of fluid.

Table 2.2: Comparison of the currently available image-based techniques - advantages and major drawbacks [19, 20, 21, 24]

Technique	**Primary Use**	**Advantages**	**Disadvantages**
Radiography	Cartilage Thickness	Inexpensive, Fast, Simple, Easy applicable	Indirect measurements, 2D images, Radiation exposure
CT	Bone characteristics; Articular cartilage assessment	Multiplanar 3-D images; Good resolution	Higher exposure to radiation; Contrast agent maybe needed
Ultrasound	Inflammation	Cheap; Real-time; Multiplanar imaging; Direct measurements; Enables movement visualization; Dismiss the use of ionizing radiation	User Dependent; Tissue depth dependent on sound's physical properties
MRI	Articular cartilage assessment	3-D joint imaging; Multiple tissues monitoring Good tissue contrast Direct measurements; Dismiss the use of ionizing radiation	High cost; Complexity; Long acquisition times; Time-consuming analysis

2.4.5 Arthroscopy

Arthroscopy is still nowadays the gold standard method for knee joint evaluation (see Figure 2.9). It remains the reference for diagnosis of internal derangements of the knee providing to the surgeon helpful information of the knee joint actual condition to confirm the extent of the problem or even contradict the first clinical impression [25, 26]. Despite this, other alternative diagnostic tools have been equationated due to the arthroscopy's invasive character (incisions are made in the knee and a tiny camera is inserted) and the required need of anesthesia [19, 27].

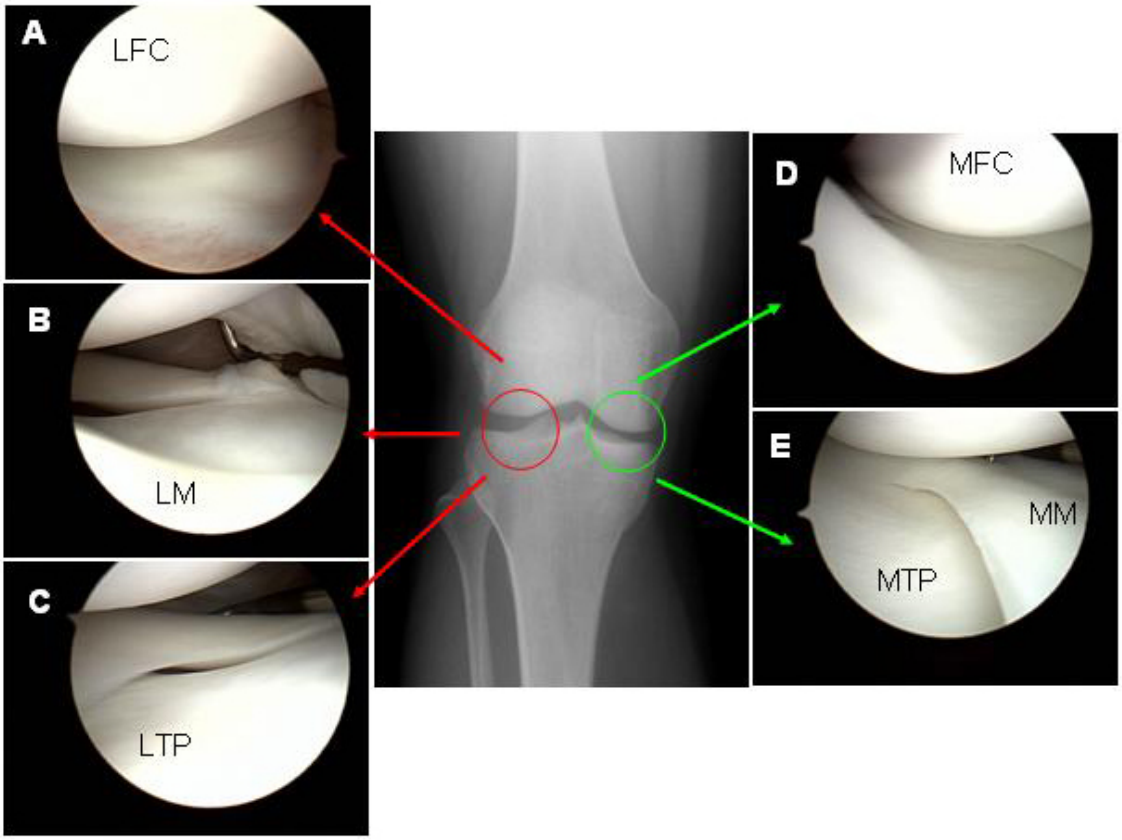

Figure 2.9: Knee Joint X-ray image with arthroscopic views of the (A) lateral femoral condyle (LFC), (B) the lateral meniscus (LM), (C) the lateral tibial plateau (LTP), (D) the medial femoral condyle (MFC) and (E) the medial meniscus (MM) [28].

Chapter 3

Statement of the problem

In order to overcome current limitations of the available diagnostic tools a new approach should be developed to assess cartilage status over time at microscopic level without the need to use invasive or highly expensive methods. Degenerated joint produces a complex set of sounds known as crepitus resulting from cartilage friction during range of motion of the knee [1, 29]. These knee sounds represent the acoustic and vibrational signals of articular surfaces rubbing together and can be very useful to evaluate joint actual condition. These particular sounds can be evaluated recurring to vibroarthrography (VAG).

VAG signals may allow the differentiation between a healthy and an injured knee recurring only to the use of a miniature accelerometer during a knee joint extension/flexion test [1, 30]. VAG may avoid the use of exploratory surgeries, invasive diagnostic methods as the arthroscopy, reducing diagnostic costs and may even improve the rehabilitation process by providing detailed insight about articular structures condition.

3.1 A novel solution - Introduction to the Vibroarthrography

Ever since in the medicine field there is particular interest in understanding the sounds emerging from the human body for diagnostic purposes. One example of this use is cardiac auscultation in which the sound emitted by the heart valves when they are closing/opening is listened to assess cardiac rate and rhythm [31]. Degenerated joint produces a complex set of sounds known as crepitus.

Crepitus or crepitation is defined as the crackling or grinding sound emitted during passive or active range of motion of the joint resulting from cartilage friction [29, 32, 33, 34]. These generated sounds are non-stationary involving multiple components and are thought to be related with the joint actual condition [34, 35]. Moreover, it is believed that crepitus its related to different pathologies affecting distinct structures within the joint [31, 32, 33, 34, 35].

Mechanical vibratory signals arising from the defected joint were recorded recurring initially, to microphones and most recently to miniature accelerometers, giving place to a new method for joint assessment, so called vibroarthrography [36]. VAG signal is the acoustic and vibrational

signal generated during a leg active flexion and extension caused by the vibration of articular surfaces of the defected joint. Healthy cartilage is smooth and slippery producing minimum vibration while deteriorated cartilage is more irregular producing additional vibrations which can be audible in some cases [37]. Vibrations generated by the friction of deteriorated articular surfaces are different in terms of frequency and amplitude compared to healthy ones, originating distinct VAG signals (see Figure 3.1) [31, 35, 36, 38].

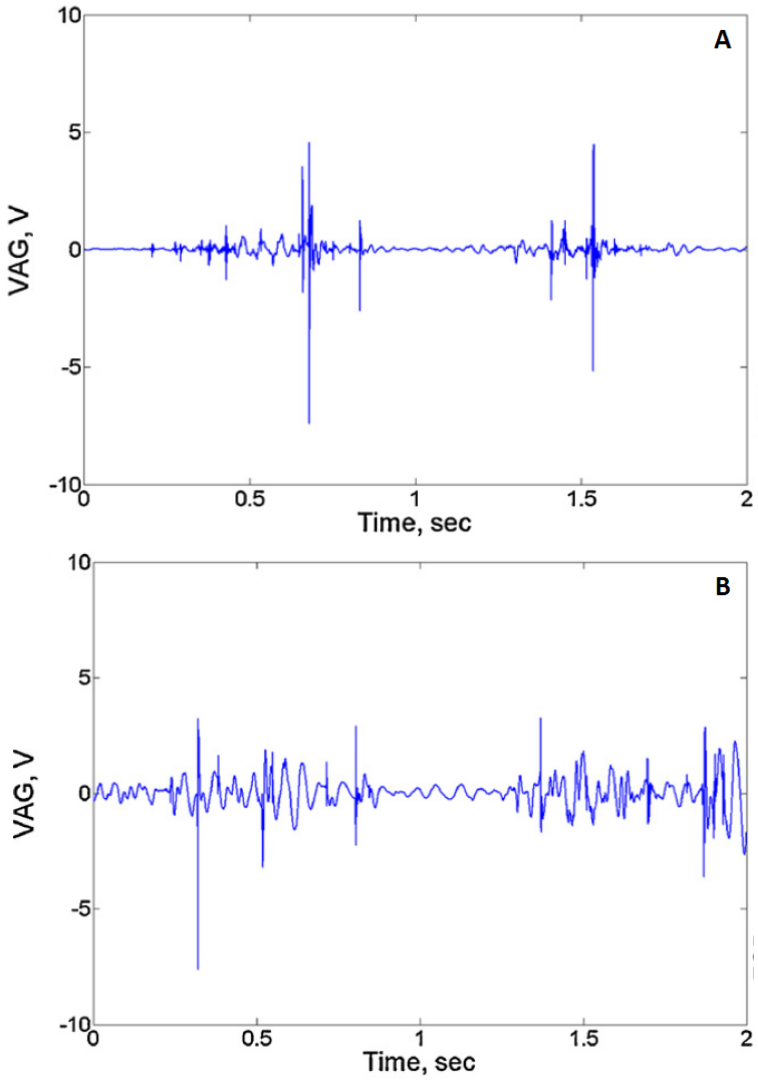

Figure 3.1: Representation of a VAG signal of (A) healthy and (B) pathological knee joint [39].

VAG signals analysis may allow the differentiation between a healthy and an injured knee. Additionally, it is known that several sub-pathologies can be identified through the VAG signal analysis as a torn meniscus, mild/severe chondromalacia patella and several types of arthritis (osteoarthritis, rheumatoid arthritis and spondylarthritis) [30, 34, 35, 36, 37, 38, 39, 40, 41]. Rangayyan et al. reported that meniscal lesions demonstrated as sharp and short energy duration bursts in the sound signal into the 0 to 200 Hz frequency range, while mild chondromalacia has

exhibited long duration bursts in the frequency range of 0 to 300 Hz [35, 42]. Severe chondromalacia signals reveal to be of even lower frequencies within the 0 to 100 Hz range due to greater loss of cartilage tissue between articulating surfaces [35, 42]. Moreover, Reddy et al. demonstrated that mean power of the acceleration signal in the range of 100 to 500 Hz was significantly different for OA patients compared to rheumatoid arthritis patients [35, 41].

Despite the great potential of this method, several signal processing techniques must be applied to the VAG signal in order to eliminate background noise, muscular activity and knee joint movement-related component. These undesirables components obscure the truly wanted signal since they basically mask the low amplitude component, that corresponds to knee joint abnormal vibrations [31]. Ideally, the whole experiment should be performed in an anechoic chamber and without muscular activation being the recorded signal the true signal of interest [31].

Chapter 4

Theoretical Fundaments

A literature review of VAG related studies for knee OA detection is provided in this chapter. The whole process since the signal acquisition until the final classification is described, focusing on the current available strategies for OA signal classification, its advantages and major drawbacks.

4.1 Signal Acquisition

In order to obtain a reliable and feasible signal that describes and fully characterizes the knee joint status several considerations must be taken into account. Among them it must be considered the type of used sensors, its inherent limitations (e.g. sampling frequency, noise, etc.), its placing on the knee joint, the preprocessing techniques, signal analysis methodologies and the adequate classifiers. A carefully choice of those and good interpretation of its limitations may lead to a successful and rewarding work.

4.1.1 Sensors

Recent developments in the electronics field are now changing completely the medical diagnosis, rehabilitation paradigm and even the research field. Nowadays it is possible, for instance, to monitor human movement for clinical purposes by comparing normal with pathological movements classifying them accurately recurring to newly developed algorithms. Knee-joint assessment is now possible recurring to new algorithms which use data from sensors such as accelerometers, stethoscopes, electro-goniometers and gyroscopes, among others [43].

4.1.1.1 Accelerometer

Accelerometer is a positional type sensor device that measures acceleration along its axis relatively to Earth's surface. Commonly, accelerations measurements are provided in terms of g-force (g) [43, 44]. Generally, accelerometers use a sensing method as a proof mass excited in a mass-spring damper system as shown in Figure 4.1 [43].

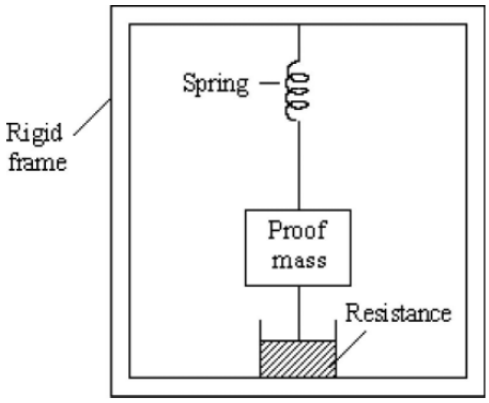

Figure 4.1: Schematics of the general functioning of an accelerometer. In the mass-spring-damper system, the loading force drives a second order damped harmonic oscillator where the displacement of the proof mass relative to the rigid frame is considered. When acceleration is kept constant, the displacement is directly proportional to the given acceleration [43].

Single and multi-axis accelerometers are available to detect magnitude and direction of the given acceleration that can be used to sense orientation, coordinate acceleration, vibration, shock and falling in a resistive medium [29, 43, 44, 45]. There are three major types of accelerometers, namely piezoelectric, piezoresistive and capacitive types [43]. General characteristics of each type of accelerometer are provided in the Table 4.1.

Capacitive accelerometers have higher stability, sensitivity and resolution than the others, enabling the measurement of two components of acceleration: the gravitational acceleration component and the specific acceleration component due to a given force [43]. Dual acceleration components accelerometers are more suitable for human posture monitoring being now widely available on market [43].

Table 4.1: Comparison of the characteristics of different types of accelerometers [43]

Parameters	**Piezoelectric**	**Piezoresistive**	**Capacitive**
Gravitational component	No	Yes	Yes
Bandwidth	Wide	Moderate	Wide
Self-generating	Yes	No	No
Impedance	High	Low	Very High
Signal Level	High	Low	Moderate
Temperature Range (^{o}C)	-55 to 100	-55 to 150	-200 to 200
Linearity	Good	Moderate	Excellent
Static Calibration	No	Yes	Yes
Cost	High	Low	High
Ruggedness	Good	Moderate	Good
Suitable for shock	Yes	No	No

4.1.1.2 Stethoscope

Stethoscope creation in 1815 by René Laennec was a landmark essentially for heart diseases diagnostics [46]. The need to better hear the sounds emanated from the body lead to the creation of a device that amplifies sound's intensity in order to obtain a more accurate diagnosis [46, 47].

The stethoscope is majorly composed of three parts: the chest piece, tubes and headset. The chest piece usually consists of two sides: a diaphragm (plastic disc) and bell (hollow cup) [48]. When the chest piece contacts the patient, body sounds cause its vibration creating acoustic pressure waves which travel through the tubes to the listener's ears. The bell transmits low frequency waves while the diaphragm transmits higher frequency sounds [48].

There are two types of stethoscopes: the acoustic and the electronic stethoscope. The acoustic stethoscope is the most well-known and the one that is most familiar devices. It is a popular and trusted device among doctors. Acoustic stethoscope remains the most commonly used device in clinical practice, however electronic stethoscope are gaining more popularity these days [48]. The electronic stethoscope function is similar to the acoustic stethoscopes however the sound in the latter one is converted to an electric signal for posterior analysis. The electronic stethoscope allow a better listening of the body sounds since the signal can be digitally amplified, filtered (for noise reduction) and transmitted to a computer for optimal listening [47, 48]. Moreover, electronic stethoscopes allow the data transmission in a wireless way (e.g. bluetooth) and a graphical representation of pathological sounds for further interpretation [48]. The advantages and drawbacks of the acoustic and electronic stethoscopes are displayed in the Table 4.2.

Table 4.2: Acoustic vs electronic stethoscope comparison - advantages and major drawbacks [47, 48].

Parameter	Acoustic Stethoscope	Electronic Stethoscope
Cost	Low	High
Signal Amplification	Moderate	High
Signal Enhancement (filtering)	No	Yes
Data Transmission	No	Yes
Storing Data	No	Yes
Graphical Displaying	No	Yes
Battery	No	Yes
Interference with environmental	Minimal	Moderated

In addition to more popular and recognized human body sound auscultation as the cardiac or lung auscultation, a new method that allows joint sound detection and analysis is nowadays under investigation. Several studies point out in the direction that the knee joint sound can be captured and evaluated recurring to the use of electronic stethoscope along with some signal processing algorithms [1, 31, 38, 39].

4.1.2 Experimental Setup

4.1.2.1 Positioning of Sensors

The correct positioning of sensors is crucial for an accurate and feasible assessment of knee joint condition. Regarding this matter, the optimal location is generally accepted to be the best contact area for knee auscultation, as the medial compartment slightly below the midline of the patella (medial condyle on the patella) [1, 37]. This spot (see Figure 4.2) is the closest to the area of contact between moving knee joint surfaces, assuring greater sensitivity. Besides that, it also offers a relatively stable position for the sensor in a way that is not greatly affected by the actual knee joint movement as well as by the muscle contraction interference [34, 35, 37, 39, 40, 41, 49]. Additionally, Kernohan et al. [50] reported that meniscal injuries produce not only characteristic signals but also larger signals on the affected side suggesting the placement of one or two sensors laterally in the knee [1, 51].

Figure 4.2: Optimal sensor position for knee joint assessment [34, 35, 37, 40, 41].

4.1.2.2 Experimental Protocol

Traditionally, one of most common performed tasks for knee joint assessment is the knee motion from flexion to full extension (see Figure 4.3) whereas in the full extension position the knee is making an angle of 0^o between the femur and the tibia while in the flexion position the knee is making a 90^o angle [1, 40]. This movement from the full flexion to full extension is defined as one cycle ($90^o \rightarrow 0^o \rightarrow 90^o$) [1, 39]. During the task, the subject is always seated and without their feet touching the ground, performing the mentioned movement. Some training should be done before the experiment onset in order to warm up the knee joint as well as for the establishment of a constant velocity during the whole exercise (usually 2 or 4 s/cycle) [1, 39, 40, 52]. The velocity

of the movement across trials should remain constant in order not to introduce artifacts in the VAG signal spectral content. The VAG signal is recorded during the whole experiment simultaneously with angular data retrieved by a electro-goniometer/gyroscope placed on the lateral aspect of the knee with the axis of rotation at the joint line [53]. This angular data is crucial for VAG signal segmentation since it gives precise information about the phase of the movement the VAG signal belongs [39, 41].

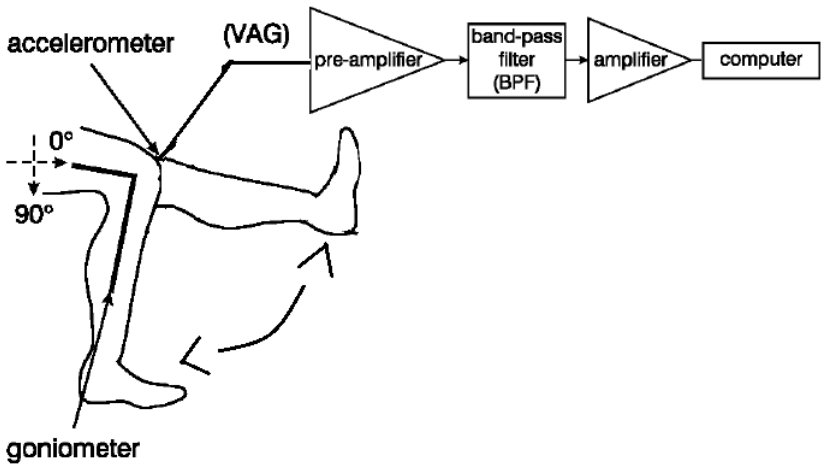

Figure 4.3: Experimental setup. VAG and angular signals simultaneously recorded during the flexion-extension movement. [1, 54].

4.2 Pre-processing

VAG acquired signal is of a very complex nature and therefore very complex to analyse since the recorded accelerations arising from the knee joint result from the combination of several components such as random, muscular and even knee-joint movement related noise. The true challenge when analysing a VAG signal is to accurately unmask the truly desirable component present in the VAG signal [31, 39, 55].

The wanted signal component of interest of a VAG signal is basically the signal's remaining low amplitude signal component after the removal of the noisy parts. Ideally, after the pre-processing step the VAG signal has only the information corresponding to the knee joint vibrations. In order to overcome these limitations several approaches are documented in the literature in order to remove signal's artifacts from different sources such as:random and background noise; baseline wandering artifacts; muscular contraction interference; movement-related artifacts (gravitational component included).

The more simpler and generalistic noise removal strategies rely on the minimization of the noise/artifacts generation process during the data gathering process/ signal's collection. Optimal placement of the sensors and the use of conductive gels or double-sided tape between the probe surface and the skin are the most commonly used strategies documented in the literature. By just

optimal placing the sensor and using double-sided tape the friction between the skin and the sensor can be greatly reduced, thus, reducing also the overall noise generation process [1, 2, 34, 35, 37, 39, 40, 41, 49, 53, 54, 56].

Also, more advanced and complex strategies are used for noise removal as signal's normalization, (fixed) bandpass filtering, adaptive filtering, noise identification and reduction algorithms or even signal's segmentation [39, 49, 53, 54, 56].

4.2.1 Normalization

In order to increase the overall robustness by taking into account the observed differences in terms of the signal's amplitude values range and/or the speed of the leg swing across different subjects and trials, several normalization methods can be applied to the VAG signals [57].

4.2.1.1 Amplitude Normalization

Each collected signal has its own range of amplitude values that may or may not substantially differ either from subject to subject or from trial to trial. Thus, with the purpose of providing a more general comparison between signals arising from different subjects, an amplitude modulation technique can be applied to the VAG signals [58].

Signal's amplitude normalization can be achieved in a simple fashion way by only adjusting the measured values on different scales to a common scale or by more advanced strategies based on statistics, such as the probability density distribution of the signal's amplitude values.

The simplest amplitude normalization method is based on the signal's maximum and minimum (min-max normalization). Each signal's amplitude value can be normalized in order to have a new amplitude within a certain and pre-defined interval of values. The minimum-maximum normalization method can be obtained according to the following equation:

$$x_{normalized}[n] = (x[n] - x_{min}) * \frac{new_{max} - new_{min}}{x_{max} - x_{min}} + new_{min} \tag{4.1}$$

where $x_{normalized}$[n] is each one of the new normalized samples, new_{min} = -1 and new_{max} = 1 the new normalized signal's amplitude range (in this case [-1, 1]), *xmin* and *xmax* the original signal's minimum and maximum, respectively.

4.2.1.2 Velocity Normalization

Another important factor when considering this kind of signals is the differences obtained regarding the knee joint movement velocity during, essentially, the extension/flexion phases. This lack of coherence in terms of leg swing velocity may affect frequency content characteristics of the analyzed signals. Therefore, some recent studies have reported the use of a time axis normalization algorithm called dynamic time warping (DTW) [2, 39, 53].

DTW algorithm measures similarity between two sequences which may vary in phase and amplitude by computing a distance coefficient between them enabling the alignment of two signals with similar patterns even if they are not on the same time axis [59].

4.2.2 Filtering

Digital filtering, if correctly applied, may allow a relatively easy and simple elimination of several undesired signal parts. Fixed filtering and more recently adaptive filtering are the most common used filtering strategies to solve this type of problem. While the fixed filtering is related to a band pass or high pass filter with certain pre-defined characteristics, adaptive filtering involves the changing of filter parameters over time adapting to the signal changing characteristics. Adaptive filtering is more appealing and also more complex than fixed filtering, but it provides more satisfying results when comparing with fixed filtering [60].

4.2.2.1 Fixed Filtering

VAG signal is usually pre-filtered by a bandpass filter with a bandwidth of 10 Hz to 2 kHz in order to remove low-frequency movement artifacts, high-frequency noise, muscle contraction interference and to prevent aliasing effects [39, 53, 54, 56].

In spite of the usefulness of this technique, fixed filtering cannot be performed correctly when the noise or outside interference overlaps the VAG signal spectrum requiring the need of modified, appropriated and adaptable techniques [54].

4.2.2.2 Adaptive Filtering

Due to signals inherent non-stationary character and difficult interpretation, adaptive filtering is needed to clean the signal. Baseline wandering and overlapping noise removal is needed in the case were the fixed filtering does not solve the problem [49, 56].

Baseline wandering or baseline drift is a very important phenomenon that occurs in biomedical signals making the signal to fluctuate from the straight baseline line over short periods of time affecting essentially diagnostic decision making in the medical field [61, 62].

In some cases, baseline wandering is seen when patients with knee joint disorders tremble its legs during the experiment procedure (e.g. during flexion or extension movement phase) causing baseline oscillations in the raw vibration signal [61]. On the other hand, random noise is a random fluctuation in an electric signal usually associated with the thermal effect of all circuit constituents [49, 61].

Baseline wandering and random noise removal algorithms such as the least-mean squares (LMS) and recursive least-squares (RLS) algorithms, were early implemented by Zhang et al. [63] and Rangayyan et al. [64].

More recently, Lu et al [56] implemented an adaptive filter technique based on the signal power error minimization method to successfully eliminate random noise from the VAG signal. While, in other studies the combined use of ensemble empirical mode decomposition (EEMD)

and detrended fluctuation analysis (DFA) methods proofed to be effective into the identification and removing of baseline wander and random noise from the original signal [49].

Another simple and effective adaptive filtering technique that estimates and removes baseline wandering from the VAG signals, widely documented on the literature, is a special version of a moving average filter, namely the cascade moving average (CMA) filter [61, 65, 66]. The cascade moving average filter is a hierarchical model that combines the used of two successive moving average operators (see Figure 4.4).

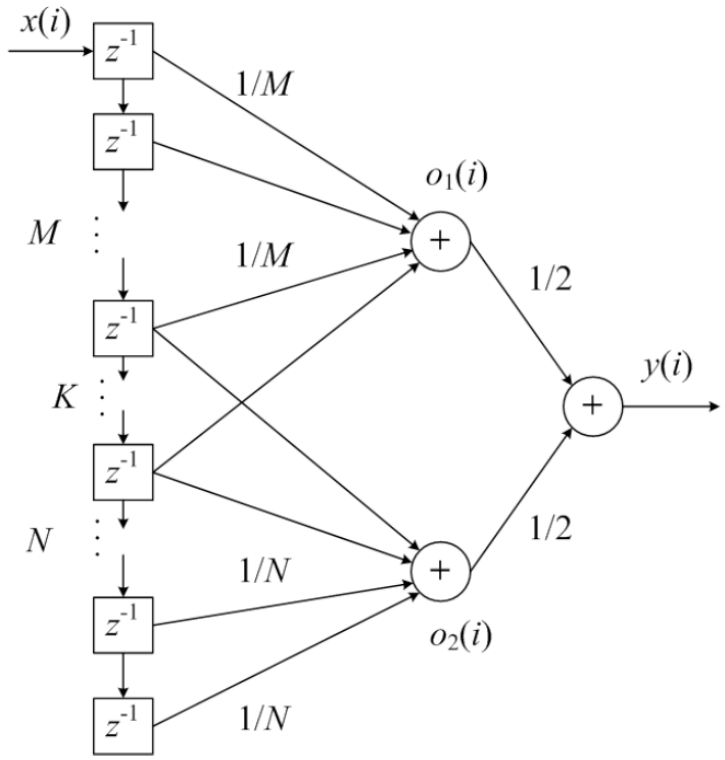

Figure 4.4: Double layer cascade moving average filter hierarchical structure [61, 66].

The first layer of the cascade filter contains a M-order and a N-order moving average operators(see Equations 4.2 and 4.3), while the second layer of the hierarchical moving average filter is used to smooth the piecewise linear trends obtained from the outputs of the previous two moving average operators in the first layer [61, 66].

The K inputs in the tail end of the M-order operator are overlapping with the beginning inputs of the N-order operator being the output of the M-order operator $o_1(i)$ and the N-order operator $o_2(i)$ expressed by following equations:

$$o_1(i) = \frac{1}{M}\sum_{m=1}^{M} x(i-m) \tag{4.2}$$

$$o_2(i) = \frac{1}{N}\sum_{n=1}^{N} x(i-M+K-n) \tag{4.3}$$

where N, M and K are the selected number of points/samples to use in the cascade moving average. The final output of the cascade moving average filter $y(i)$ is given by:

$$y(i) = \frac{1}{2M}\sum_{m=1}^{M} x(i-m) + \frac{1}{2N}\sum_{n=1}^{N} x(i-M+K-n) \tag{4.4}$$

4.2.3 Segmentation

Another used strategy in several studies to overcome noise-related issues is to segment the VAG signal into smaller segments according to a simultaneously recorded angular information (usually recorded with an electrogoniometer). This strategy allows the exclusively extraction of the segments that are less affected by noise [34, 35].

In a knee extension/flexion test, one full leg swing cycle comprises an angular movement range of approximately 90º. Having this in mind, several studies reported the exclusion of the initial and end phase movement segments correspondent to the initial 0º to 25º angles and to the last 75º to 90º angles in the total 90º movement range. Only the segments correspondent to the middle phase of the movement, i.e., segments with correspondent angles between 25º and 75º, were kept for further analysis. The exclusion is based on the fact, that anatomically, in those phases the patella is not fully contacting the femur surface and so, it is not interesting to analyze [7]. Additionally, a lot of ambient noise related due to the inherent acceleration/deceleration of knee joint movement/leg movement is also more pronounced during this period [34, 35].

4.2.4 Feature Extraction

An extremely vital part for the development of an accurate, feasible and robust analysis/classifier is the capability of each selected feature to discriminate the different classes, i.e., distinguish an affected arthritic knee joint from a healthy one [58]. A proper selection of relevant features with high discriminant capability is essential for a proper development of the classification system.

It is well-known that the VAG signal is a non-stationary signal and its properties may vary according to time. So, some pathological events may only occur in certain and specific time periods, demanding a reliable time-related/ time-localized and adaptive approach in order to obtain a good feature extraction and consequent selection.

Feature extraction can be performed either in the time as in the frequency domain, resulting in a different set of characteristics fully describing the signal.

4.2.4.1 Time-domain Features

Time domain features are usually more simpler to obtain and are often more used to describe and characterize the raw content of the VAG signals. Most of these metrics are based on simple mathematical and statistical measurements of the signals.

Several statistical parameters observed in histograms of normal and abnormal VAG signals as skewness, kurtosis and entropy are widely used as discriminant features [1, 58].

Skewness measures the asymmetry of the probability density function (PDF); Kurtosis measures the tendency of the PDF to have peaks, i.e., measures whether the data are peaked or flat relative to a normal distribution; Entropy measures the inherent randomness observed in a probability distribution and it is commonly used to represent the nature and spread of a PDF [58].

Skewness, kurtosis and entropy were defined as it follows:

$$S = \frac{\frac{1}{n}\sum_{i=1}^{n}(x_i - \bar{x})^3}{(\sqrt{\frac{1}{n}\sum_{i=1}^{n}(x_i - \bar{x})^2})^4} \tag{4.5}$$

$$K = \frac{\frac{1}{n}\sum_{i=1}^{n}(x_i - \bar{x})^4}{(\sqrt{\frac{1}{n}\sum_{i=1}^{n}(x_i - \bar{x})^2})^4} \tag{4.6}$$

$$H = -\sum_{L=0}^{L-1} p_x(x_l) log_2[p_x(x_l)]) \tag{4.7}$$

Where n is the total number of samples, x_i the sample with the i index and $\bar{x}$ the mean value of all samples. $p_x(x_l)$ is the probability density function of the given signal with x_l, l = 0, 1, 2, ..., L - 1, representing the L bins used to represent the range of the values of the signal x.

Other features such as the mean, standard deviation (std), variance, variance of the mean-squared (VMS) and the form factor (FF) values have been described in the literature. VMS values describe the local spread or dispersion degree of the signal in a short time span while form factor values measure the VAG signal shape complexity [7, 30, 40, 58]. The FF value is computed as the ratio of mobility of the first derivative of the signal $M_{x'}$ to the mobility of the signal itself M_x [40]. Previous findings reported that Kruskal-Wallis test results regarding VMS values reached the level of significant difference (p<0.01) when comparing normal with abnormal VAG signals [40]

VMS and FF values were defined as it follows:

$$\sigma_x^2 = \sum_{l=0}^{L-1}(x_l - \mu_x)^k p_x(x_l) = VMS \tag{4.8}$$

$$M_x = \left[\frac{\sigma_{x'}^2}{\sigma_x^2}\right]^{0.5} = \frac{\sigma_{x'}}{\sigma_x} \tag{4.9}$$

$$FF = \frac{M_{x'}}{M_x} = \frac{\frac{\sigma_{x''}}{\sigma_{x'}}}{\frac{\sigma_{x'}}{\sigma_x}} \tag{4.10}$$

Where σ_x^2 represents the variance of the signal x, μ_x is the mean value of the signal x and $p_x(x_l)$ is the probability density function of the given signal with x_l, l = 0, 1, 2, ..., L - *1*, representing the L bins used to represent the range of the values of the signal.

The signal's sample variability over time was also suggested as a feature which was named as the turns count (TC) parameter. TC parameter measures the number of significant changes in direction for a given signal [52, 66, 67]. The total number of the signal turns computed over the time series indicates the degree of fluctuation dynamics in the presented signal. This parameter was firstly introduced by Willison [68] for Electromyography (EMG) myopathy signal analysis.

A signal sample can be considered as a turn if it satisfies, simultaneously, the following two conditions: 1) it represents an alteration in direction in the signal, i.e., a change in the sign of the derivative (either positive or negative); 2) the difference (considering its absolute values) between the amplitude of the current alteration and that of the preceding alteration is greater than a threshold.

$$TC_{candidade}[k] = \big[x[n]-x[n-1]][x[n+1]-x[n]\big] < 0, 2 \leq n \leq N-1 \tag{4.11}$$

$$TC_{final} = |TC_{candidade}[k] - TC_{candidade}[k-1]| \geq Th \tag{4.12}$$

where $x[n]$ is the nth sample, with n=0,1,...,N, $TC_{candidade}[k]$ the extracted sample candidates that satisfies the first admissible condition, Th the pre-defined threshold and TC_{final} as the final TC sequence.

The threshold value can be predefined recurring to fixed or adaptive style. For fixed threshold, it is reported by the work of Rangayyan and Wu [52] the use of a threshold value of 0.2 considering an amplitude-normalized VAG signal bounded to the interval [-1,1].

As an adaptive approach, threshold value were selected by taking into account signals standard deviation, usually 0.5 σ. However, due to pathological VAG signal inherent variability, such standard deviation-based approach revealed to be non-satisfactory. VAG pathological signals have a higher standard deviation value due to the signal's higher degree of variability, resulting into a greater threshold value when compared to the healthy group. Consequently, TC parameter values from the arthritic group are smaller than the healthy controls, deviating from the true expectations. Such adaptive and standard deviation based approach reveal not to be suitable for TC threshold purposes.

4.2.4.2 Frequency-domain Features

Frequency domain features are of a more complex nature however being more suitable for this kind of purposes since it can more easily provide detailed insight of the hidden signal's patterns [69].

Signal processing techniques such as Fourier Transform (FT), time-frequency distributions (Wigner-Ville distribution) and Wavelet Transform (WT) are widely used to characterize VAG signals [39, 54, 58, 70].

One of the most conservative and used approaches for frequency content information extraction is the Fast Fourier Transform. FFT (see Equation 4.13) is based in the decomposition of the input signal x(t) into its harmonics (sinusoidal functions) of different frequencies revealing its

frequency content. Fourier transform is independent of time, i.e., the frequency decomposition is the averaged over the total duration of the signal by assuming that the random process behind the signal creation is stationary and do not change with time.

$$F(k) = \sum_{n=0}^{N-1} x(n).e^{-2\pi ikn/N}, k \in \mathbb{Z} \tag{4.13}$$

Therefore, despite its simplicity, Fourier transform is not adequate for the characterization of transient signals such as the VAG signals. Fourier-based analysis provides a poor localization of signals in time, difficulty the capability to detect signal's time-varying spectral characteristics. Although this, previously findings in VAG signal analysis reveal different power spectral densities patterns through the Fourier Transform in certain frequency intervals regarding the arthritic and healthy groups either [1, 30, 41]. VAG signal spectral content revealed that the power spectral density in the 0-500 Hz frequency range is significantly higher for the arthritic group compared to healthy controls [35].

FT poor time resolution was partially surpassed with the creation of the Short Time Fourier Transform (STFT), that can be considered more suitable for non-stationary signals analysis than the general Fourier Transform. Although, STFT implies a fixed time-frequency resolution due to its fixed window size. In general, STFT method is nothing more than the application of the Fourier Transform over a window that slides over time. STFT is defined in the Equation 4.14

$$X(n,k) = \sum_{m=-\infty}^{\infty} x(m)w(n-m).e^{-jkm2\pi/N} \tag{4.14}$$

where the $w(n-m)$ is the window function. The length of the window function is intrinsically related with the bandwidth of the frequency spectrum, thus STFT cannot provided a high resolution in both time and frequency domain.

Similarly to the STFT, other time-frequency representation of signals were used with the introduction of the Wigner-Ville distribution (WVD). Basically, WVD correlates the input signal with a time-translated and frequency-translated version if itself, i.e., the window is essentially a shifted version of the same input signal. The WVD can be calculated as it follows:

$$W_s(t,w) = \sum_{-\infty}^{\infty} x(t+\frac{\tau}{2})x^*(t-\frac{\tau}{2})e^{-iw\tau}d\tau \tag{4.15}$$

In the work of Kim et al. [39], four time-frequency parameters namely the energy parameter (EP), energy spread parameter (ESP), frequency parameter (FP) and frequency spread parameter (FSP) were obtained from a denoised time-frequency distribution (TFD) version of the VAG signal obtained by the Wigner-Ville distribution [39, 53].

The EP is nothing more than the mean of the signal along each time slice representing energy variation with time. The ESP measures the spreadability of energy over the frequency range across time and is calculated as the standard deviation of the signal along each time slice. The FP stands for the instantaneous mean frequency being computed as the first moment of the signal *(t,f)* along

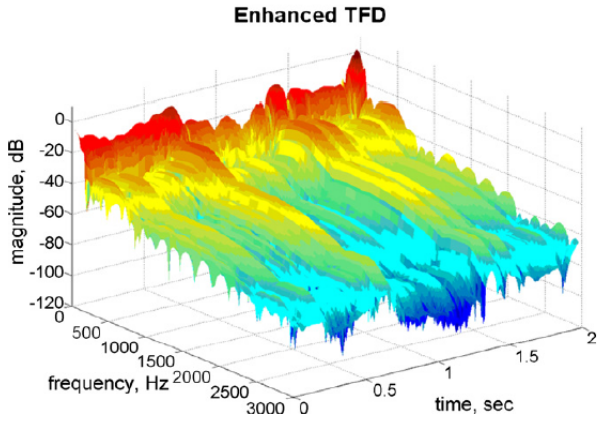

Figure 4.5: Denoised time-frequency representation of the VAG signal obtained by the Wigner-Ville distribution [39].

each time slice. The FSP measures the spread of frequencies across time and is given by the second central moment of the signal *(t,f)* along each time slice. Additionally, the average and standard deviation values of each enounced parameter were also found to be meaningful features for the classifier [39, 53].

EP, ESP, FP and FSP were defined as it follows:

$$EP(t) = \frac{\sum_{f=0}^{fm} X_e(t,f)}{f_m} \tag{4.16}$$

$$ESP(t) = \left[\frac{\sum_{f=0}^{fm} |X_e(t,f) - EP(t)|^2}{f_m}\right]^{1/2} \tag{4.17}$$

$$FP(t) = \frac{\sum_{f=0}^{fm} fX_e(t,f)}{\sum_{f=0}^{fm} X_e(t,f)} \tag{4.18}$$

$$FSP(t) = \left[\frac{\sum_{f=0}^{fm} |X_e(t,f) - EP(t)|^2}{\sum_{f=0}^{fm} X_e(t,f)}\right]^{1/2} \tag{4.19}$$

Where $X_e(t,f)$ is the value of the enhanced matrix derived from the TFD of the VAG signal at a given t time and f frequency and f_m as the maximum frequency present in the signal.

However, a well-known disadvantage of the use of WVD is that it may lead to a misguided or difficult interpretation of the result, not being easy to fully understand its meanings majorly in those cases where the analyzed signal is constituted by multiple components [71].

In order to overcome this fixed time-frequency resolution issues and/or time-frequency representation difficult understanding (e.g. WVD), the wavelet-based analysis appeared. The WT (see Equation 4.21) has provided a more flexible time-frequency resolution by instead of breaking down the input signal into its harmonics as the Fourier-based transforms, it seeks to break it down into a series of local basis function called wavelets.

These family of functions are generated from a single function $\psi_{(a,b)}$ by the operation of dilations and translations being the wavelet transform of a continuous signal defined as:

$$\psi_{a,b}(t) = |a|^{(1/2)}\psi(t-b)a \tag{4.20}$$

$$X(n,k) = \frac{1}{|a|^{(1/2)}}\sum_{-\infty}^{\infty} x(t)\psi^*(\frac{t-b}{a})dt \tag{4.21}$$

where * represents the complex conjugation.There are several families of wavelets, namely the Morlet, Haar, Daubechies, Biorthogonal, Coifflets, among many others.

WT provides a multi resolution decomposition of the input signal into a set of frequency intervals with the same bandwidth (in a logarithmic scale - logarithmic sampling of the frequencies). This property enables the analysis of higher frequencies in shorter windows and lower frequencies in longer windows in time providing a good trade-off between time and frequency resolution.

However, time-frequency resolution in the high frequency region may be compromised since according to WT properties the discrimination between signals that have close high-frequency component in time can be difficult (see Figure 4.6).

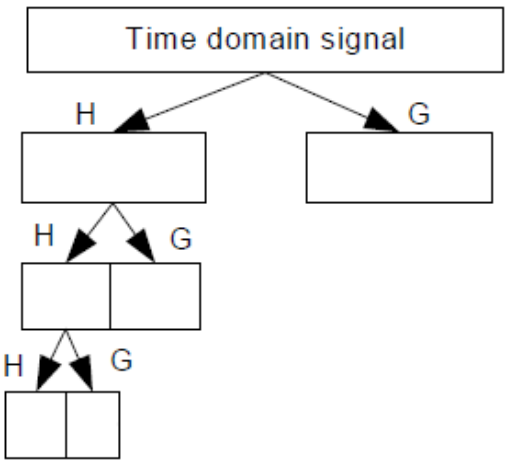

Figure 4.6: Wavelet transform decomposition scheme [72]. At the first level, the input signals is passed to a low pass-filter resulting into two new signals described by set of wavelet coefficients (approximation (H) and detail(G) coefficients). Moreover, for the remaining levels, the approximation coefficients signal is recursively passed through the low-pass filter creating once more two set of detailed and approximation coefficients, until the last level is reached.

Having this in mind, a more generalistic approach of the wavelets has arised, called wavelets packets or wavelet packet decomposition (see Equation 4.22). These wavelet packets are formed by taking linear combination of the common wavelets functions preserving some inherited properties such as orthonormality, smoothness and location from their corresponding mother functions.

The equation describing the discrete wavelet packets transform is defined as it follows:

$$W_{j,k}^{n}(t) = 2^{j/2} W^{n}(2^{j}t - k) \tag{4.22}$$

where the index n is the modulation parameter. The first two wavelet packet functions are the usual scaling and motherwavelet function, respectively.

$$W_{0,0}^{0}(t) = \Phi(t) \tag{4.23}$$

$$W_{0,0}^{1}(t) = \psi(t) \tag{4.24}$$

The remaining wavelet packet functions for n=2,3,..., N are defined recursively by the following relationships:

$$W_{0,0}^{2n}(t) = \sqrt{2}\sum_{k} h(k) W_{1,k}^{n}(2t - k) \tag{4.25}$$

$$W_{0,0}^{2n+1}(t) = \sqrt{2}\sum_{k} g(k) W_{1,k}^{n}(2t - k) \tag{4.26}$$

where h(k) and g(k) are the quadrature mirror filters (QMF). Specific time-frequency information measurements of a signal can be obtained by taking the inner product of the signal and that particular basis function resulting in a set of wavelet packets coefficients of the given function f(t) according to the Equation 4.27:

$$W_{j,n,k} = \langle f.W_{j,k}^{n} \rangle = \int f(t) W_{j,k}^{n}(t) dt \tag{4.27}$$

The full wavelet packet decomposition (WPD) of a discrete-time signal is calculated by applying both low and high pass filters followed by the decimation procedure (usually downsampling by a factor of 2) to the input signal and then recursively to each intermediate signal's version until the last level of decomposition is reached (see Figure 4.7).

The WPT full tree can be viewed in Figure 4.6 but a modified version with the WPT tree displayed in increasing frequency order can be obtain by only switching the order of some tree nodes known, also called as the Paley ordering (see Figure 4.8). This representation is easier for data interpretation.

The major advantages of the using WPT instead the regular WT is that the latter only decompose the low-frequency components of the intermediate signals at each node while the WPT decomposes not only the low but also the high-frequency components of all signals (see Figure 4.9) providing a more deep analysis of the input signal providing the extraction of features or

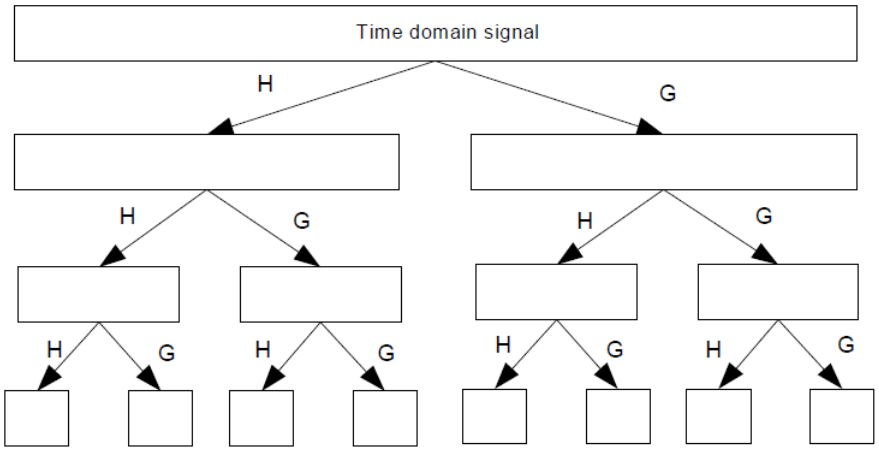

Figure 4.7: Wavelet packets transform decomposition scheme [72]. For the first level of decomposition the input signal is passed to a high pass and low pass filter, respectively, resulting into two new intermediate signals (the low and high pass versions of the input signal). Moreover, until the last level of decomposition is reached, each one of the intermediate signals are then passed to the same high pass and low pass filters at each iteration.

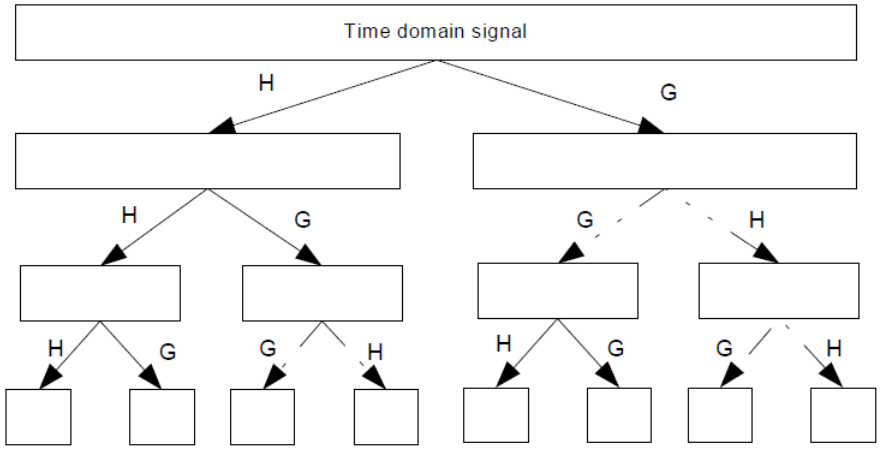

Figure 4.8: Paley WPT order scheme [72]. Dash-lines tree nodes are re-ordered so than can the tree be displayed in increasing frequency order.

even signal's characterization for stationary and repetitive events but also for the punctual or non-stationary events.

Equivalent approaches for time-frequency representations of a signal was also introduced by Mallat and Zhang [73] using the so called "greedy" algorithm. This matching pursuit (MP) decomposition algorithm is able to decompose the signal using basis functions with good time-frequency properties, referred also as atoms [54, 70]. Gabor function, local cosines trees and even the wavelet packets are often applied to build up dictionaries for this type of applications.

In the work of Krishnan and Rangayyan [54] the average and standard deviation values of

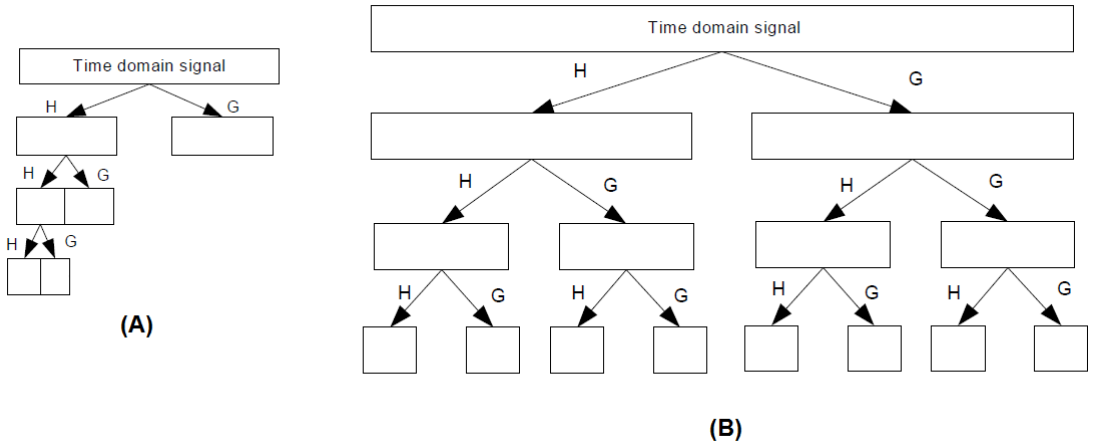

Figure 4.9: (A) Regular wavelet transform and (B) Wavelet Packets decomposition schematics [72]. Regular WT only decomposes the low frequency intermediate components into two new subsets of wavelet coefficients while the WPT decomposes not only the low frequency intermediate component as well as the high frequency component.

the number of MP iterations using a Gaussian function was used to classify VAG signals with a relatively good accuracy. Later on, Cai et al. [70] also used the number of atoms obtained with MP algorithm with Daubechies 8 filter and the number of turn counts (time-domain feature) to classify VAG signals.

4.3 Classification

Classification can be thought as the problem of assigning a given observation in a collection to target categories or classes (labels). Classification consists of predicting a certain outcome based on a given input or model. The goal of classification is to accurately predict new observation/data based on its similarity to previous used examples, i.e., by extracting essential information from a data set and transform it into an understandable structure/model for further use. Classification can be divided into subgroups: the supervised and unsupervised classification.

In supervised classifications, as the name suggests, it is provided a set of correctly labelled observations, also called the ground truth, that are used in the process of constructing the classifier model. In unsupervised classification, no labels are provided, and the observations are assigned to a certain number of classes based on their properties, by aggregating (clustering) instances that display similar properties according to some metrics. For this work purposes (binomial classification), only supervised classification techniques will be used.

In order to predict the outcome, a classifier, usually, requires five major steps, which can be more or less complex depending on the used methods [74, 75, 76]. These five steps are described below (see Figure 4.10).

Figure 4.10: General mechanism behind of a classifier system.

4.3.1 Data Transformation

4.3.1.1 Dataset Normalization

Data collected from multiple sources (i.e. different subjects), not always display the same range of values, units or scales for each collected parameter. Therefore, the original dataset needs to suffer a transformation process involving smoothing, generalization and normalization of the data [57, 77].

Data transformation, more specifically, data normalization is used to standardize all dataset features into a specified predefined criterion (e.g. specific range of values) in order to remove noisy or redundant objects which are not reliable neither good for increasing classification results [57]. Several different techniques are available for data normalization. Among them, the most commonly used are the minimum-maximum and Z-Score [57, 78]. There is not a universal criterion for optimal choice of the normalization method, being the particular choice of normalization technique responsible to the user choice [57].

The minimum-maximum normalization method involve the linear transformation of the input data to specific interval range such as 0.0 to 1.0. This method takes into account each variable minimum and maximum and performs a linear transformation to the desired the interval, e.g. [0,1], based on both ends [57, 78].

The Z-Score normalization is more used when the actual minimum and maximum value of an attribute is unknown, using instead the mean value and standard deviation of that attribute to perform the attribute transformation [57, 78].

4.3.1.2 Feature Selection

Feature selection is one of the most important and frequently used techniques for data mining [79, 80]. Discriminant power of the available features is crucial to obtain a good overall classification accuracy. Therefore, redundant, irrelevant features or noisy data present in the original dataset needs to be removed in order to create a subset with only the best and highly discriminant features. The optimal subset of features is measured by an evaluation criterion. This evaluation criteria can

be quite different in terms of its nature but the final purpose remains always the same, i.e., to increase predictive accuracy and result comprehensibility [80].

Several techniques are available for this purposes being the most commonly used the sequentially forward selection (SFS), sequential backward selection (SBS), bidirectional search and principal component analysis (PCA).

Sequential search methods such as the SFS, SBS or bidirectional search creates, iteratively, a subset of features (by adding and/or removing features) that is posteriorly evaluated according to a certain criterion, usually, predictive accuracy. The search may start with a empty set and successively add features (e.g. SFS), or start with all available features and iteratively removing some (e.g. SBS) or to start with a certain set of features and simultaneously add and remove features (bidirectional search)[80].

PCA is a statistical-based procedure that uses an orthogonal transformation to convert a set of variables into a new set of values of linearly uncorrelated variables called principal components (pc), with less than or equal to the number of original variables [81]. PCA identify patterns in data and express them in a way that highlights their similarities and differences. PCA is often used not only to unmask patterns but simultaneously to reduce the number of dimensions of a high dimensional dataset [81].

The PCA transformation of data is based on dataset attributes variance. The first principal component has the largest possible variance seen in the data and each succeeding component has the second, third and N-th highest variance possible under the constraint that orthogonality must be satisfied to the preceding components. This sequence of principal components are order by its order of significance being the first the most important one. By discarding the components of lesser significance, dimensionality reduction is accomplished without the loss of any vital information [82].

PCA is sensitive to feature scaling of the original variables, so feature range values must be taken into account for a correct application of the PCA.

4.3.2 Model Building and Selection

After the data transformation step, the next step is to choose the desired model to use in the classification. There are two general classes of distribution and density models:

- **Parametric Models:** this type of models assumes a particular functional form to separate the data. Parametric models are simple, easier to implement and interpretate since makes some assumptions about the data. Parametric classifier is based on the statistical probability distribution of each class [83]. Although this type of models are not always advantageous because real data may not obey the assumed functional form [84]. There are many available parametric classifiers such as the the Bayesian, Naive-Bayes, Decision Tree and Support Vector Machine (SVM)[83].

- **Non-Parametric Models:** makes relatively few assumptions about the functional form and are more data-driven, i.e., it adapt the boundary shape that discriminate the classes to the

data being modelled [74, 75, 76, 84, 85]. The most commonly used non parametric classifiers are the k-Nearest Neighbors (k-NN) and the logistic regression. [83].

4.3.2.1 KNN

The k-NN is one of the simplest and trivial used classifiers in the data mining field [65, 86]. The k-NN is a type of instance-based learning algorithm that based its decision regarding the classification of new unlabelled instances by their similarity with each of instances in the training set. For each new observation the k-NN classifier computes a distance metric between the feature vector unlabelled data and (labelled) data in the training set and then the k-th closest objects from the training set are identified, being the assignment of the label based on the predominance of a particular class in that specific neighbourhood [65, 86]. In this non-parametric procedure of the k-NN classification, a new instance is classified by a majority vote of its neighbours, being the predicted label assigned to the most represented class among the k nearest neighbours. The are several used distance metrics as the Mahalanobis, Haming, city block, cosine or the Euclidean distance, being the latter one the most used [65].

The k-NN classifier is one of the most easiest classifier to understand and implement because its process is straightforward and intuitive being only needed a given integer k, training dataset and a distance metric for decision. Despite its simplicity, it comes with several limitations as the optimal choice of the k nearest neighbours, computational costs (computing the distance metrics in large datasets can be expensive) and the required need of storage of the training dataset for the classification procedure of new instances [65, 86].

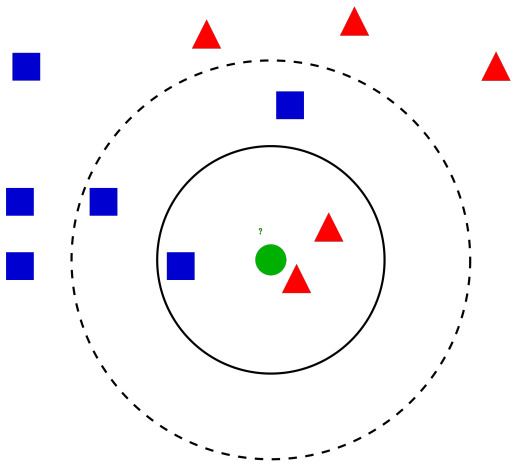

Figure 4.11: Decision-making voting mechanism behind the k-NN classifier. The unlabelled data (green circle) class is going to be set as a red triangle, in the case where k=3 (contiguous circle) and as a blue square in the case where k=5 (dashed circle), respectively. Class decision is defined by the a majority vote of its neighbours class which are defined according to k parameter.

4.3.2.2 SVM

Support vector machines are considered to be a must try method for machine learning purposes because it offers one of the most robust and accurate methods among all well-known algorithms [86]. For instance, in a binomial classification task the SVM goal is to find the best classification function that better separates the members of each class. This separation is obtained via geometrically corresponding to hyperplanes in the feature space which separate the classes. The best function is found by maximizing the margin between the two classes, i.e., by maximizing the distance between the closest data points to the hyperplane and a point of the hyperplane. Once this function is found, new data can be classified by simply testing if it belongs to the positive or negative classes, i.e., if it belongs to one side of the hyperplane or to the other [86].

SVM allows the use of kernel functions (e.g. linear, quadratic, exponential) to defined a variety of non-linear relationships between its inputs. Thus, such approach provides an accurate generalization ability, improving the chances of correctly predicting new unseen data in the future [86].

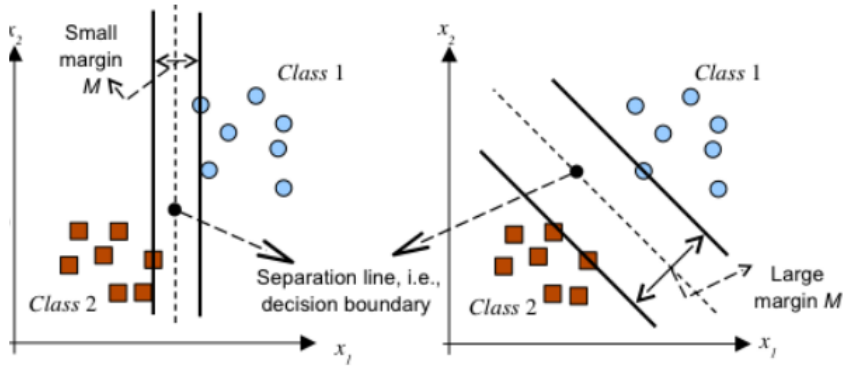

Figure 4.12: SVM hyperplane projection schematics. On the left side image, it is displayed a hyperplane with smaller margin for class separability which was enlarged by optimization of the classification function (by maximizing the distance between the closest data points to the hyperplane and the points of the hyperplane) which displayed on the right side image proving better class separability.

4.3.2.3 Decision Tree

Decision Tree is a widely used and one of the most easy to understand classification algorithms in the data mining field due to its practical and feature-guided nature. The decision tree algorithm uses a tree-like shape model to classify the data by sorting the instances to be classified based on their features values [87, 88]. A decision tree uses a divide and conquer strategy using nodes and leafs to predict the classes of given set of features. Each node represents a dataset feature to be classified and each leaf represents a set of values that the node can assume. The assignment of a given label is achieved by going through the path from the root node to the leaf. The most discriminant feature that best divides the training data is the root node of the tree [87].

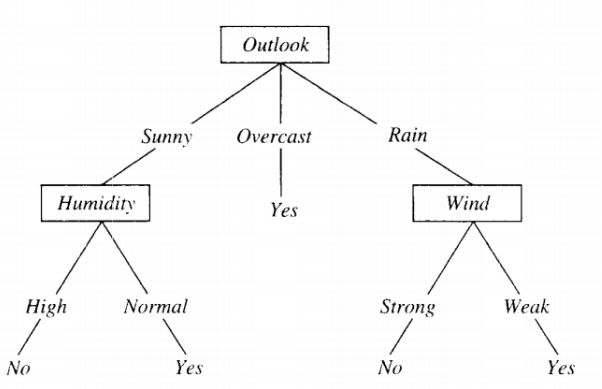

Figure 4.13: A decision tree concept applied to a binomial classification problem of "Play Tennis". This tree classifies a given morning as suitable or not (yes or no) for tennis practising. Classification label is obtained by navigating to the tree to the appropriate leaf node [88].

The in-between path since the root node and the final leaf is constituted by branches that represents the set of features and the possible range of values used to predict the final class label. At each node, a given feature is "tested" and each branch stands for the possible outcome being the final leaf the predicted class label. The decision tree algorithm splits the original set of attributes into subsets that are tested resulting into new branches, i.e., the path, this process is repeated recursively on each derived subset until splitting no longer adds value to the final predictions. There are many stopping criterion being the most used the information gain or the overall accuracy.

4.3.2.4 Model Estimation

In order to choose the best model that fits the data and increase overall prediction accuracy, it is required to train and test that specific model with the available data. The model may be a simple linear equation or complex as a neural network, mapped out by sophisticated software.

There are several methods to accomplish this purposes that basically share the same principle that is to build a model in a subset of data, called the training set, and to test the resulting model in unseen subset of data, called the testing set.

The input dataset may be splitted recurring to most used techniques such as split-validation and cross-validation methods.

In the split-validation technique, the dataset is subdivided into training and testing dataset with predefined weights. The weights of the training and testing dataset can be chosen being majorly used 70% for training and 30% for the testing dataset. The training dataset is used to train the classifier according to the chosen model and the testing dataset is used for performance evaluation of that same model. The division of the input dataset into training and test is done randomly, being possible to repeat the split process k times and then estimate the global accuracy as the averaging of all runs [89, 90].

On the other hand, cross-validation technique revealed to be of more interest since it is identical to the split-validation technique but simultaneously ensure the universality of the data splitting

heuristics [89, 90]. More specifically, the so called k-fold stratified cross validation splits the data into k folds (e.g. 10 folds) with same classes ratio proportion and then uses one fold as the validation set while the remaining nine folds are combined and used as the training set. The validation accuracy is then computed for the mentioned test dataset and afterwards the validation set is changed to the next fold, being the remaining nine folds combined again and used as the training set. This process is repeated for k times, by changing the validation set at each run and then the model global prediction accuracy estimated by the averaged accuracy obtained at each run (see Figure 4.14).

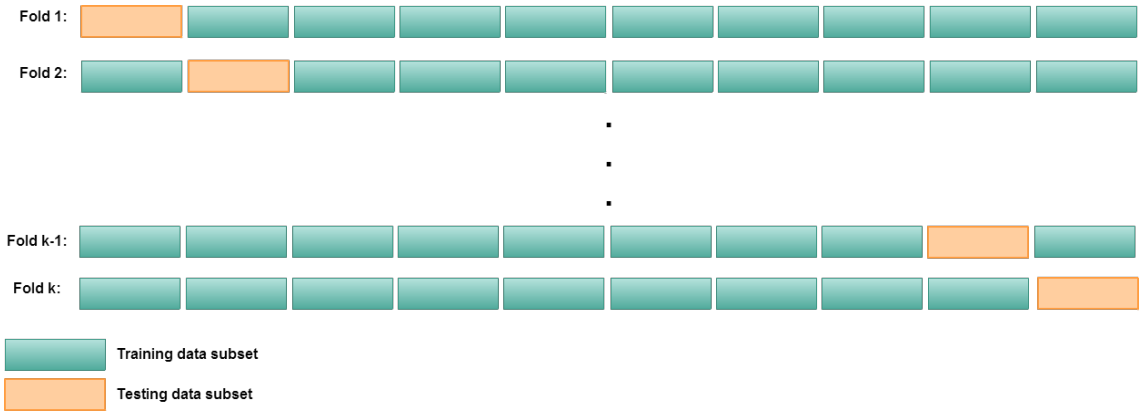

Figure 4.14: k-Fold cross validation schematics.

Generally, classification evaluation is accomplished by measuring the amount of correctly and incorrectly predicted samples for each class, being the result displayed in a so called confusion matrix [91, 92, 93, 94]. The confusion matrix for a binary classification problem (e.g. healthy (positive class) vs pathological (negative class)) is represented in the Table 4.3:

Table 4.3: Confusion matrix structure [91, 92, 93, 94].

		Predicted	
		positive	negative
Ground Truth	positive	*tp*	*fn*
	negative	*fp*	*tn*

The false positives (fp), false negatives (fn), true positives (tp) and true Negatives (tn) are defined as being :

- fp: number of samples predicted as positive, which the true class is negative.
- fn: number of samples predicted as negative, which the true class is positive.
- tp: number of samples predicted as positive, which the true class is also positive.
- tn: number of samples predicted as negative, which the true class is also negative.

The most important performance measure is the accuracy, which evaluate the effectiveness of the classifier by its overall percentage of correct predictions (see Equation 4.28). Additionnaly, some other metrics as recall and precision are used to measure the capability of the classifier to effectively predict the outcome for each class in a binary problem.

Recall, known also as sensitivity is the proportion of samples belonging to the positive class which were correctly predicted as positive (see Equation 4.29). Precision measures the proportional of positive samples that were correctly predicted from the total predicted patterns in a positive class (see Equation 4.30). Specificity can also be measured and is the percentage of negative samples that were correctly predicted as negative (see Equation 4.31).

Finally, a combined measure namely F-measure can also be determined representing the weighted average of the precision and recall (see Equation 4.32).

$$Accuracy = \frac{t_p + t_n}{t_p + f_p + t_n + f_n} \tag{4.28}$$

$$Recall/Sensitivity = \frac{t_p}{t_p + t_n} \tag{4.29}$$

$$Precision = \frac{t_p}{t_p + f_p} \tag{4.30}$$

$$Specificity = \frac{t_n}{t_n + f_p} \tag{4.31}$$

$$F - Measure = \frac{2 * Precision * Recall}{Precision + Recall} \tag{4.32}$$

4.4 State of the art studies

The constant pursuit for an higher degree of classification accuracy and a simultaneously lower generalisation error is the ultimate goal of a generic classification system. Therefore, over the years, several studies have implemented different classification methods in order to obtain the best classifier performance.

Early studies from Krishnan and Rangayyan [95] demonstrated a global classification accuracy of 68.9% using a statistical pattern classifier based on stepwise logistic regression analysis with only 6 time-frequency features; Kim et al. [96] obtained a classification accuracy of 92.3% using the back-propagation neural network (BPNN) with 43 time-frequency extracted features from each signal segment and later on [39], an 91.4% with the same dataset using an improved denoised version of the TFD of the signal. Rangayyan and Wu [52] obtained 0.857 screening efficiency, in terms of the area under the receiver operating characteristics curve (AUC), using statistical-based features and a neural network classifier based on radial basis functions; Wu and Krishnan [97] obtained 80.9% accuracy using statical features derived from the time-frequency wavelet MP decomposition of the signals with a multiple classifier system based on recurrent neu-

ral network. Another work from Rangayyan and Wu [98] demonstrated a global classification accuracy of 77.53% using PDF-derived statistical features using a neural network classifier with radial basis functions; Son et al [53], showed an accuracy of 91.4% using TFD extracted features and the BPNN classifier; Filip Leszko [55] obtained a considerable high accuracy of 96.1% in its study using several different statistical and frequency-based features with a Bayesian minimum-error-rate classifier; in another study, Wu et al [99] showed an overall accuracy of 0.8230 in terms of AUC using statistical features from the signals with a multiple classifier system group of component least squares support vector machine classifiers with a linear and normalized fusion model.

More recently, Chen et al. [100] demonstrated a screening accuracy of the statistical pattern classifier of 85.3% using time-frequency extracted features; Wu et al. [40] obtained 86.67% accuracy with the maximal posterior probability decision criterion classifier using only two-statistical based features; Lin et al. [35] obtained 81.52% as the total accuracy rate evaluated by statistical analysis and using statistical and Fourier analysis-based features; Yang et al. [101], showed an overall classification accuracy of 88% using the fractal scaling index parameter and the averaged envelope amplitude as features with a Bayesian decision rule classifier; Another work from Lin et al. [65] demonstrated a global accuracy of 80% using only 2 statistical features (FF and VMS) with the k-NN classifier.

In Table 4.4, a more detailed description of the studies done so far are presented.

Author(s)	Sensor	Dataset (Healthy-Pathological)	Features	Classification Method	Classification Evaluation
Krishnan and Rangayyan [95]	ACC	51-39 subs	TF Features	Statistical pattern classifier based on stepwise logistic regression analysis	68.9% Accuracy
Kim et al. [96]	Stethoscope Goniometer	1031-377 ACC segments	TF Features	BPNN	92.3%
Rangayyan et al. [52]	ACC Stethoscope	51-38 subs	Statistical Parameters	Neural Network Classifier Based on radial basis functions	0.82 AUC
Wu et al. [97]	ACC Stethoscope	51-38 subs	Statistical-based features extracted from the TF wavelet MP decomposition method	Multiple Classifier System using the adaptive weighted fusion method	80.9% Accuracy
Kim et al. [39]	Stethoscope Goniometer	1031-377 Acoustic Segments	Enhanced TFD Features	BPNN	91.4% Accuracy
Rangayyan et al. [98]	ACC Stethoscope	51-38 subs	PDF-derived statistical features	Neural Network Classifier Based on radial basis functions	77.53% Accuracy
Song et al. [53]	Stethoscope Goniometer	21-11 subs	TF features	BPNN	91.4% Accuracy
Filip Leszko [55]	ACC	23-52 subs	Signal's Frequency-based Features	Bayesian Minimum Error Classifier	96.1% Accuracy
Wu et al. [99]	ACC	51-38 subs	Statistical-based Features	Multiple Classifier System	0.823 AUC
Chen et al. (2013) [100]	ACC	12-23 subs	TF Features	Statistical Pattern Classifier	85.3% Accuracy
Wu et al. [40]	ACC Stethoscope	47-28 subs	Statistical-based Features (VMS and FF)	Maximum Posterior Probability Decision Criterion	86.67% Accuracy
Lin et al. [35]	ACC Goniometer	85-59 subs	Statistical and Fourier analysis features	Statistical Analysis	81.52% Accuracy
Yang et al. [101]	ACC Goniometer	47-28 subs	Fractal scaling index and averaged envelope amplitude parameter	Bayesian Decision Rule	88% Accuracy
Liu et al. [65]	ACC Goniometer	47-28 subs	Statistical-based Features (FF and VMS)	k-NN	80% Accuracy

Table 4.4: Comparison of several different knee joint vibrational based classification results reported in the literature. ACC - accelerometer; TF - Time Frequency; TFD - Time Frequency Distribution; PDF - Probability Density Function; AUC - Area Under the Curve

Chapter 5

Vibroartrhographic Analysis

This chapter describes the used methodology and achieved results that were obtained during the course of this study to meet the final goal of creating a knee joint vibration-based classification system. Signal processing and machine learning techniques were implemented for an accurate analysis and are described in detail during this chapter.

5.1 Data Acquisition

5.1.1 Accelerometer Sensor

The Fraunhofer (FhP) Pandlets sensor was used in this study. The FhP sensor contains a Bluetooth 4.0 interface, a 16 Mhz ARM M0+ processing unit, inertial (IMU) and environmental (EMU) measurement units. The IMU unit is composed of three inertial sensors: an accelerometer, a gyroscope and a magnetometer. Only the accelerometer unit was used during the course of this study for signal's collection. The 3 axis accelerometer has 16 bits resolution, 4 kHz sampling rate and a dynamic range of 2 to 16 g. Specifically, for this study, the FhP sensor was predefined to record at 500 Hz sampling rate being the data stored in a secure digital (Sd) card. Due to hardware and firmware limitation, the maximum available sampling rate for acceleration recordings was set to 500 Hz which may be enhanced in a near future.

5.1.2 Knee Flexion/Extension Protocol

Each subject was requested to sit either on a rigid table or on the doctor's examination table (if applicable) in a relaxed position, with their back straight up and both feet suspended in the air (without contacting the ground at all times). The accelerometer sensor was placed in the medial compartment of the knee slightly below the midline of the patella (medial condyle on the patella) recurring to double-sided tape. Thereafter, an elastic knee brace was used to fix and assure that the sensor would not move during the whole experiment. Each subject was asked to perform a leg swing movement that consisted in swinging the leg over an approximate angle range of 90^{o} starting with the knee bended (at 90^{o}), going to full extension (0^{o}) and backwards with an approximately

period of the 4 seconds per cycle. Each trial consisted in performing 4 cycles of the mentioned movement.

5.1.3 Dataset

In the present study a dataset was collected with 19 healthy volunteers (46.6 ± 13.1 years old) that underwent medical physical examination and evidentiating no sign of having any knee joint problems and 20 arthritic volunteers (62.5 ± 9.1 years old) that have medical history based on physical examination and medical x-ray. All signals were collected in hospital environment recurring to knee flexion/extension protocol under doctors supervision and using FhP Pandlets Sensor. Any additional information provided by the doctor's was kept for further subject characterization. The collected dataset resulted in a total of 30 arthritic signals and 24 healthy signals, acquired from both knees (when applicable).

5.2 System Implementation

In order to create and implement a classification system for the assessment of the knee joint status, an algorithm based on the vibration analysis and machine learning techniques was developed and applied to the signals. An overview of the pipeline of the algorithm is provided in the Figure 5.1

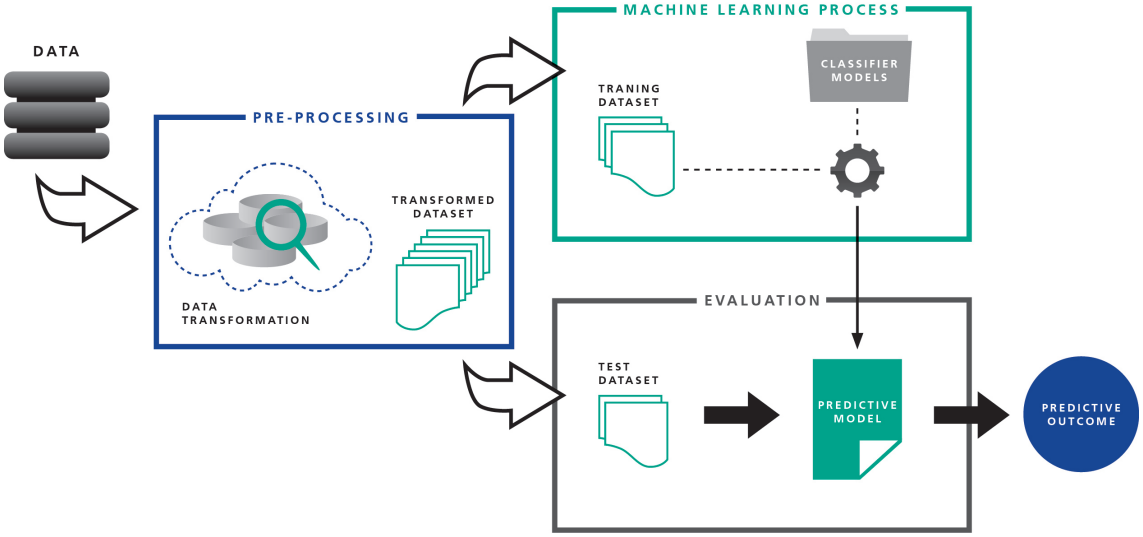

Figure 5.1: Classification system pipeline.

5.2.1 Signal's Acquisition

For each trial, the three acelerations components, under the form of x, y and z axis signals, were collected for all time instants. Additionally, the magnitude signal which is a combination of the

three components of the acceleration signal was computed according to the Equation 5.1:

$$Mag(t) = \sqrt{x(t)^2 + y(t)^2 + z(t)^2} \tag{5.1}$$

where the $Mag(t)$ is the resulting magnitude signal and the $x(t)$, $y(t)$ and $z(t)$ are each one of the recorded acceleration from the x, y and z axis, respectively.

5.2.2 Pre-processing

VAG signal pre-processing plays a major role for the achievement of an accurate and reliable analysis. Therefore several pre-processing steps were applied to the original (raw) VAG signals. Techniques such as amplitude range normalization and digital filtering (fixed and adaptive) were applied to the signals.

5.2.2.1 Normalization

In order to increase algorithm robustness by taking into account the observed differences in terms of the signal's amplitude values range across subjects and trials, an amplitude normalization method was applied to all the available signals. Each signal's amplitude was normalized in order to have a new range of amplitude values bounded to the interval [-1, 1]. This amplitude range normalization method is based on the minimum and maximum amplitude values of each signal, being each sample normalized according to the Equation 4.1. An illustrative example of this procedure is displayed in the Figure 5.2.

As we can see in the Figure 5.2, the minimum-maximum amplitude based normalization was successfully apply to the accelerations signals by bounding their original amplitudes values to the interval [-1,1]. This technique was able to keep the shape of the waveform (acceleration signal's shape) and to re-scale the amplitude values to a new predefined interval. This pre-processing step is vital for inter-subjects comparisons since the recorded accelerations values may vary in terms of scale from subject to subject and from trial to trial.

5.2.2.2 High-Pass Filtering

In order to eliminate the unwanted signal's components as movement, gravitational and muscular components that mask the wanted components from the VAG signals, a high pass filter was applied.

The applied high pass filter was a 9th order Butterworth filter with a cut off frequency of 20 Hz. The used cut off frequency value was chosen according to the reported literature however different cut off frequencies should be tested in future studies to evaluate the overall system performance. An example of the filtering procedure of each one of the acceleration signals is provided in the Figure 5.3):

By filtering the signals according to the given cut off frequency, the more simpler artifacts arising from movement related issues, gravity or even muscular interference can be removed,

being the "remaining" signal constituted only by specific knee joint vibrations emitted during the knee flexion/extension test which characterizes the knee joint status.

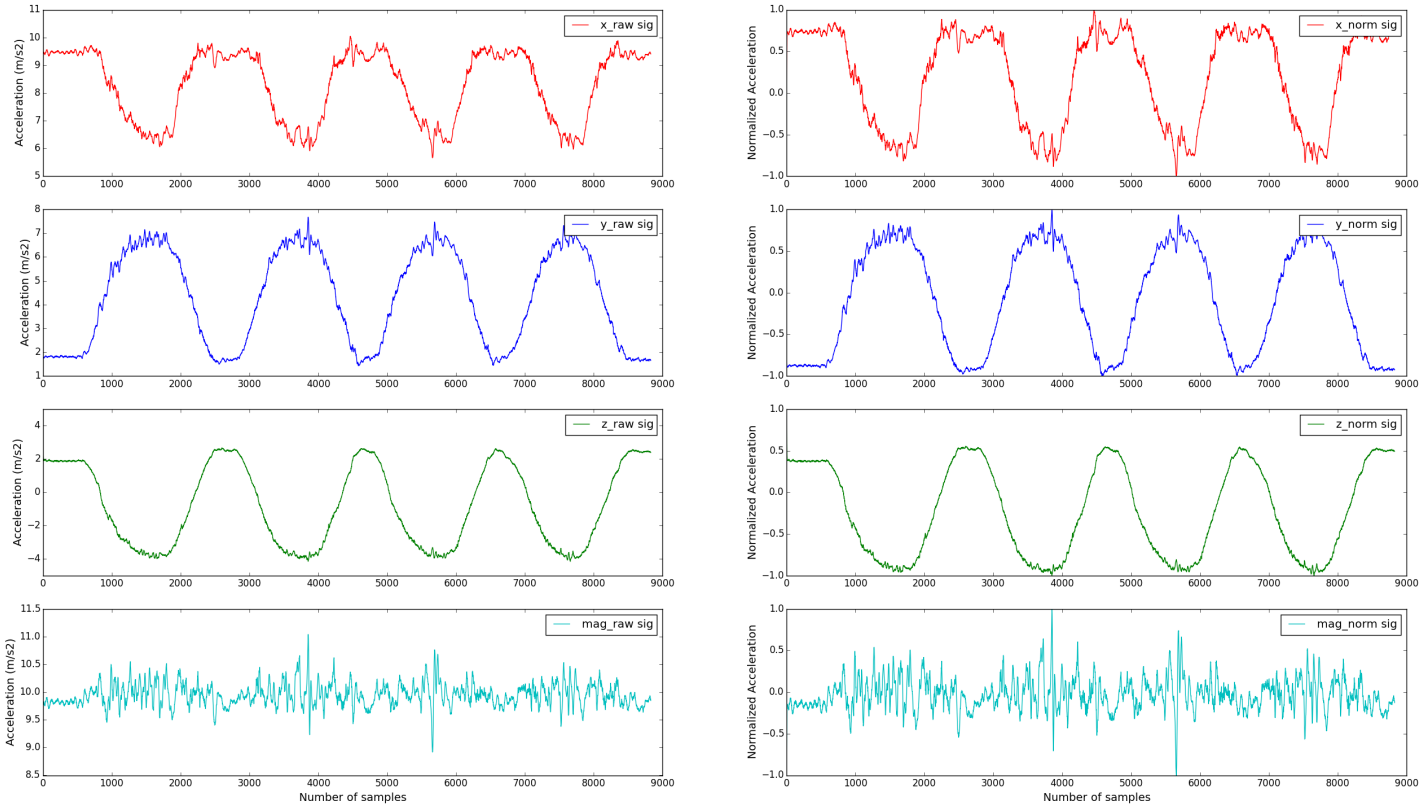

Figure 5.2: Amplitude range normalization illustration of the x, y, z and magnitude accelerations signals.

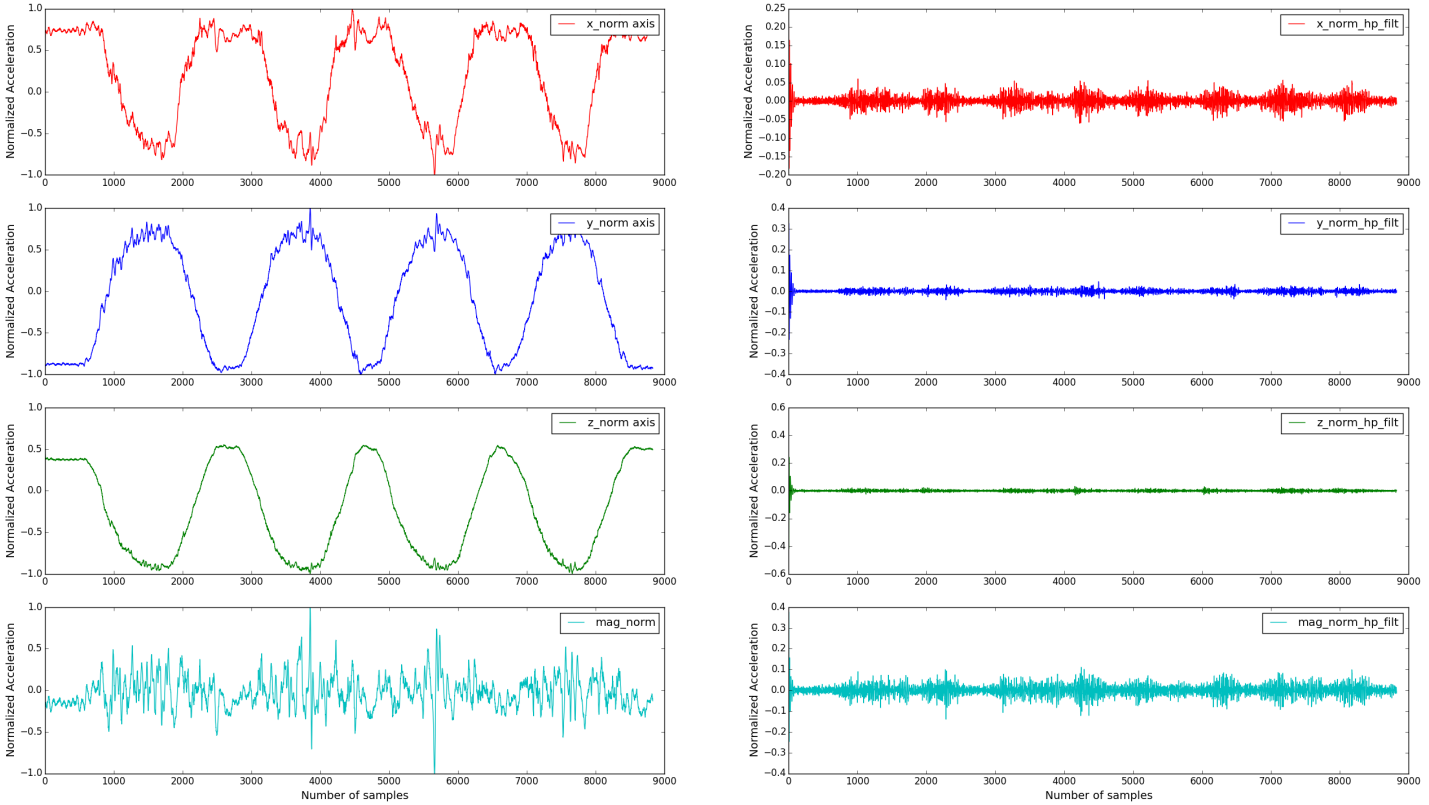

Figure 5.3: Illustrative example of the high-pass filtering process. Raw (left side) and high-pass filtered (right side) acceleration signals of the x, y, z and magnitude.

5.2.2.3 Baseline wandering removal

Baseline wandering estimation and subsequently removal from the VAG signal was accomplished via adaptive filtering, more specifically, by using the CMA filter algorithm. A more detailed description of this technique was provided in the Chapter 4. An illustration of the application of such filter is provided below:

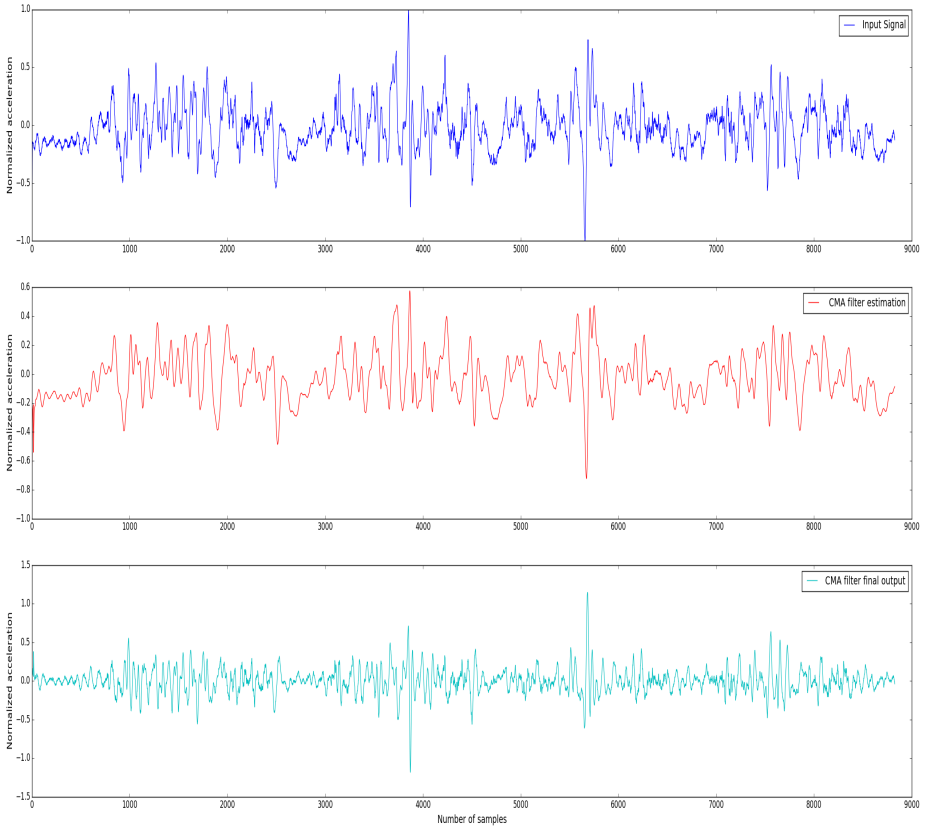

Figure 5.4: Illustrative example of the cascade moving average filter. For input signal (blue line), the algorithm estimates the mean component (red line) being the bottom signal (cyan line) the final filter output given by cascade moving average filter.

As it can be seen in the Figure 5.4, the cascade moving average filter was able to estimate and remove the mean component of the signals for all time instants recurring to the application of a hierarchical structure consisting in two successive moving average operators resulting in a baseline wandered free version of the input signal. The latter one is more interesting for this kind of analysis purposes since it focuses more on the signal's changes regarding to the mean and thus provides a more reliable source for feature extraction.

5.2.3 Segmentation

In order to select the most meaningful and desired segments of the VAG signals a segmentation approach was applied to all the available signals. The VAG signals were segmented according to the angular data into segments corresponding only to a specific phase of the knee flexion/extension movement, i.e., the middle phase of the movement.

Initial and end phase of the leg swing movement are not essential for the analysis not only because the femur is not in fully contact with the tibia in those moments as for the inherent noise that is present in those parts due to the test's characteristics (self initiation and stoping of the movement induced a lot of noise into the signals). Having this in mind, only the VAG signals correspondent to middle phase movement was kept for further analysis.

The selection of those specific segments was obtained by keeping only the corresponding accelerometer time series values where the calculated angle for those same instants belonged to a predefined range of values. The latter interval was defined as being 2/4 of the total angular displacement obtained during one leg swing corresponding to the mentioned middle phase of the movement.

The angles during the leg swing movement for all time instants were determined by calculating the dot product between two vectors see Equation 5.2).

$$A \cdot B = |A||B|.cos(\theta) \tag{5.2}$$

$$\theta = acos(\frac{A \cdot B}{|A||B|}) \tag{5.3}$$

By definition, the result of the dot product between two vectors (e.g. vector A and B) is a third vector which is perpendicular to both A and B (see Figure 5.5). To find the angle between the two vectors the dot product calculation is performed according to the equation 5.3:

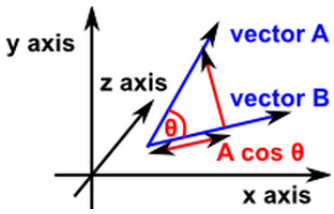

Figure 5.5: Dot product schematics.

A reference frame composed of three vectors was defined as Ref_x, Ref_y and Ref_z (see Figure 5.6). Additionally for each x, y and z acceleration values, a vector with the coordinates (x,y,z) was created and the dot product equation applied to calculate the angle between each one of the reference vectors (Ref_x, Ref_y and Ref_z) and the acceleration-derived vector for all the time instants resulting into 3 different angular signals describing the angle between the sensor and the reference frame at each time instant.

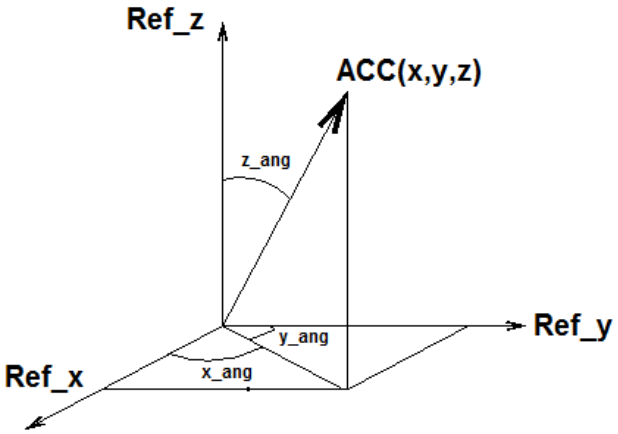

Figure 5.6: Reference frame composed of three directional vectors (Ref_x, Ref_y and Ref_z) and sensor's three dimensional position $ACC_{x,y,z}$ for each time instant. The x_{ang}, x_{ang} and x_{ang} are the resulting angle between the sensor and Ref_x, Ref_y and Ref_z,respectively.

The predefined reference frame consisted into 3 different directional vector as it can be seen below:

- $Ref_x - (1,0,0)$
- $Ref_y - (0,1,0)$
- $Ref_z - (0,0,1)$

The resulting angular signals for all time instants described the angle between the sensor at each time point and each one of the reference vectors. An automatic segmentation algorithm which only selects the segments correspondent to the middle phase of the leg swing movement was developed based on the initial and maximum angles obtained during one leg swing.

The range of angular values was determined by the total angular displacement obtained during the experiment. The angular displacement was calculated by subtracting the initial angle (when the knee is bended - initial position) from the maximum angle obtained in the angular signal (correspondent to the position where the leg is fully extended). Angular displacement measures the range of motion of the leg during each swing. By keeping the accelerations values correspondent to the middle 2/4 of the total angular displacement, an automatic segmentation approach was provided for the segmentation of each trial. With the value of the total angular displacement, two thresholds are created for the segmentation, one for the lower cut off angle and another for the higher cut off angles according to the Equation 5.4 and 5.5 , respectively. A detailed example of the segmentation mechanism is provided below for better understanding:

$$Th\_ang1 = Init\_angle + \frac{2}{4} * \delta_{ang} \tag{5.4}$$

$$Th\_ang2 = Max\_angle - \frac{2}{4} * \delta_{ang} \tag{5.5}$$

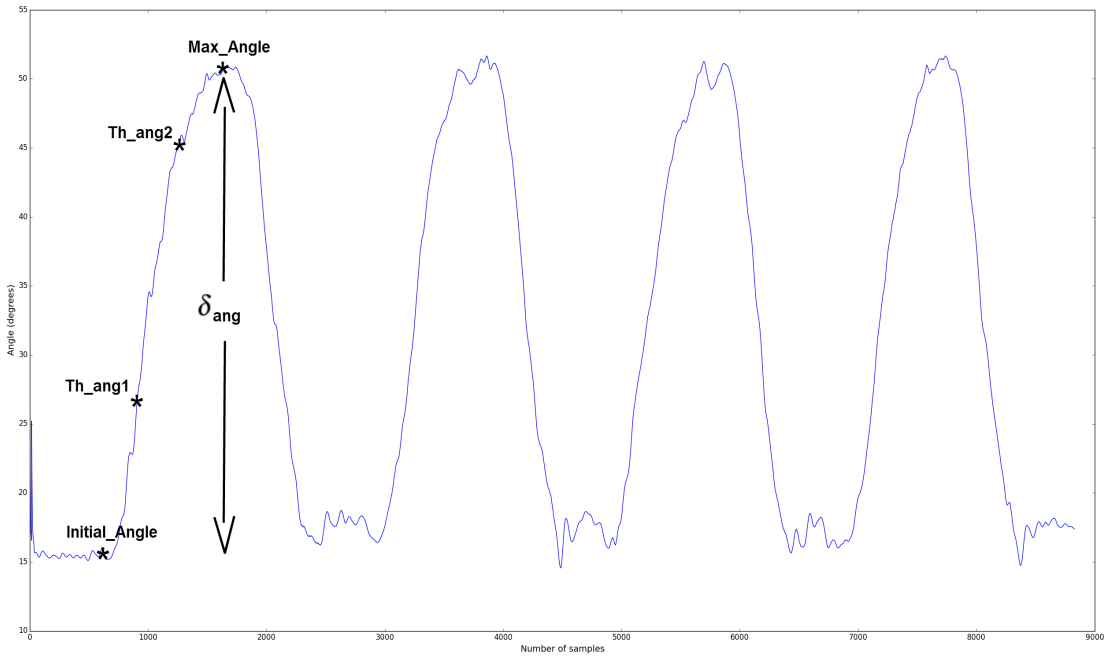

Figure 5.7: Angular segmentation mechanism. Init_ang and Max_ang are the initial and maximum angles obtained in the leg swing movement being the δang the total angular displacement. Th_ang1 and Th_ang2 are the threshold angles for the lower and upper part segmentation, respectively.

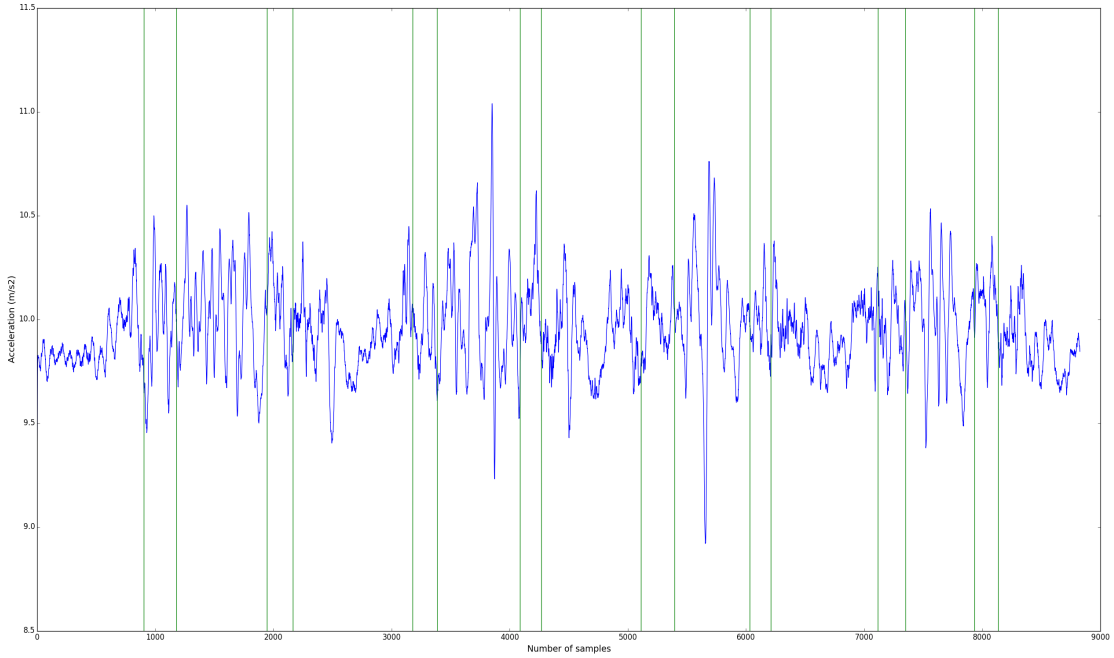

Figure 5.8: Example of the automatic angular segmentation algorithm performed on a magnitude raw signal. Samples within the green rectangles represents the chosen accelerations segments correspondent to the middle phase of the leg swing movement.

The maximum angle is obtained when the leg is fully extended, being this angular value the maximum angle. The angle when the knee is bended (correspondent to the initial position) is the minimum angle. The difference between the maximum and minimum angles is the total angular displacement. Based on this angular displacement the two threshold values are generated for the correspondent segmentation (see Figure 5.8).

5.2.4 Feature Extraction

For the creation of an accurate and reliable classification system the provided extracted feature from the VAG signals needs to be highly discriminant by providing a good and specific characterization of the knee joint status.

In this study, a set of features based on the time and frequency domains were extracted from the VAG. Usually, time domain features are often used to characterize the shape of the raw signals are mostly based in simple mathematical and statistical metrics extracted from each signal in order to extracted its most basic information. Additionally, frequency-domain features are more often related to the discovery of the signal's hidden patterns by identifying and capturing information from repetitive events that occurs through time. The VAG signals are of non-stationary nature, therefore it requires an analysis which simultaneously based on time and frequency domain. In order to pursuit this goal, the wavelet transform, more specifically the wavelet packets transform, was used to perform an accurate time-frequency analysis of the VAG signals. As mentioned before, due to VAG signals inherent non-stationary and irregularity the wavelets transform approach revealed to be more suitable for this kind of purposes because it would allow not only the extraction of frequency content of the signal but also its localization regarding to time.

5.2.4.1 Signal's Array Creation

The four initial raw signals, namely x, y, z and magnitude signals, were pre-processed with amplitude range normalization. This new set of four signals were defined as the basic signals corresponding to the raw and pure collected signals. Posteriorly for each one of these signals a high pass filter and/or a cascade moving average filter were applied, being able to create several x, y, z and magnitude new versions of the original signals by combining the application of only the high pass filter, or only the cascade moving average filter or both (first the cascade moving average filter and then the high pass filter). Several versions of the four input signals were computed according to the possible combinations of the high pass and cascade moving average filter. An illustrative example of the resulting array of signals is represented in the Figure 5.9.

As it can be seen in the Figure 5.9 the 4 initial normalized signals (the x, y, z and magnitude) were pre-processed in order to obtain 12 other different versions of the same ones by: 1) high pass filtering; 2) applying the cascade moving average filter; 3) both applying the cascade moving average and the high pass filtering to the input normalized signals. These twelve versions of the input signals in addition to the four original normalized signals were used together to form the final signal array for the analysis. This strategy of combining several signals versions into a final array

was used in order to determined which type of signals (normalized, high pass filtered, cma filtered or both cma and high pass filtered signals) provide the most discriminant features, i.e., the optimal separability among classes. Thus, for future studies, only the signals which provide essential and most discriminant features will be used. This will be accomplished by applying feature selection techniques among all available features extracted from each signal version in order to determine which are the most important ones.

Each one of the signals in the final signal array was segmented, as mentioned before, recurring to angular segmentation by keeping only the middle phase of the leg swing movement, i.e., the segments corresponding to the middle ascendant and descendent phases of the leg swing movement. Therefore, feature extraction was applied to these segments in order to extract meaningful and highly discriminant metrics with a wavelet-based time-frequency analysis. For each signal a total of 197 features were extracted from each signal's segment.

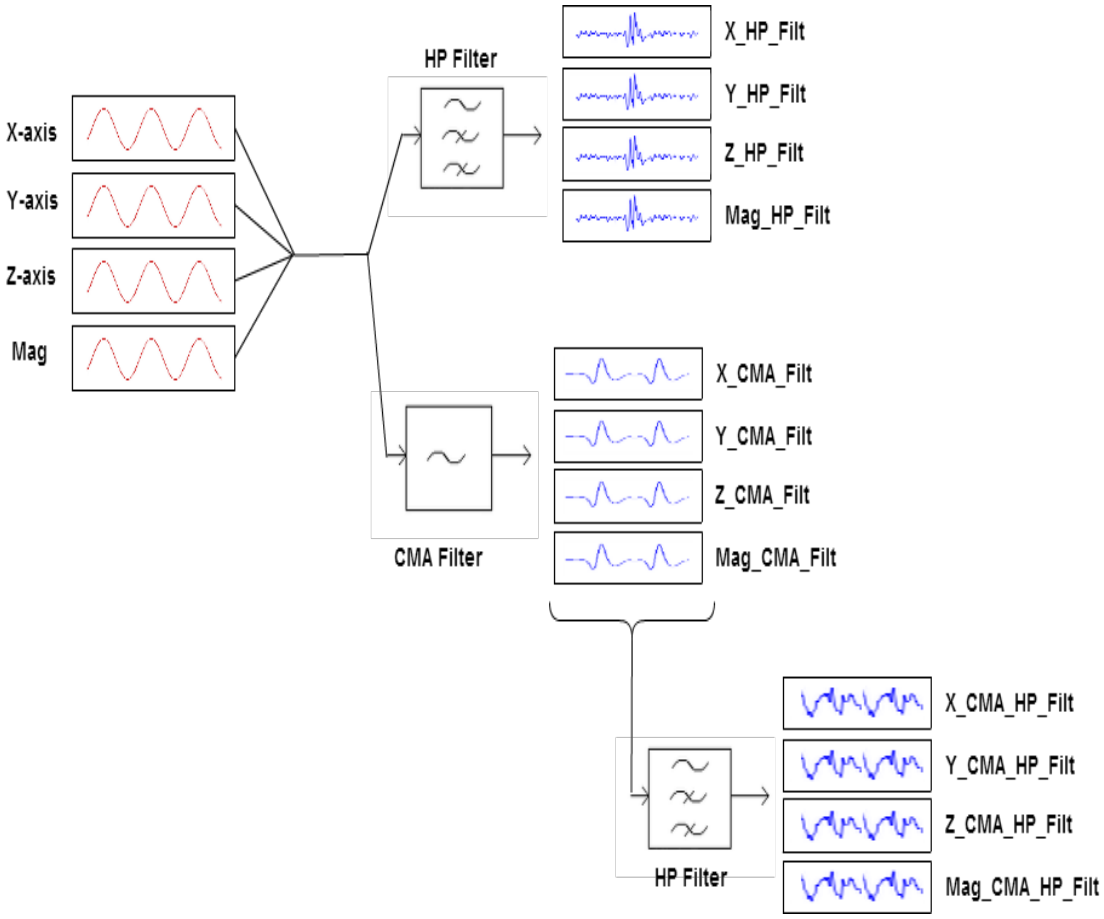

Figure 5.9: Signals array creation schematics. A final signal's array with a total of 16 signals was created for further analysis. The latter one was composed of the x, y, z and magnitude signals derived from the normalization of the raw signals, high pass filtering, cascade moving average filtering and cascade moving average with high pass filtering, respectively.

The extracted features can be divided into 2 major groups: the sample statistics and the time-frequency features. A detailed description of the all extracted features is provided below:

- **Sample Statistics (SS)**
  - **SS_ft1:** Mean - calculates the average of a given set of numbers,i.e., calculates the "central" value of a given set of numbers;
  - **SS_ft2:** Standard deviation - measures the spreadability of a given set of numbers;
  - **SS_ft3:** Variance - is also a measure of spreadability like standard deviation (by definition it is equal to the squared value of standard deviation) given by the average of the squared differences from the mean;
  - **SS_ft4:** Skewness - measures the asymmetry of the probability distribution of a real-valued variable about its mean;
  - **SS_ft5:** Kurtosis - measures the tendency of a probability distribution of a real-valued variable to have peaks. It is considered to be a descriptor of the shape of a probability distribution.
  - **SS_ft6:** Turn Counts - with measures the number of significant "turns" observed in the seen with an adaptive (mean and/or std based threshold) and universal (threshold=0.2) threshold.
- **Time-Frequency (TF) Statistics**
  - **Frequency based features**
    - **TF_ft1:** Mean wavelet coefficient power of each frequency band distribution over the entire time - it measures the mean wavelet coefficient value obtained during the entire signal's segment length;
    - **TF_ft2:**Standard deviation of wavelet coefficients distribution of each frequency band over the entire time - measures the spreadability of the wavelet coefficients values of a given frequency interval over time;
    - **TF_ft3:** Variance of wavelet coefficients distribution of each frequency band distribution over the entire time - measures the dispersion of the wavelet coefficients values of a given frequency interval over time;
    - **TF_ft4:** Skewness of the wavelet coefficients distribution of each frequency band distribution over the entire time - measures the asymmetry of the wavelet coefficient distribution of a given frequency interval over time;
    - **TF_ft5:** Kurtosis of wavelet coefficients distribution of each frequency band distribution over time - measures the tendency of the wavelet coefficient distribution of a given frequency interval to have peaks over the entire time;
    - **TF_ft6:** Number of significant differences (above a given threshold) observed between successive wavelet coefficients (in terms of absolute value) of each frequency band distribution over the entire time - measures the number of times that

the difference between consecutive wavelet coefficients values, in terms of absolute value, was higher than a certain threshold. Two types of threshold were used: one based on the mean and another based on the standard deviation of that wavelet coefficient difference distribution over time.

– **Instantaneous time-based features**

  * **TF_ft7:** Instantaneous mean wavelet coefficient value - provides the instantaneous mean wavelet coefficient value of all frequency bands at each time slice;
  * **TF_ft8:**Instantaneous standard deviation - measures the instantaneous spreadability of the wavelet coefficients values of all frequency bands at each time slice;
  * **TF_ft9:** Instantaneous variances of frequencies - measures the instantaneous dispersion of the wavelet coefficients values of all frequency bands at each time slice;
  * Instantaneous skewness - measures the instantaneous asymmetry of the wavelet coefficient distribution of all frequency bands at each time slice;
  * **TF_ft10:** Instantaneous kurtosis - measures the instantaneous tendency of the wavelet coefficient distribution of all frequency bands to have peaks at each time slice;
  * **TF_ft11:** Mean frequency band with most power/activity - indicates the frequency band which displayed greater activity during the whole experiment by averaging the frequency band with most power at all time instants;
  * **TF_ft12:** Standard deviation of the band with most power/activity - indicates the amount of frequency changes, in terms of absolute power differences, of the band with the most power across the entire time, i.e., measures if the power is concentrated always in the same frequency band or if it changes drastically from one frequency band to another as time elapses;
  * **TF_ft13:** Energy parameter - mean of the signal along each time slice representing energy variation with time;
  * **TF_ft14:** Energy spread parameter - measures the spreadability of energy over the frequency range across time;
  * **TF_ft15:** Frequency parameter - instantaneous mean frequency being computed as the first moment of the signal (t,f) along each time slice;
  * **TF_ft16:** Frequency spread parameter - spreadability of frequencies across time;
  * **TF_ft17:** Number of times that the frequency band with most power is greater than a given threshold - counts the number of times that the band with most power is greater than a certain threshold. Three types of threshold were used: one based on the mean distribution of the frequency band with most power obtained for each time instant; another based on the standard deviation of that distribution and finally, another based on the combination of the previous two (mean + standard deviation).

For the time-frequency analysis, it was used the wavelet packets transform with four levels of decomposition and the Daubechies 2 (dB2) wavelet (see Figure 5.12) resulting into a set of sixteen different frequency bands computed for all time instants (see Figure 5.10). All mentioned features were extracted for all segmented signal's corresponding to ascendant and descendent phases of the leg swing movement. For each full leg swing cycle, i.e., for the segment correspondent to the ascendant phase and for the segment correspondent to the descendant phase a total of 394 features were extracted. The latter number of features were extracted for all the available versions of the input signals that are in the final signal's array with a total of 6304 features distributed among the sixteen different signals in the final signal's array.

With the collected dataset, the maximum level used for the wavelet packets decomposition was 4, producing a tree with 16 different frequency bands (see Table 5.1 for detailed description of the frequency interval range). Due to the wavelet packets transform inherent characteristics the maximum tree depth was established to be 4 because the segmented acceleration signals have a limited number of samples (not sufficient for an analysis with 5 or more levels) which impossibilitate the analysis for greater decomposition levels than 4. This constraint does not allow a more detailed analysis of the frequency content of each VAG signal, being only possible to analyze each signal in terms of frequency using 16 equality spaced frequency intervals. This kind of limitation could be surpassed by performing the leg swing movement more slowly or/and by increasing sensor's sampling frequency. Despite this, 16 different frequency bands were found to be sufficient for the development of a relatively accurate analysis.

Table 5.1: Number of frequency bands obtained using 4 levels of decomposition with the correspondent frequency interval range.

Band number	**Frequency interval (Hz)**
Band 1	0 - 15.6
Band 2	15.6 - 31.3
Band 3	31.3 - 46.9
Band 4	46.9 - 62.5
Band 5	62.5 - 78.1
Band 6	78.1 - 93.7
Band 7	93.7 - 109.4
Band 8	109.4 - 125
Band 9	125 - 140.6
Band 10	140.6 - 156.2
Band 11	156.2 - 171.9
Band 12	171.9 - 187.5
Band 13	187.5 - 203.1
Band 14	203.1 - 218.7
Band 15	218.7 - 234.4
Band 16	234.4 - 250

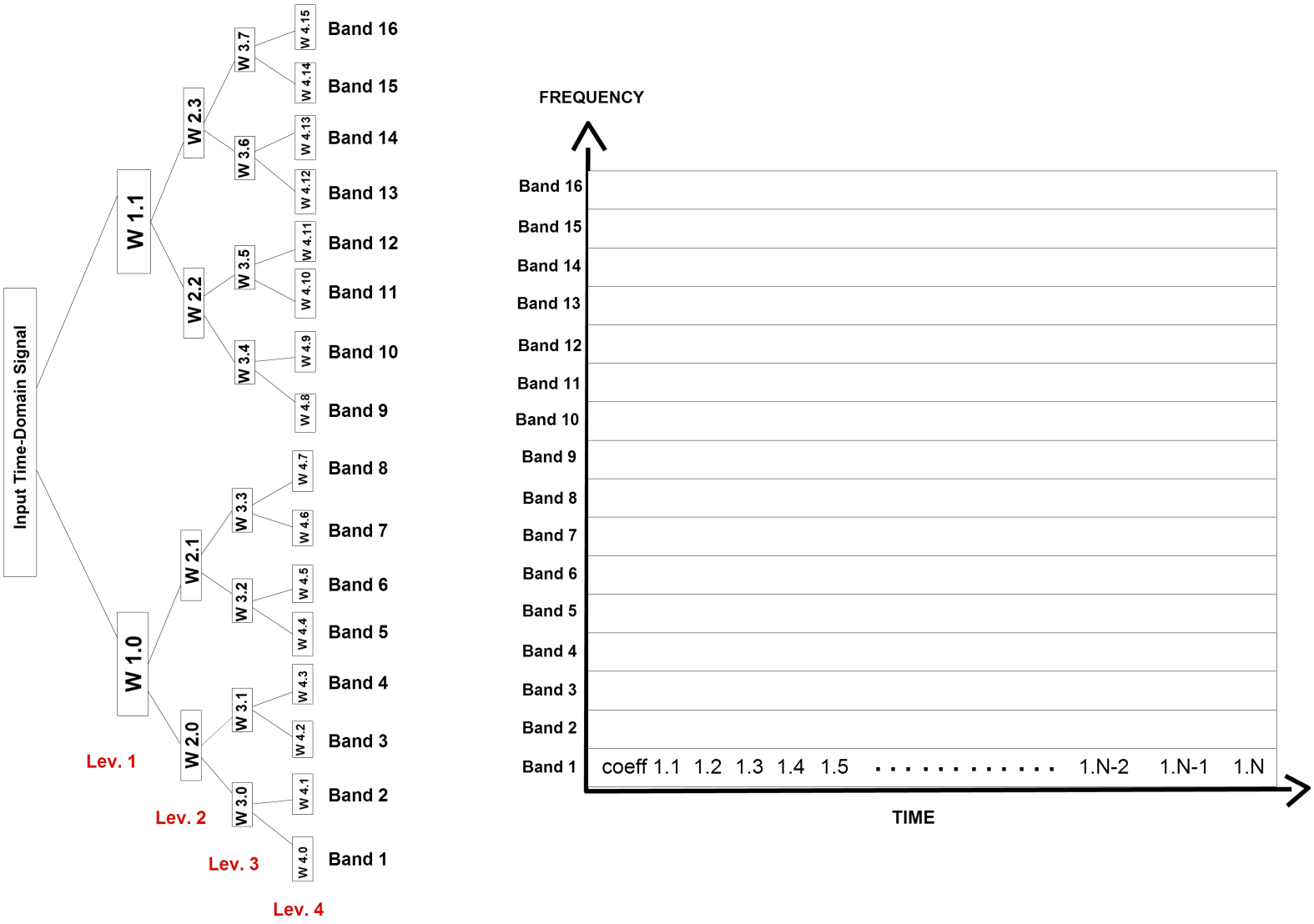

Figure 5.10: 4 Level Wavelet Packets decomposition scheme (left side) and time-frequency representation of the signal (right side) obtained via wavelet coefficients from all the 16 frequency bands. Each frequency band have N coefficient values which characterizes the behaviour of the input the signal at that specific frequency range over the entire time.

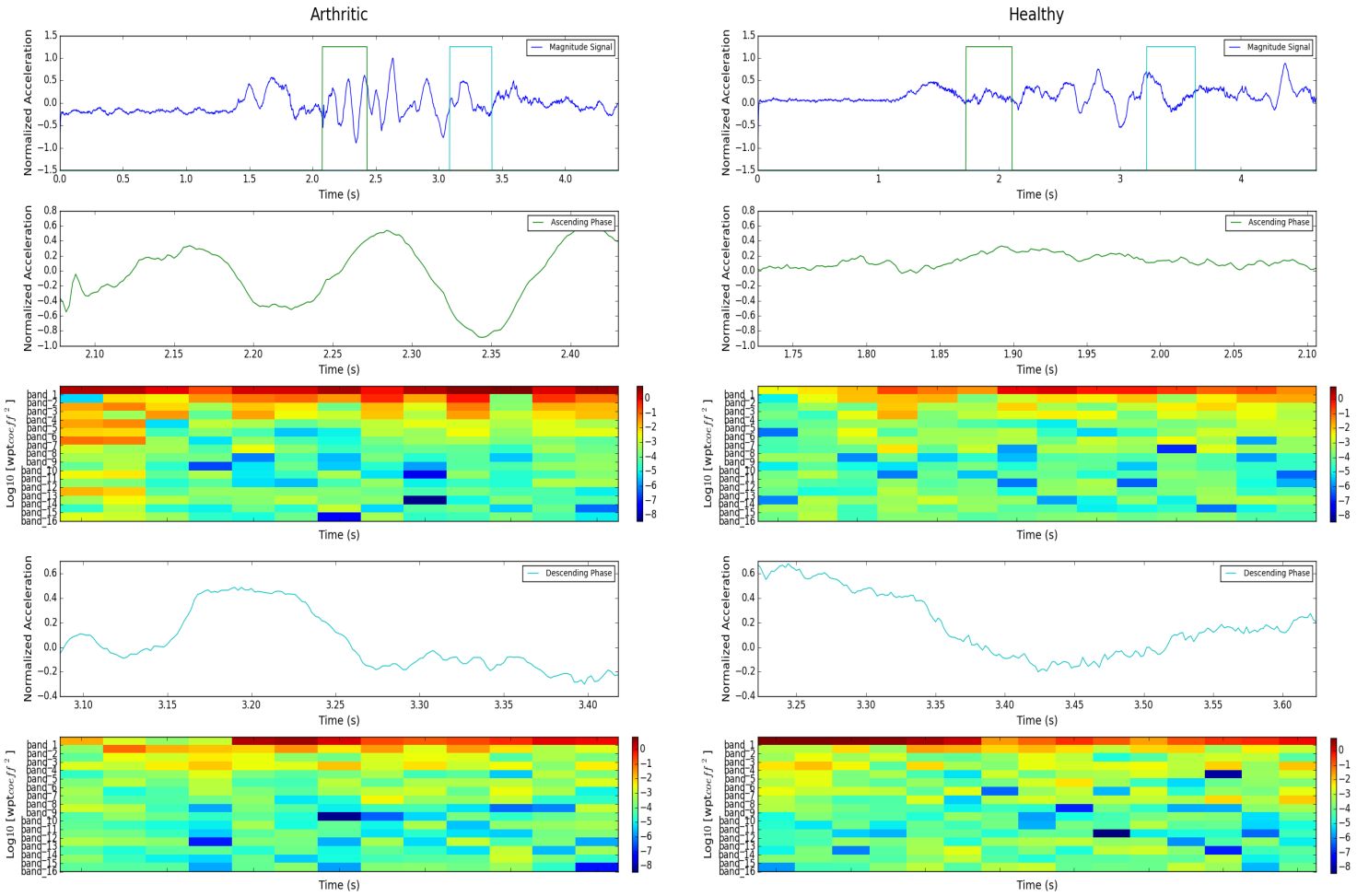

Figure 5.11: Illustrative example of the wavelet-based time-frequency signal analysis for an arthritic (left side) and healthy subject (right side). The raw magnitude signal (blue line), ascending phase (green line) and descending phase (cyan line) of the leg swing movement are represented along with its scalograms. Waveform, amplitude and frequency content changes over time of each signal are quite distinct when comparing arthritic and healthy knee joints signals. Time-frequency extracted features are crucial for an accurate characterization and differentiation between defected and healthy knee joints.

A representative example of the wavelet packet decomposition analysis is provided in the Figure 5.11 where the magnitude raw signal, the ascending and descending movement phases with the correspondent wavelet-based time-frequency analysis from an arthritic and a healthy subject are presented, respectively. As can be seen in the Figure 5.11, signals arising from a healthy and from an arthritic knee are quite distinct when considering the signal's waveform, amplitude and frequency content. Healthy knee joints produce signals with less oscillations and with a reduced amplitude range while arthritic knee joints produce signals that are more irregular over time and with higher fluctuations in terms of amplitude and frequency content. Generally, the ascendant phase of the leg swing movement produces more characteristic and distinct signals when comparing arthritic and healthy subjects, carrying information that is more suitable for classification purposes with higher discriminant power, as reported in several other studies [58]. Moreover, the ascendant and descendent phases signals scalogram are also provided. A scalogram is nothing more that a visual method to display or inspect the wavelet transform where the x, y and z axis represents time, frequency and wavelet coefficient values. The frequency changes over time are displayed by varying the colour or brightness, being clearer that frequency content of the signals changes over time being quite different when comparing healthy and arthritic signals. The already mentioned time-frequency features were extracted from these wavelet-based scalograms.

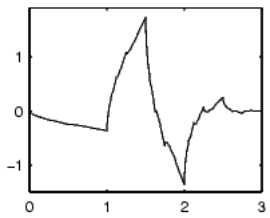

Figure 5.12: dB 2 Wavelet.

Moreover, the dB2 wavelet (see Figure 5.12) was chosen among the all available family of wavelets functions because it was reported in previous studies to be the best type of wavelet for vibroarthrography analysis due its similarity with the VAG signals [66].

5.2.5 Dataset construction

For each trial, four complete leg swing cycles (ascendant and descendant) were collected. Moreover, each trial result into four dataset new instances being each one composed of 6304 features carrying the information from sixteen different accelerations signals. Therefore, the final dataset was composed of 120 pathological and 92 healthy instances, derived from 30 arthritic and 24 healthy collected signals, respectively.

5.3 Feature Selection

In order to reduce the number of features, a dimensionally reduction algorithm was applied to the collected dataset. Correlated and irrelevant features for the analysis may be removed using this kind of approach leaving behind only the most discriminant and highly characteristic features when considering a healthy or an arthritic knee joint. To achieve this purpose, the SFS algorithm and principal component analysis were applied (for detailed description of the SFS and PCA see Chapter 4).

Depending on the model/classifier used for the evaluation of accuracy of the binomial classification of the collected dataset, a different set of features were selected by the SFS method. SFS algorithm with the SVM classifier had selected a set of 5 relevant features while with the k-NN classifier, 6 relevant features were chosen. On the other hand, PCA had selected 11 principal components as the optimum number of principal components for entire dataset characterization which were subsequently evaluated in terms of performance with the SVM, k-NN and Decision Tree classifiers, respectively .

A table with detailed description about how many features were chosen and correspondent classifier evaluation metric is provided is provided below:

- SVM (gamma=0.004334, C=4889, kernel_type=rbf, epsilon=0.001)
  - **TF_ft3_x_norm_raw** - standard deviation of the variance parameter obtained for each time instant from the ascendant phase segment of the x-axis normalized signal;
  - **TF_ft6_y_norm_raw** - number of times that the frequency band number 1 was greater than the mean of that same distribution over the entire time, extracted from the ascendant phase of the y-axis normalized signal;
  - **TF_ft4_y_norm_raw** - skewness of the distribution over time of the frequency band number 14, extracted from the ascendant phase of the y-axis normalized signal;
  - **TF_ft6_x_cma_filt** - Wavelet-based feature - number of times that the frequency band number 16 was greater than the standard deviation of that same distribution over the entire time, extracted from the ascendant phase of the x-axis cascade moving average filtered signal version;

  - **TF_ft4_y_cma_filt** - skewness of the distribution over time of the frequency band number 11, extracted from the ascendant phase of the y-axis cascade moving average filtered signal version;

- k-NN (k=5, distance_metric=Euclidean Distance)

  - **TF_ft1_x_norm_raw** - average value of the frequency band number 1 coefficients over the entire time, extracted from the ascendant phase of the x-axis normalized signal;
  - **TF_ft1_y_norm_raw** - average value of the frequency band number 1 coefficients over the entire time, extracted from the ascendant phase of the y-axis normalized signal;
  - **TF_ft1_z_norm_raw** - average value of the frequency band number 1 coefficients over the entire time, extracted from the ascendant phase of the z-axis normalized signal;
  - **TF_ft6_x_filt_norm** - number of times that the frequency band number 16 was greater than the standard deviation of that same distribution over the entire time, extracted from the ascendant phase of the x-axis high pass filtered signal;
  - **SS_ft6_y_filt_norm** - number of significant "turns" observed in the y-axis high pass filtered signal;
  - **TF_ft6_z_filt_norm** - number of times that the frequency band number 2 was greater than the mean of that same distribution over the entire time, extracted from the ascendant phase of the z-axis high pass filtered signal;

For illustrative purposes of the feature selection step, several different combinations of some of the selected features are displayed in the Figure 5.14 and 5.14 (see also Appendix A). This allows the evaluation for class separability, in a coarse and visual form, of the effect of combining two different features.

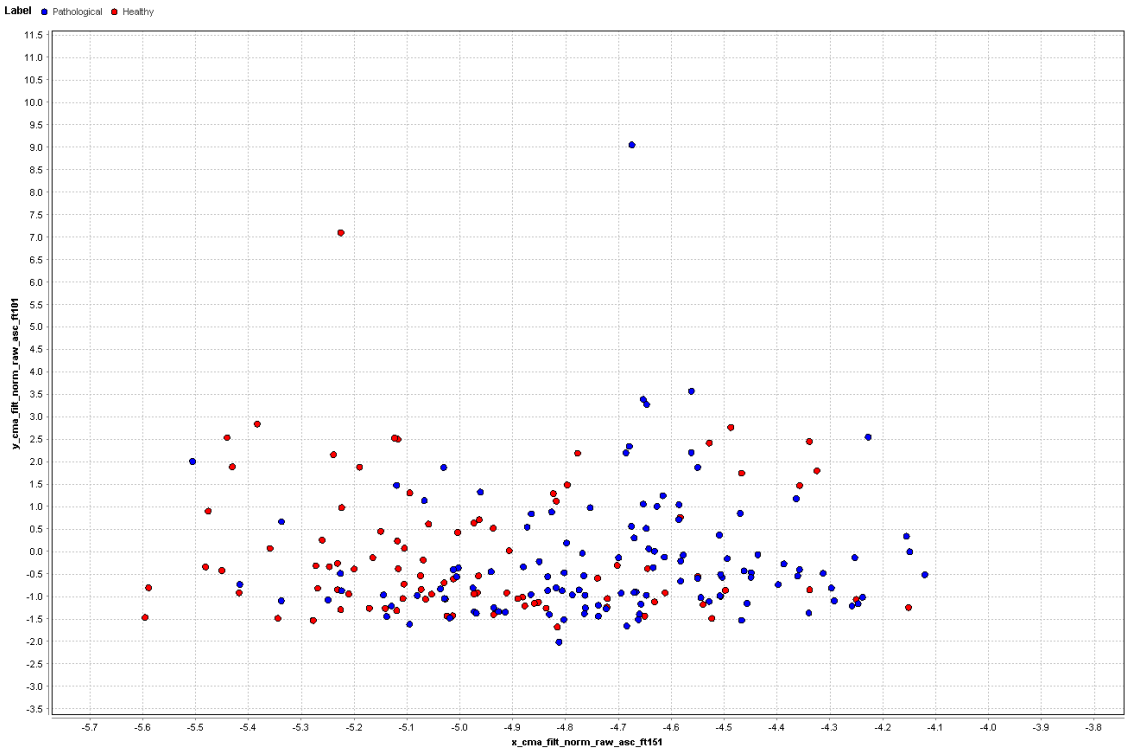

(a)

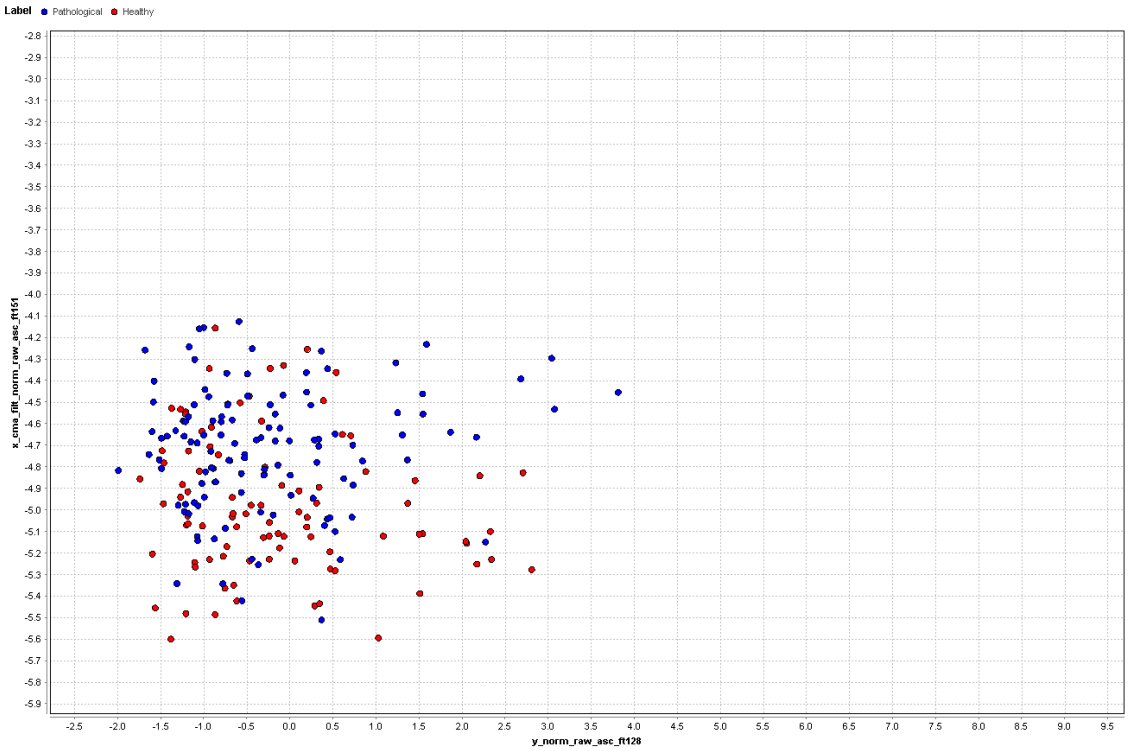

(b)

Figure 5.13: Scatter plot images of the combination two features for inter-class evaluation (blue dots - Pathological; red dots - Healthy). Discriminative power of the selected features with SVM classifier, can be visually inspected for different sets of two features: (a) TF_ft6_x_cma_filt vs TF_ft4_y_cma_filt and (b) TF_ft4_y_norm_raw vs TF_ft4_x_cma_filt.

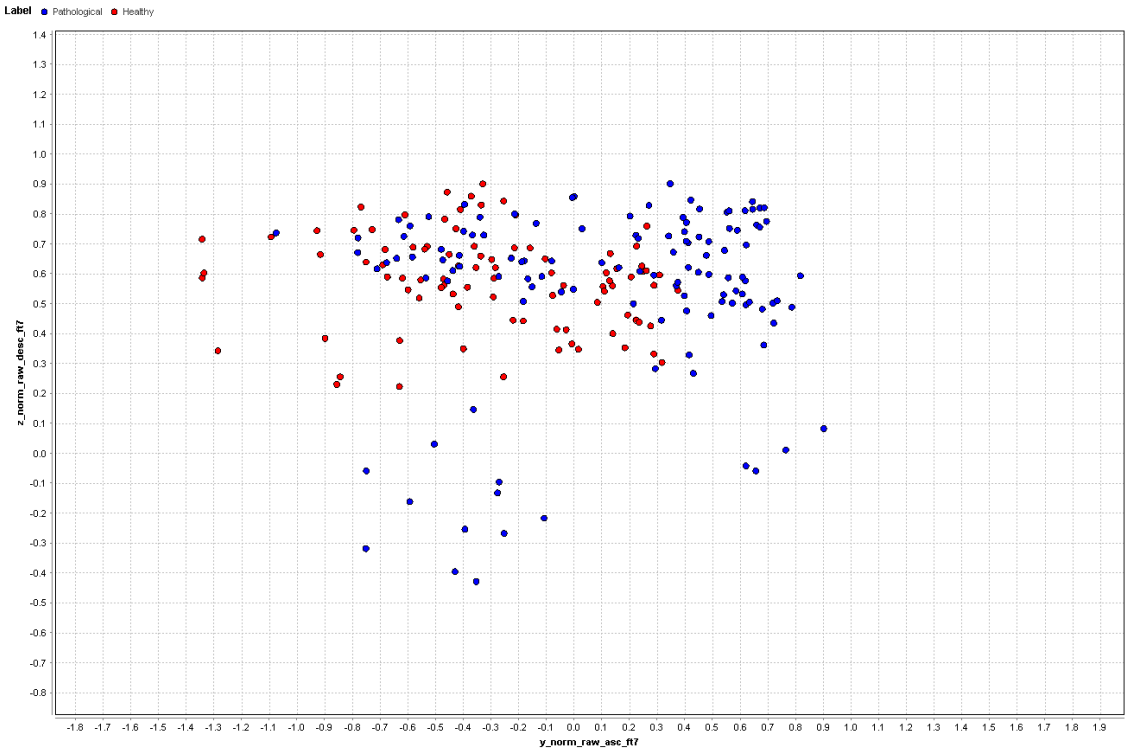

(a)

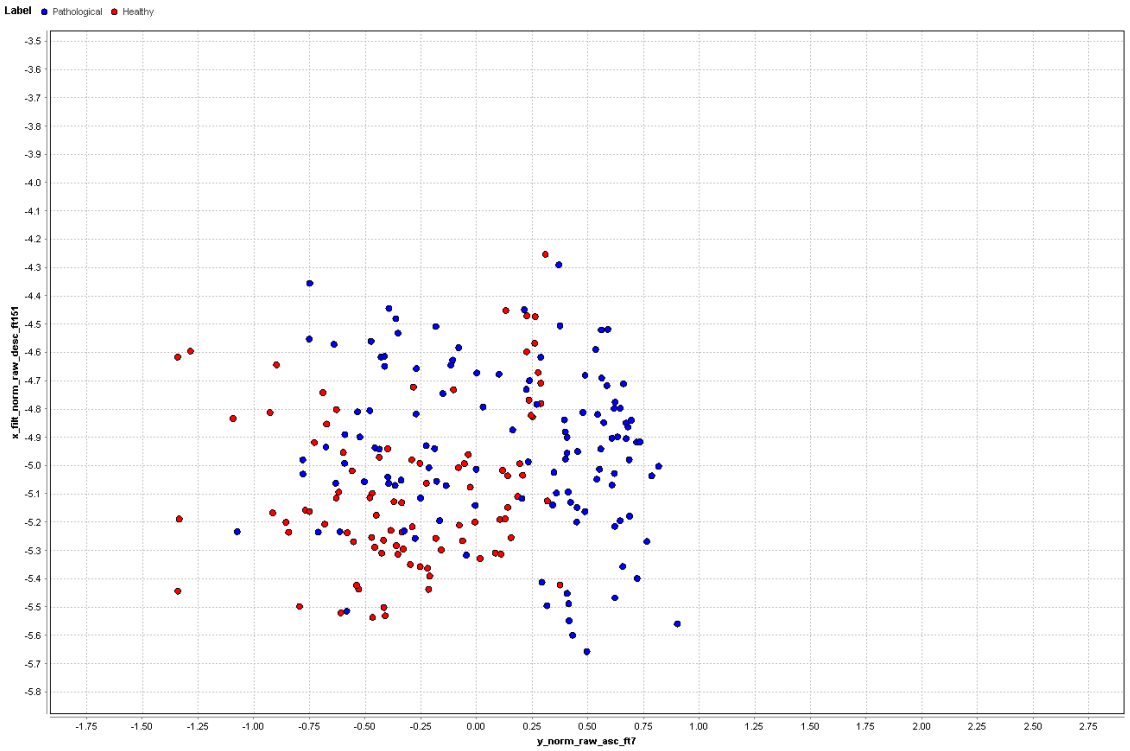

(b)

Figure 5.14: Scatter plot images of the combination two features for inter-class evaluation (blue dots - Pathological; red dots - Healthy). Discriminative power of the selected features with k-NN classifier, can be visually inspected for different sets of two features: (a) TF_ft1_y_norm_raw vs TF_ft1_z_norm_raw and (b) TF_ft1_y_norm_raw vs TF_ft6_x_filt_norm.

5.4 Classification Results

Several classifiers were tested in order to choose the one that most fits to the data. Thus, having this in mind, SVM, k-NN and Decision Tree classifiers were applied to a subset of equally balanced instances (50:50) in terms of healthy/arthritic ratio. The evaluation of each classifier was accomplished using the 10 fold cross validation method with stratified sampling (preserve also the 50:50 healthy/arthritic ratio at each partition/subset) and recurring to the accuracy, recall, precision and F-measure parameters. The average classification results are presented in the Table 5.2.

Table 5.2: Overall classification results for each tested classifier.

Classifier	Feature Selection	Accuracy	Precision	Recall	F-Measure
SVM	none	80.41	80.16	83.89	80.67
SVM	SFS (5 features)	84.3	83.19	86.89	84.54
SVM	PCA (11 pc)	78.45	80.01	80.33	78.76
k-NN 5	none	77.2	78.9	78.22	77.21
k-NN 5	SFS (6 features)	89.77	88.27	92.44	90.13
k-NN 5	PCA (11 pc)	82.66	82.87	85.89	83.26
Decision Tree	none	67.81	69.94	64.22	65.14
Decision Tree	PCA (11 pc)	81.99	82.98	82.67	82.06

As it can be seen in the Table 5.2, all tested classifiers produced relatively good results in terms of classifying a knee joint as healthy or arthritic. In overall, better classification performances were obtained when a feature selection procedure was applied to the dataset, independently of being the SFS technique or PCA, highlighting the need for dimensionality reduction step for removal of meaningless or redundant features.

In terms of classification performance, the k-NN classifier (k=5, 6 selected features) revealed to be best among all tested. The used k-NN algorithm was able to correctly discriminate 89% signals with sensitivity of 92.44% and specificity of 88.27% , which is superior to the global accuracy obtained in the work of [65] of 80% (sensitivity: 71%, specificity: 85%) using the same type of classifier. Previous studies (see Table 4.4) have reported similar or better performances using other types of classifiers being quite difficult to directly compare the results obtained in this study with those studies, not only because the differences in the methodology (signal processing, extracted features and classifier models) but also the differences in the total number of analyzed subjects and/or differences in the type and characteristics of the sensors used in the mentioned studies.

Despite this, the overall classification performance obtained with this dataset, highlights once more, the potentiality of such kind of technique for knee joint assessment. In order to obtain a better classification performance and to overcome several limitations in the data collecting and processing steps, several aspects needed to be improved as:

- Sensor's sampling frequency - a higher sampling rate would allow a more detailed and flexible signal analysis of the VAG signals.
- Angular segmentation - the use of a second sensor (electro-goniometer or a 2nd accelerometer) would allow a better signal segmentation and provide essential information about the leg swing velocity which could be used for leg swing velocity normalization.
- Leg swing velocity - by controlling and defining a constant velocity for all subjects and trials, the variable velocity would no longer influence the analysis.

Chapter 6

Conclusions and Future Work

The development of a vibrational-based classification system for knee joint assessment was successfully obtained during the course of this preliminary study recurring only to the use of a miniature accelerometer during a knee extension/flexion test. This innovative system showed that it may provide the differentiation between a healthy and pathological knee with relatively good accuracy, as reported in several other studies.

Such system could be used as a reliable, accurate, cheap and non-invasive screening diagnostic tool in the clinical practice or even at home for preliminary screening. Additionally, it would provide detailed insight, at cartilage level, about the knee joint status and affected structures that may not be detected with other current diagnostic tool (only gross and symptomatic changes are detected with the current image-based techniques), possibly enabling the early detection of knee joint disorders (e.g. OA).

Moreover, such system may also be used as potential monitoring tool in combination with physiotherapy which would improve the overall rehabilitation process.

Despite the promising results, future work needs to be performed in the data gathering and analysis process to increase the overall robustness of the classification system. As for future work, it is suggested to study the biomechanical properties of the knee joint emitted vibrations under different types of friction and/or loading conditions, increase the sensor's sampling frequency, to use of a second sensor (e.g. electro-goniometer or a second accelerometer), optimize the experimental protocol (differences in the leg swing velocity and knee size must be considered for a better classification) and testing several other different classifier (e.g. neural networks).

Bibliography

[1] Tsair-Fwu Lee, Wei-Chun Lin, Li-Fu Wu, and Hung-Yu Wang. Analysis of Vibroarthrographic Signals for Knee Osteoarthritis Diagnosis. In Shieh, CS and Watada, J and Pan, TS, editor, *2012 SIXTH INTERNATIONAL CONFERENCE ON GENETIC AND EVOLUTIONARY COMPUTING (ICGEC)*, International Conference on Genetic and Evolutionary Computing, pages 223–227. Kaohsiung Univ Appl Sci (KUAS); Waseda Univ; IEEE Comp Soc; IEEE; IEEE Tainan Sect; IEEE Signal Processing Soc, Tainan Chapter; IEEE Computat Intelligence Soc Tainan Chapter; Taiwan Assoc Web Intelligence Consortium; Japan Soc Evolutionary Computat; Int Soc Management Engineers, 2012. 6th International Conference on Genetic and Evolutionary Computing (ICGEC), Kitakyushu, JAPAN, AUG 25-28, 2012.

[2] KS Kim, DY Yoon, SO Lee, JH Seo, and CG Song. Classfication of arthritic pathology using acoustic signal processing. 2005.

[3] Cinnamon L VanPutte, Jennifer Regan, and Andrew Russo. *Seeley's Anatomy & Physiology*. McGraw-Hill, 2014.

[4] K Messner and JZ Gao. The menisci of the knee joint. Anatomical and functional characteristics, and a rationale for clinical treatment. *JOURNAL OF ANATOMY*, 193(2):161–178, AUG 1998.

[5] Erik Schulte and Udo Schumacher. *Thieme atlas of anatomy: Latin nomenclature: general anatomy and musculoskeletal system*. Thieme, 2006.

[6] Keo Sik Kim, Jeong Hwan Seo, and Chul Gyu Song. An acoustical evaluation of knee sound for non-invasive screening and early detection of articular pathology. *Journal of medical systems*, 36(2):715–722, 2012.

[7] Rangaraj M Rangayyan and YF Wu. Screening of knee-joint vibroarthrographic signals using statistical parameters and radial basis functions. *Medical & Biological Engineering & Computing*, 46(3):223–232, 2008.

[8] Peter J Millett, Thomas L Wickiewicz, and Russell F Warren. Motion loss after ligament injuries to the knee part i: Causes. *The American journal of sports medicine*, 29(5):664–675, 2001.

[9] Anthony D Woolf and Bruce Pfleger. Burden of major musculoskeletal conditions. *Bulletin of the World Health Organization*, 81(9):646–656, 2003.

[10] Ewa M Roos. Joint injury causes knee osteoarthritis in young adults. *Current opinion in rheumatology*, 17(2):195–200, 2005.

[11] Gary S Firestein. Evolving concepts of rheumatoid arthritis. *Nature*, 423(6937):356–361, 2003.

[12] Daniel Aletaha, Tuhina Neogi, Alan J Silman, Julia Funovits, David T Felson, Clifton O Bingham, Neal S Birnbaum, Gerd R Burmester, Vivian P Bykerk, Marc D Cohen, et al. 2010 rheumatoid arthritis classification criteria: an american college of rheumatology/european league against rheumatism collaborative initiative. *Arthritis & Rheumatism*, 62(9):2569–2581, 2010.

[13] Celebrex - Understanding Arthritis.

[14] David T Felson, Reva C Lawrence, Paul A Dieppe, Rosemarie Hirsch, Charles G Helmick, Joanne M Jordan, Raynard S Kington, Nancy E Lane, Michael C Nevitt, Yuqing Zhang, et al. Osteoarthritis: new insights. part 1: the disease and its risk factors. *Annals of internal medicine*, 133(8):635–646, 2000.

[15] David T Felson and Yuqing Zhang. An update on the epidemiology of knee and hip osteoarthritis with a view to prevention. *Arthritis & Rheumatism*, 41(8):1343–1355, 1998.

[16] F Berenbaum. Osteoarthritis as an inflammatory disease (osteoarthritis is not osteoarthrosis!). *Osteoarthritis and Cartilage*, 21(1):16–21, 2013.

[17] Richard F Loeser, Steven R Goldring, Carla R Scanzello, and Mary B Goldring. Osteoarthritis: a disease of the joint as an organ. *Arthritis & Rheumatism*, 64(6):1697–1707, 2012.

[18] Dieuwke Schiphof, Marienke van Middelkoop, BM De Klerk, EHG Oei, Albert Hofman, BW Koes, Harrie Weinans, and SMA Bierma-Zeinstra. Crepitus is a first indication of patellofemoral osteoarthritis (and not of tibiofemoral osteoarthritis). *Osteoarthritis and Cartilage*, 22(5):631–638, 2014.

[19] Johannes WJ Bijlsma, Francis Berenbaum, and Floris PJG Lafeber. Osteoarthritis: an update with relevance for clinical practice. *The Lancet*, 377(9783):2115–2126, 2011.

[20] Frank W Roemer, Felix Eckstein, Daichi Hayashi, and Ali Guermazi. The role of imaging in osteoarthritis. *Best Practice & Research Clinical Rheumatology*, 28(1):31–60, 2014.

[21] Ali Guermazi, Daichi Hayashi, Frank W. Roemer, and David T. Felson. Osteoarthritis: A review of strengths and weaknesses of different imaging options. *Rheumatic Disease Clinics of North America*, 39(3):567 – 591, 2013. The Use of Imaging in Inflammatory Joint and Vascular Disorders.

[22] European Society of Radiology - Synovial chondromatosis: a pictorial review (Poster).

[23] P Mandl, M Brossard, P Aegerter, M Backhaus, GA Bruyn, I Chary-Valckenaere, A Iagnocco, E Filippucci, J Freeston, F Gandjbakhch, et al. Ultrasound evaluation of fluid in knee recesses at varying degrees of flexion. *Arthritis care & research*, 64(5):773–779, 2012.

[24] F.W. Roemer and A. Guermazi. Osteoarthritis year in review 2014: imaging. *Osteoarthritis and Cartilage*, 22(12):2003 – 2012, 2014.

[25] Ruth Crawford, Gayle Walley, Stephen Bridgman, and Nicola Maffulli. Magnetic resonance imaging versus arthroscopy in the diagnosis of knee pathology, concentrating on meniscal lesions and acl tears: a systematic review. *British medical bulletin*, 84(1):5–23, 2007.

[26] Stuart Brooks and Mamdouh Morgan. Accuracy of clinical diagnosis in knee arthroscopy. *Annals of the Royal College of Surgeons of England*, 84(4):265, 2002.

[27] V Goëb, CA Walsh, RJ Reece, P Emery, and F Ponchel. Potential role of arthroscopy in the management of inflammatory arthritis. *Clinical and experimental rheumatology*, 30(3):429–435, 2011.

[28] UW Medicine - Orthopaedics and Sports Medicine.

[29] Pagamas Piriyaprasarth and Meg E Morris. Psychometric properties of measurement tools for quantifying knee joint position and movement: a systematic review. *The Knee*, 14(1):2–8, 2007.

[30] D Bączkowicz and K Kręcisz. Vibroarthrography in the evaluation of musculoskeletal system-a pilot study. *Ortopedia, traumatologia, rehabilitacja*, 15(5):407–416, 2013.

[31] Hassan M Bassiouni. *Phonoarthrography: A New Technique for Recording Joint Sounds*. INTECH Open Access Publisher, 2012.

[32] MD Crema, A Guermazi, EC Sayre, FW Roemer, H Wong, A Thorne, J Singer, JM Esdaile, MD Marra, JA Kopec, et al. The association of magnetic resonance imaging (mri)-detected structural pathology of the knee with crepitus in a population-based cohort with knee pain: the modeko study. *Osteoarthritis and Cartilage*, 19(12):1429–1432, 2011.

[33] Jolanda Cibere, Nicholas Bellamy, Anona Thorne, John M Esdaile, Kelly J McGorm, Andrew Chalmers, Simon Huang, Paul Peloso, Kam Shojania, Joel Singer, et al. Reliability of the knee examination in osteoarthritis: effect of standardization. *Arthritis & Rheumatism*, 50(2):458–468, 2004.

[34] Tsair-Fwu Lee, Wei-Chun Lin, Li-Fu Wu, and Hung-Yu Wang. Analysis of vibroarthrographic signals for knee osteoarthritis diagnosis. In *Proceedings of the 2012 Sixth International Conference on Genetic and Evolutionary Computing*, pages 223–228. IEEE Computer Society, 2012.

[35] Wei-Chun Lin, Tsair-Fwu Lee, Shu-Yuan Lin, Li-Fu Wu, Hung-Yu Wang, Liyun Chang, Jia-Ming Wu, Jing-Chuan Jiang, Chiu-Ching Tuan, Mong-Fong Horng, et al. Non-invasive knee osteoarthritis diagnosis via vibroarthrographic signal analysis. *Journal of Information Hiding and Multimedia Signal Processing*, 5(3):497–507, 2014.

[36] Noriyuki Tanaka and Minoru Hoshiyama. Vibroarthrography in patients with knee arthropathy. *Journal of back and musculoskeletal rehabilitation*, 25(2):117–122, 2012.

[37] L-K Shark, H Chen, and John Goodacre. Knee acoustic emission: a potential biomarker for quantitative assessment of joint ageing and degeneration. *Medical engineering & physics*, 33(5):534–545, 2011.

[38] Hassan M Bassiouni, Mamoun El-Deeb, Nasser Kenawy, Ehab Abdul-Azim, and Mamdouh Khairy. Phonoarthrography, musculoskeletal ultrasonography, and biochemical biomarkers for the evaluation of knee cartilage in osteoarthritis. *Modern rheumatology*, 21(5):500–508, 2011.

[39] Keo Sik Kim, Jeong Hwan Seo, Jin U Kang, and Chul Gyu Song. An enhanced algorithm for knee joint sound classification using feature extraction based on time-frequency analysis. *Computer methods and programs in biomedicine*, 94(2):198–206, 2009.

[40] Yunfeng Wu, Suxian Cai, Shanshan Yang, Fang Zheng, and Ning Xiang. Classification of knee joint vibration signals using bivariate feature distribution estimation and maximal posterior probability decision criterion. *Entropy*, 15(4):1375–1387, 2013.

[41] Narender P Reddy, Bruce M Rothschild, Eon Verrall, and Anand Joshi. Noninvasive measurement of acceleration at the knee joint in patients with rheumatoid arthritis and spondyloarthropathy of the knee. *Annals of biomedical engineering*, 29(12):1106–1111, 2001.

[42] RM Rangayyan, CB Frank, GD Bell, and R Smith. Analysis of knee joint sound signals. In *Engineering in Medicine and Biology Society, 1988. Proceedings of the Annual International Conference of the IEEE*, pages 712–713. IEEE, 1988.

[43] Wai Yin Wong, Man Sang Wong, and Kam Ho Lo. Clinical applications of sensors for human posture and movement analysis: a review. *Prosthetics and orthotics international*, 31(1):62–75, 2007.

[44] Jing Song, Pamela Semanik, Leena Sharma, Rowland W Chang, Marc C Hochberg, W Jerry Mysiw, Joan M Bathon, Charles B Eaton, Rebecca Jackson, C Kent Kwoh, et al. Assessing physical activity in persons with knee osteoarthritis using accelerometers: data from the osteoarthritis initiative. *Arthritis care & research*, 62(12):1724–1732, 2010.

[45] Hooman Dejnabadi, Brigitte M Jolles, and Kamiar Aminian. A new approach to accurate measurement of uniaxial joint angles based on a combination of accelerometers and gyroscopes. *Biomedical Engineering, IEEE Transactions on*, 52(8):1478–1484, 2005.

[46] Ira Martin Grais. Proper use of the stethoscope: Three heads and one tale. *Texas Heart Institute Journal*, 40(2):120, 2013.

[47] Fábio de Lima Hedayioglu, Miguel Tavares Coimbra, and Sandra da Silva Mattos. A survey of audio processing algorithms for digital stethoscopes. In *HEALTHINF*, pages 425–429, 2009.

[48] Kuldeep Singh, Preeti Abrol, and Neelam Rathi. Review on digital stethoscope. *International Journal of Soft Computing and Engineering (IJSCE)*, 3:96–97, 2013.

[49] Yunfeng Wu, Shanshan Yang, Fang Zheng, Suxian Cai, Meng Lu, and Meihong Wu. Removal of artifacts in knee joint vibroarthrographic signals using ensemble empirical mode decomposition and detrended fluctuation analysis. *Physiological measurement*, 35(3):429, 2014.

[50] W GEORGE KERNOHAN, DAVID E BEVERLAND, GERALD F MCCOY, STEPHEN N SHAW, RICHARD GH WALLACE, GERALD C MCCULLAGH, and RAYMOND AB MOLLAN. The diagnostic potential of vibration arthrography. *Clinical orthopaedics and related research*, 210:106–112, 1986.

[51] Gerald F McCoy, John D Mccrea, David E Beverland, W George Kernohan, and RA Mollan. Vibration arthrography as a diagnostic aid in diseases of the knee. a preliminary report. *Journal of Bone & Joint Surgery, British Volume*, 69(2):288–293, 1987.

[52] Rangaraj M Rangayyan and Yunfeng Wu. Analysis of vibroarthrographic signals with features related to signal variability and radial-basis functions. *Annals of biomedical engineering*, 37(1):156–163, 2009.

[53] CG Song, KS Kim, and JH Seo. Non-invasive monitoring of knee pathology based on automatic knee sound classification. In *Proceedings of the World Congress on Engineering and Computer Science, San Francisco, USA*, 2009.

[54] S Krishnan and RM Rangayyan. Automatic de-noising of knee-joint vibration signals using adaptive time-frequency representations. *Medical and Biological engineering and Computing*, 38(1):2–8, 2000.

[55] Filip Leszko. Dynamics, electromyography and vibroarthrography as non-invasive diagnostic tools: investigation of the patellofemoral joint. 2011.

[56] Meng Lu, Suxian Cai, Fang Zheng, Shanshan Yang, Ning Xiang, and Yunfeng Wu. Adaptive noise removal of knee joint vibration signals using a signal power error minimization method. In *Computing and Convergence Technology (ICCCT), 2012 7th International Conference on*, pages 1193–1196. IEEE, 2012.

[57] Vaishali R Patel and Rupa G Mehta. Impact of outlier removal and normalization approach in modified k-means clustering algorithm. *IJCSI International Journal of Computer Science Issues*, 8(5), 2011.

[58] Rangaraj M Rangayyan, Faraz Oloumi, Yunfeng Wu, and Suxian Cai. Fractal analysis of knee-joint vibroarthrographic signals via power spectral analysis. *Biomedical Signal Processing and Control*, 8(1):23–29, 2013.

[59] Sam Chao, Fai Wong, Heng-Leong Lam, and Mang-I Vai. Blind biosignal classification framework based on dtw algorithm. In *Machine Learning and Cybernetics (ICMLC), 2011 International Conference on*, volume 4, pages 1684–1689. IEEE, 2011.

[60] Scott C Douglas. Introduction to adaptive filters. *Digital Signal Processing Handbook*, pages 7–12, 1999.

[61] Suxian Cai, Yunfeng Wu, Ning Xiang, Zhangting Zhong, Jia He, Lei Shi, and Fang Xu. Detrending knee joint vibration signals with a cascade moving average filter. In *Engineering in Medicine and Biology Society (EMBC), 2012 Annual International Conference of the IEEE*, pages 4357–4360. IEEE, 2012.

[62] R Udayakumar, V Khanaa, and T Saravanan. Noise removal and screening of knee joint vibroarthrographic signals. *Middle-East Journal of Scientific Research*, 20(12):2450–2455, 2014.

[63] YT Zhang and RM Rangayyan. Adaptive cancellation of muscle contraction interference in vibroarthrographic signals. *Biomedical Engineering, IEEE Transactions on*, 41(2):181–191, 1994.

[64] Zahra MK Maussavi, Rangaraj M Rangayyan, G Douglas Bell, Cyril B Frank, and KO Ladly. Screening of vibroarthrographic signals via adaptive segmentation and linear prediction modeling. *Biomedical Engineering, IEEE Transactions on*, 43(1):15, 1996.

[65] Kaizhi Liu, Xin Luo, Shanshan Yang, Suxian Cai, Fang Zheng, and Yunfeng Wu. Classification of knee joint vibroarthrographic signals using k-nearest neighbor algorithm. In *Electrical and Computer Engineering (CCECE), 2014 IEEE 27th Canadian Conference on*, pages 1–4. IEEE, 2014.

[66] Yunfeng Wu. *Knee joint vibroarthrographic signal processing and analysis*. Springer, 2014.

[67] Rangaraja M Rangayyan and Narender P Reddy. Biomedical signal analysis: a case-study approach. *Annals of Biomedical Engineering*, 30(7):983–983, 2002.

[68] RG Willison. Analysis of electrical activity in healthy and dystrophic muscle in man. *Journal of neurology, neurosurgery, and psychiatry*, 27(5):386, 1964.

[69] Emmanuel C Ifeachor and Barrie W Jervis. *Digital signal processing: a practical approach*. Pearson Education, 2002.

[70] Suxian Cai, Shanshan Yang, Fang Zheng, Meng Lu, Yunfeng Wu, and Sridhar Krishnan. Knee joint vibration signal analysis with matching pursuit decomposition and dynamic weighted classifier fusion. *Computational and mathematical methods in medicine*, 2013, 2013.

[71] PJ Chi and CT Russell. Use of the wigner-ville distribution in interpreting and identifying ulf waves in triaxial magnetic records. *Journal of Geophysical Research: Space Physics (1978–2012)*, 113(A1), 2008.

[72] Jesus Franklin Andrade Romero, Monica Santana D'angelo, Osamu Saotome, and Sérgio Frascino Müller. Wavelet packet feature extraction for vibration monitoring in high speed milling. submitted to the 18th International Congress of Mechanical Engineering, Ouro Preto, 2005.

[73] Stéphane G Mallat and Zhifeng Zhang. Matching pursuits with time-frequency dictionaries. *Signal Processing, IEEE Transactions on*, 41(12):3397–3415, 1993.

[74] Sotiris B Kotsiantis, I Zaharakis, and P Pintelas. Supervised machine learning: A review of classification techniques, 2007.

[75] Yuichiro Anzai. *Pattern Recognition & Machine Learning*. Elsevier, 2012.

[76] Thomas G Dietterich. Machine learning for sequential data: A review. In *Structural, syntactic, and statistical pattern recognition*, pages 15–30. Springer, 2002.

[77] Luai Al Shalabi and Zyad Shaaban. Normalization as a preprocessing engine for data mining and the approach of preference matrix. In *Dependability of Computer Systems, 2006. DepCos-RELCOMEX'06. International Conference on*, pages 207–214. IEEE, 2006.

[78] Luai Al Shalabi, Zyad Shaaban, and Basel Kasasbeh. Data mining: A preprocessing engine. *Journal of Computer Science*, 2(9):735–739, 2006.

[79] Manoranjan Dash and Huan Liu. Feature selection for classification. *Intelligent data analysis*, 1(3):131–156, 1997.

[80] Huan Liu and Lei Yu. Toward integrating feature selection algorithms for classification and clustering. *Knowledge and Data Engineering, IEEE Transactions on*, 17(4):491–502, 2005.

[81] Lindsay I Smith. A tutorial on principal components analysis. *Cornell University, USA*, 51:52, 2002.

[82] Pedro R Peres-Neto, Donald A Jackson, and Keith M Somers. How many principal components? stopping rules for determining the number of non-trivial axes revisited. *Computational Statistics & Data Analysis*, 49(4):974–997, 2005.

[83] G Sahoo et al. Analysis of parametric & non parametric classifiers for classification technique using weka. *International Journal of Information Technology and Computer Science (IJITCS)*, 4(7):43, 2012.

[84] David J Hand, Heikki Mannila, and Padhraic Smyth. *Principles of data mining*. MIT press, 2001.

[85] Yunfeng Wu and Sridhar Krishnan. Combining least-squares support vector machines for classification of biomedical signals: a case study with knee-joint vibroarthrographic signals. *Journal of Experimental & Theoretical Artificial Intelligence*, 23(1):63–77, 2011.

[86] Xindong Wu, Vipin Kumar, J Ross Quinlan, Joydeep Ghosh, Qiang Yang, Hiroshi Motoda, Geoffrey J McLachlan, Angus Ng, Bing Liu, S Yu Philip, et al. Top 10 algorithms in data mining. *Knowledge and Information Systems*, 14(1):1–37, 2008.

[87] Ilias G Maglogiannis. *Emerging artificial intelligence applications in computer engineering: real word AI systems with applications in eHealth, HCI, information retrieval and pervasive technologies*, volume 160. Ios Press, 2007.

[88] J. Ross Quinlan. Induction of decision trees. *Machine learning*, 1(1):81–106, 1986.

[89] Ron Kohavi et al. A study of cross-validation and bootstrap for accuracy estimation and model selection. In *Ijcai*, volume 14, pages 1137–1145, 1995.

[90] Sylvain Arlot, Alain Celisse, et al. A survey of cross-validation procedures for model selection. *Statistics surveys*, 4:40–79, 2010.

[91] M Hossin and MN Sulaiman. Areview on evaluation metrics for data classification evaluations. *International Journal of Data Mining & Knowledge Management Process*, 5(2):1, 2015.

[92] E Costa, A Lorena, ACPLF Carvalho, and A Freitas. A review of performance evaluation measures for hierarchical classifiers. In *Evaluation Methods for Machine Learning II: papers from the AAAI-2007 Workshop*, pages 1–6, 2007.

[93] Mehrdad Fatourechi, Rabab K Ward, Steven G Mason, Jane Huggins, A Schlogl, and Gary E Birch. Comparison of evaluation metrics in classification applications with imbalanced datasets. In *Machine Learning and Applications, 2008. ICMLA'08. Seventh International Conference on*, pages 777–782. IEEE, 2008.

[94] Charles Elkan. Evaluating classifiers. *University of San Diego, California, retrieved [01-11-2012] from http://cseweb. ucsd. edu/˜ elkan B*, 250, 2012.

[95] Sridhar Krishnan, Rangaraj M Rangayyan, G Douglas Bell, and Cyril B Frank. Adaptive time-frequency analysis of knee joint vibroarthrographic signals for noninvasive screening of articular cartilage pathology. *Biomedical Engineering, IEEE Transactions on*, 47(6):773–783, 2000.

[96] Keo-Sik Kim, Chul-Gyu Song, and Jeong-Hwan Seo. Feature extraction of knee joint sound for non-invasive diagnosis of articular pathology. In *Biomedical Circuits and Systems Conference, 2008. BioCAS 2008. IEEE*, pages 349–352. IEEE, 2008.

[97] Yunfeng Wu and Sridhar Krishnan. An adaptive classifier fusion method for analysis of knee-joint vibroarthrographic signals. In *Computational Intelligence for Measurement Systems and Applications, 2009. CIMSA'09. IEEE International Conference on*, pages 190–193. IEEE, 2009.

[98] Rangaraj M Rangayyan and Yunfeng Wu. Screening of knee-joint vibroarthrographic signals using probability density functions estimated with parzen windows. *Biomedical Signal Processing and Control*, 5(1):53–58, 2010.

[99] Yunfeng Wu, Suxian Cai, Meng Lu, and Sridhar Krishnan. An artificial-neural-network-based multiple classifier system for knee-joint vibration signal classification. In *Advances in Computer, Communication, Control and Automation*, pages 235–242. Springer, 2012.

[100] Jien-Chen Chen, Pi-Cheng Tung, Shih-Fong Huang, Shu-Wei Wu, Shih-Lin Lin, and Kuo-Liang Tu. Extraction and screening of knee joint vibroarthrographic signals using the empirical mode decomposition method.

[101] Shanshan Yang, Suxian Cai, Fang Zheng, Yunfeng Wu, Kaizhi Liu, Meihong Wu, Quan Zou, and Jian Chen. Representation of fluctuation features in pathological knee joint vibroarthrographic signals using kernel density modeling method. *Medical engineering & physics*, 36(10):1305–1311, 2014.

[102] Savitha S Upadhya. Pitch detection in time and frequency domain. In *Communication, Information & Computing Technology (ICCICT), 2012 International Conference on*, pages 1–5. IEEE, 2012.

[103] Mohd R Jamaludin, Sheikh HS Salleh, Tan T Swee, Kartini Ahmad, Ahmad KA Ibrahim, and Kamarulafizam Ismail. An improved time domain pitch detection algorithm for pathological voice. *American Journal of Applied Sciences*, 9(1):93, 2011.

[104] Suhas S Gajre, Sneh Anand, U Singh, and Rajendra K Saxena. Novel method of using dynamic electrical impedance signals for noninvasive diagnosis of knee osteoarthritis. In *Engineering in Medicine and Biology Society, 2006. EMBS'06. 28th Annual International Conference of the IEEE*, pages 2207–2210. IEEE, 2006.

Appendix A

A.0.1 Collected dataset detailed description

Detailed information about the collected dataset is provided in the Table A.1 where the differences between the healthy and pathological groups are displayed in terms of mean and standard deviation values of each group ages and k-NN selected features values.

Table A.1: Healthy and pathological group comparison in terms of mean and standard deviation of each group ages and k-NN classifier selected features. Mean and standard deviation values of the selected features indicate a good class separability for classification purposes using only a few and most relevant features.

Group / Mean ± std	Age	TF_ft1_x_norm_raw	TF_ft1_y_norm_raw	TF_ft1_z_norm_raw	TF_ft6_x_filt_norm	TF_ft6_z_filt_norm
Healthy	46.6 ± 13.1	-0.258 ± 0.295	-0.303 ± 0.423	0.582 ± 0.156	-5.079 ± 0.280	0.043 ± 0.293
Pathological	62.5 ± 9.1	-0.430 ± 0.345	0.124 ± 0.487	0.548 ± 0.301	-4.943 ± 0.287	0.025 ± 0.203

A.0.2 Scatter Plots - Feature combination for inter-class separability

Several different combinations of some of the most discriminant features obtained with FFS algorithm for visual inspection of inter-class separability are displayed in the Figure A.1 and A.2.

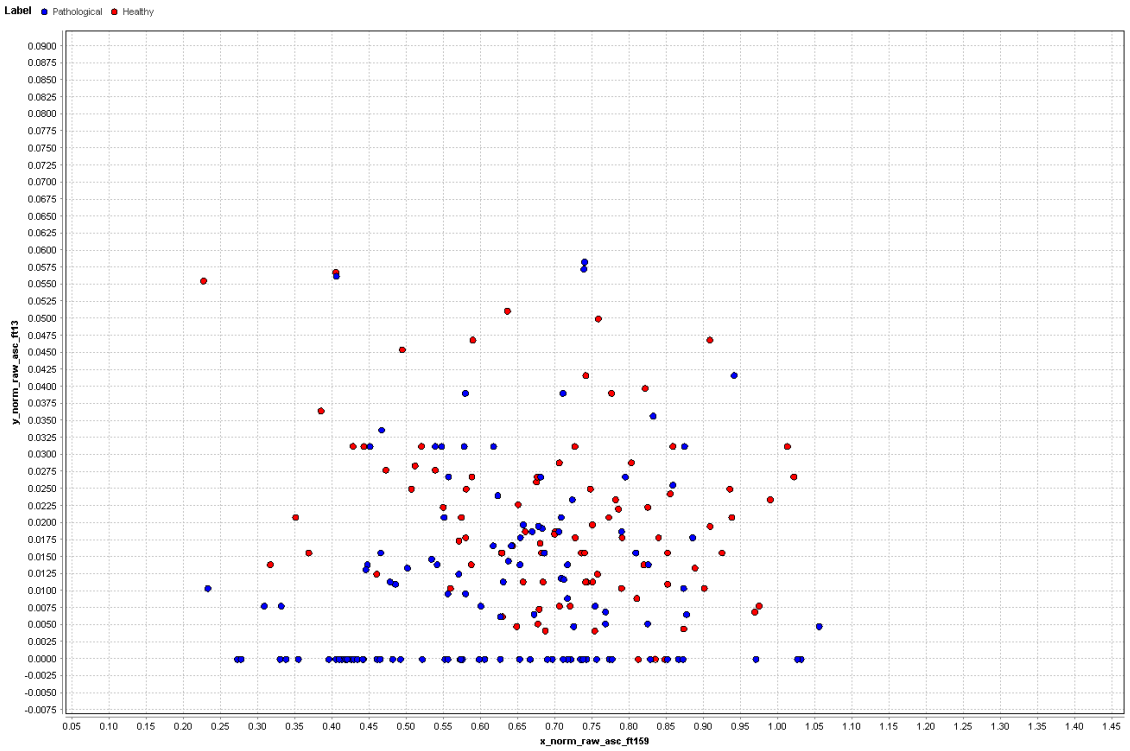
Label
Pathological
Healthy
y_norm_raw_asc_ft13
x_norm_raw_asc_ft159

(a)

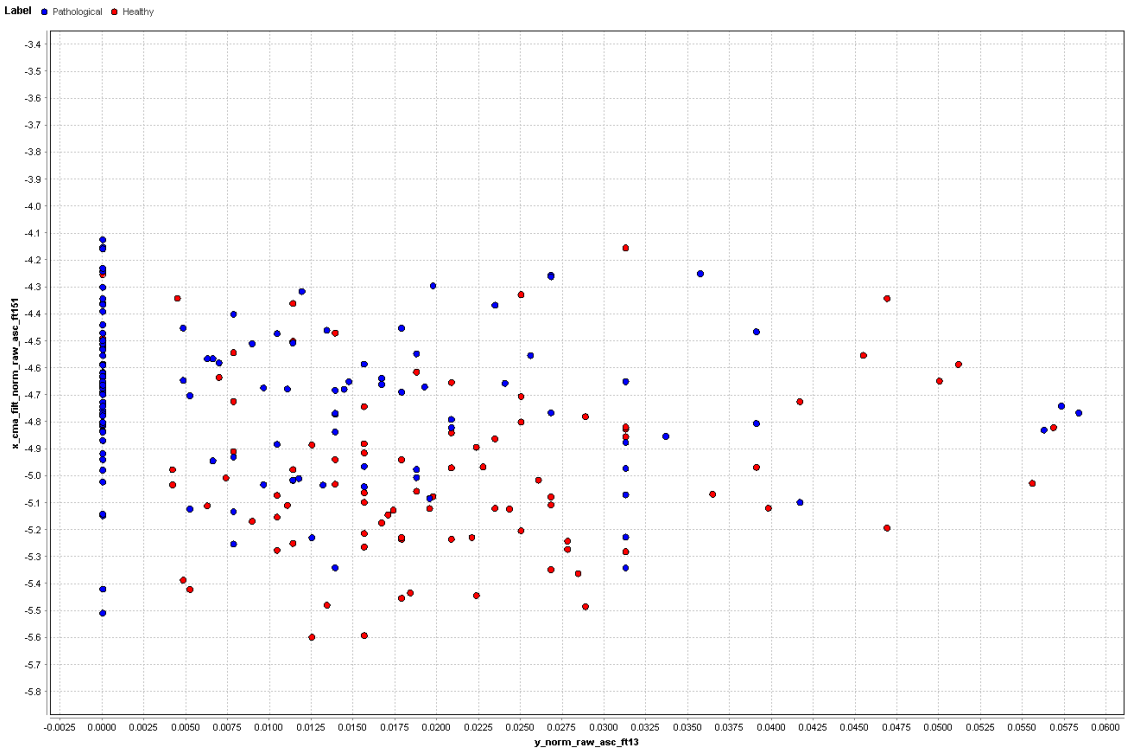
Label
Pathological
Healthy
x_cma_filt_norm_raw_asc_ft151
y_norm_raw_asc_ft13

(b)

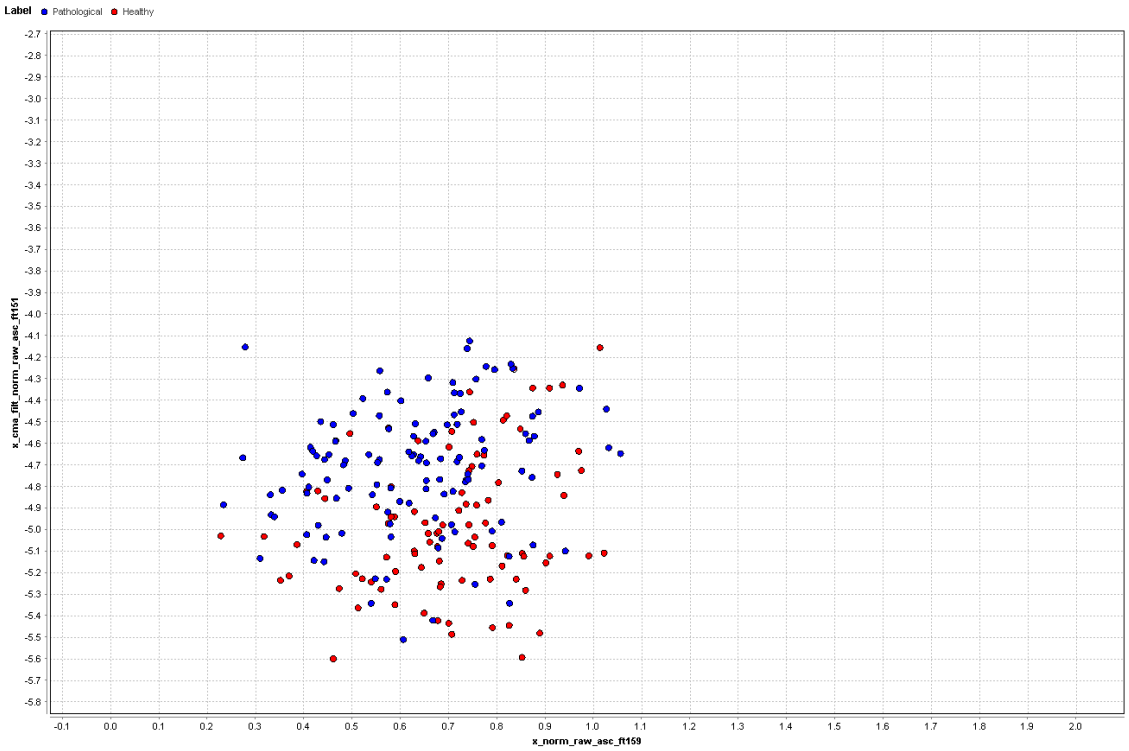
Label
Pathological
Healthy
x_cma_fit_norm_raw_asc_ft151
x_norm_raw_asc_ft159

(c)

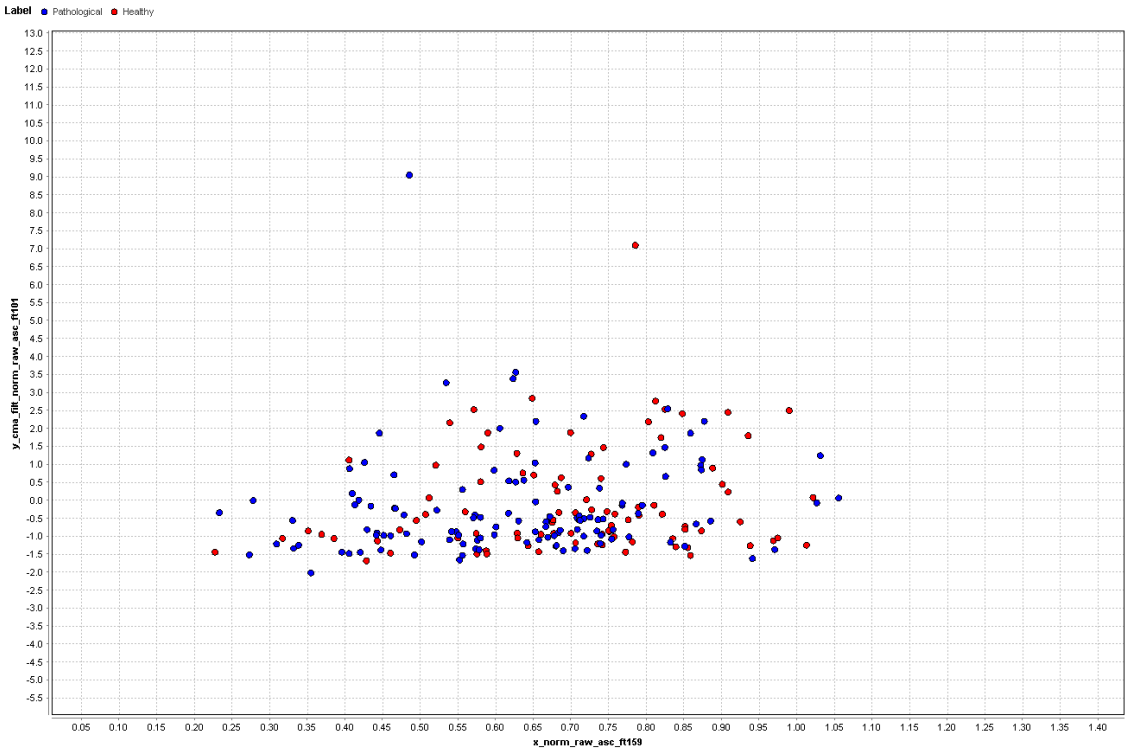
Label
Pathological
Healthy
y_cma_fit_norm_raw_asc_ft101
x_norm_raw_asc_ft159

(d)

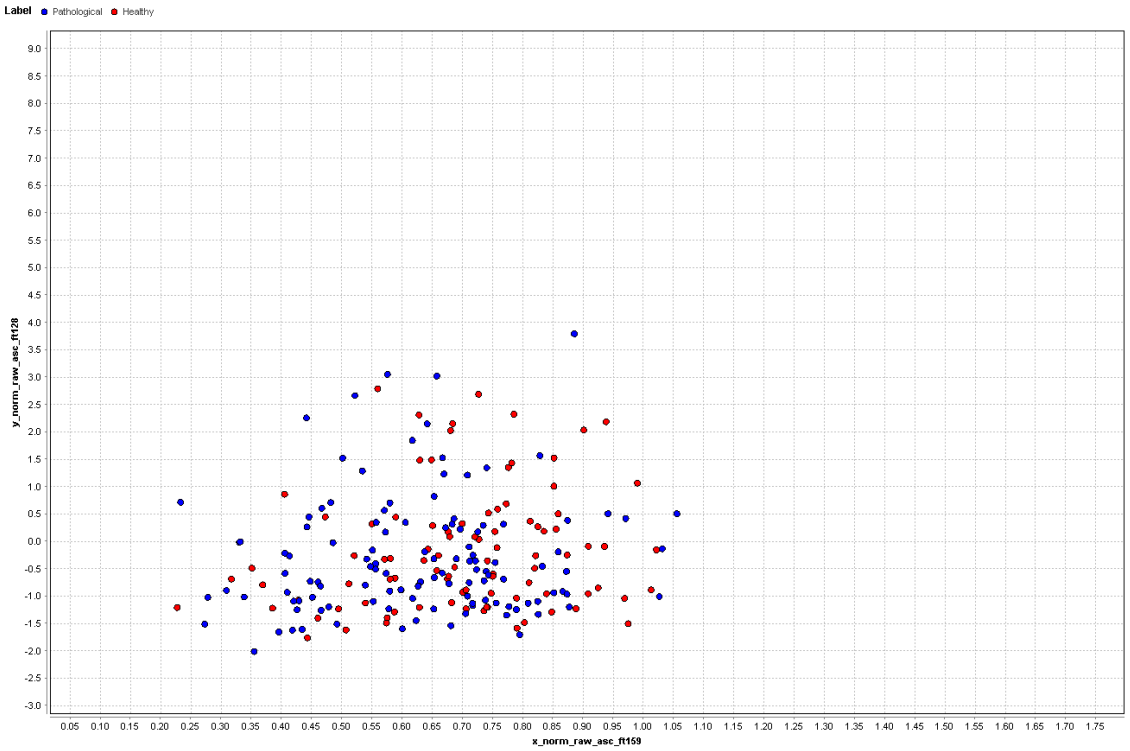
Label
Pathological
Healthy
y_norm_raw_asc_ft128
x_norm_raw_asc_ft159

(e)

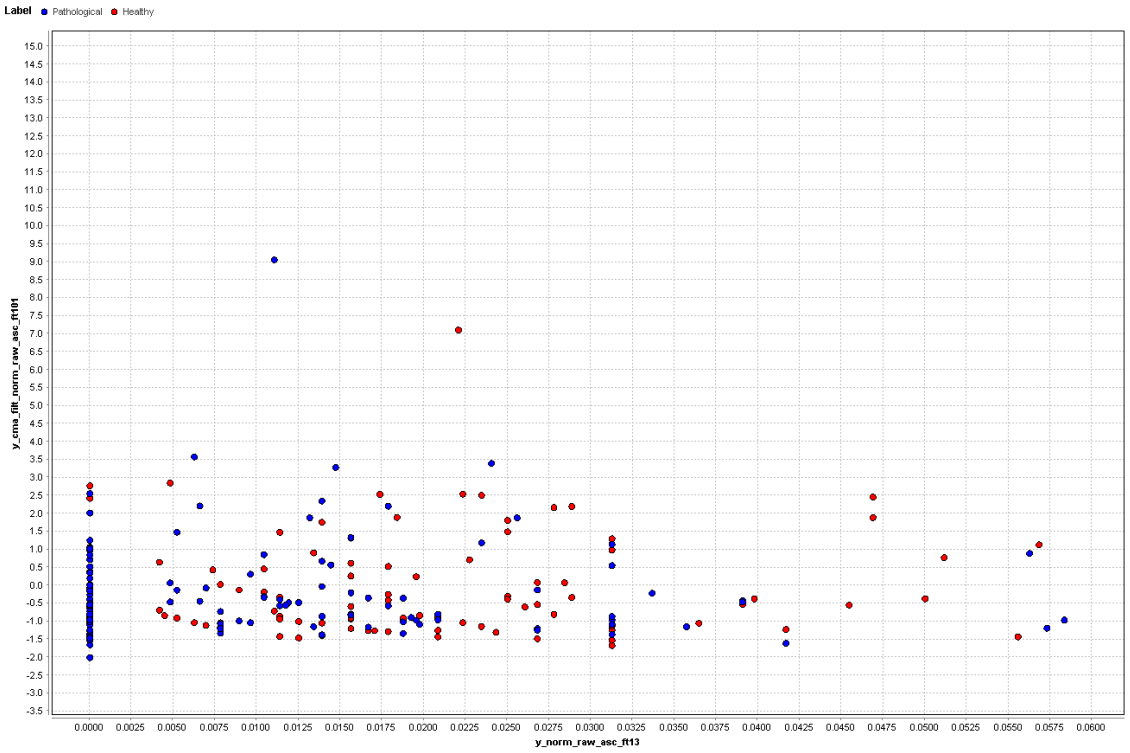
Label
Pathological
Healthy
y_cma_filt_norm_raw_asc_ft101
y_norm_raw_asc_ft13

(f)

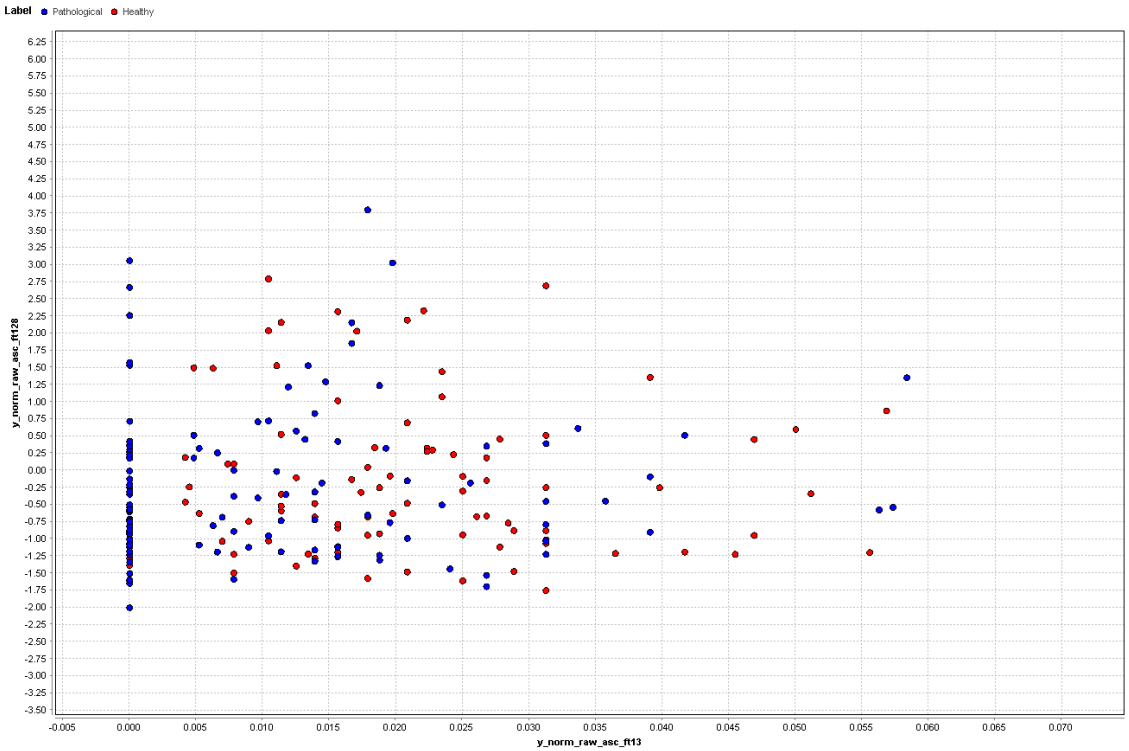

(g)

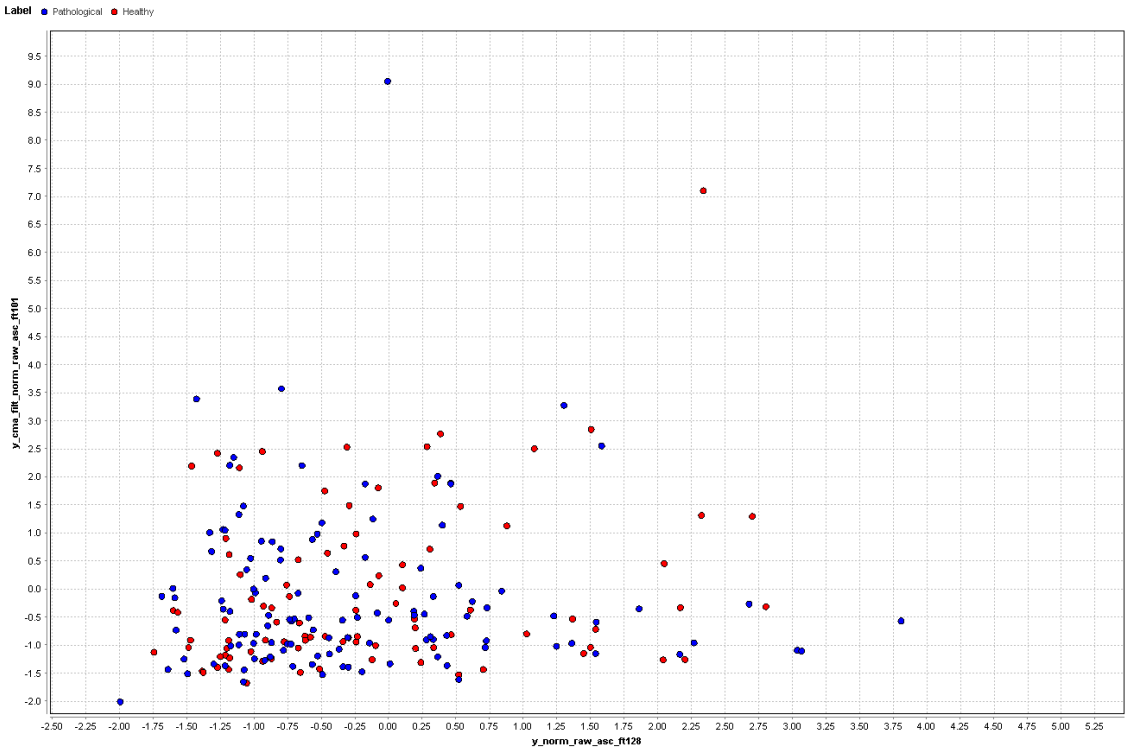

(h)

Figure A.1: Scatter plot images of the combination two features for inter-class evaluation (blue dots - Pathological; red dots - Healthy). Discriminative power of the selected features with SVM classifier, can be visually inspected for different sets of two features: (a) TF_ft3_x_norm_raw vs TF_ft6_y_norm_raw and (b) TF_ft6_y_norm_raw vs TF_ft6_x_cma_filt, (c) TF_ft3_x_norm_raw vs TF_ft6_x_cma_filt, (d) TF_ft3_x_norm_raw vs TF_ft4_y_cma_filt, (e) TF_ft3_x_norm_raw vs TF_ft6_y_norm_raw, (f) TF_ft6_y_norm_raw vs TF_ft4_y_cma_filt, (g) TF_ft6_y_norm_raw vs TF_ft4_y_norm_raw and (h) TF_ft4_y_norm_raw vs TF_ft4_y_cma_filt .

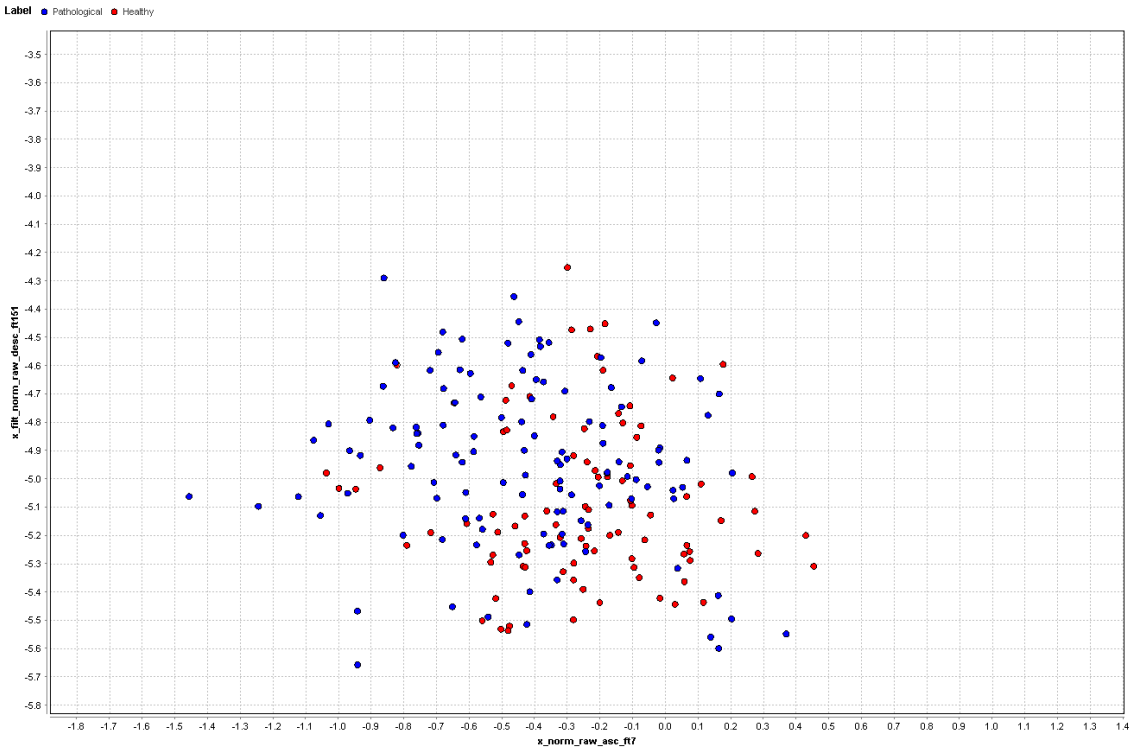
Label
Pathological
Healthy
x_filt_norm_raw_desc_ft151
x_norm_raw_asc_ft7

(a)

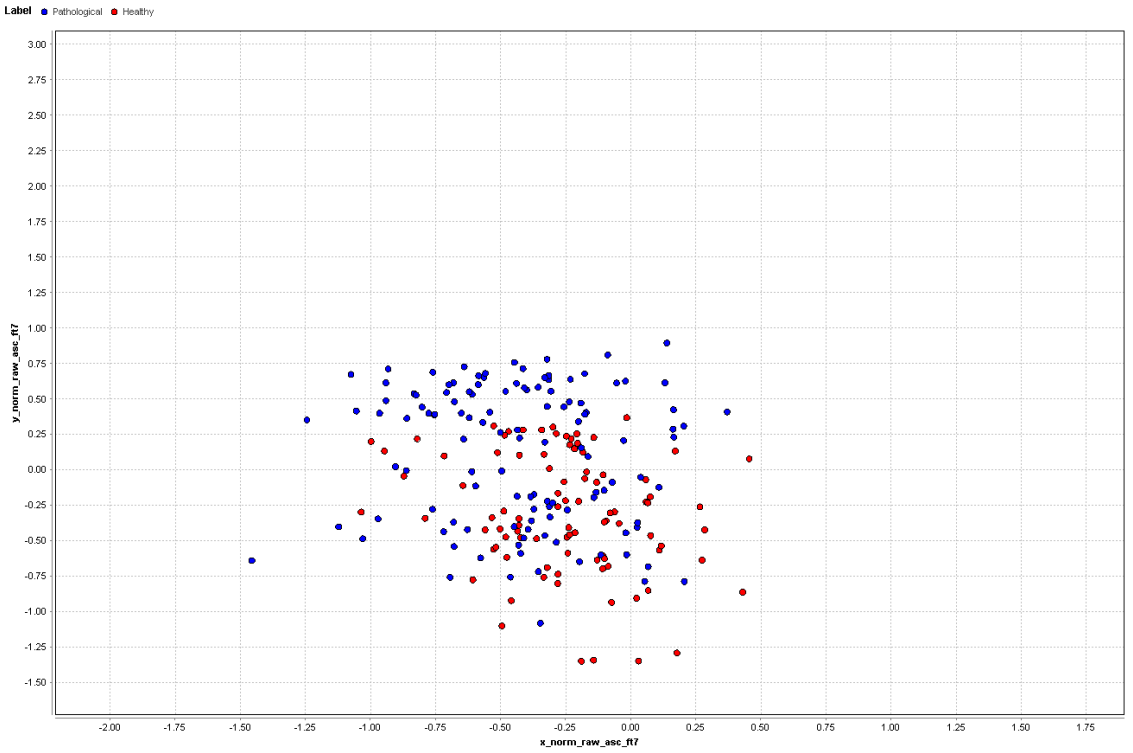
Label
Pathological
Healthy
y_norm_raw_asc_ft7
x_norm_raw_asc_ft7

(b)

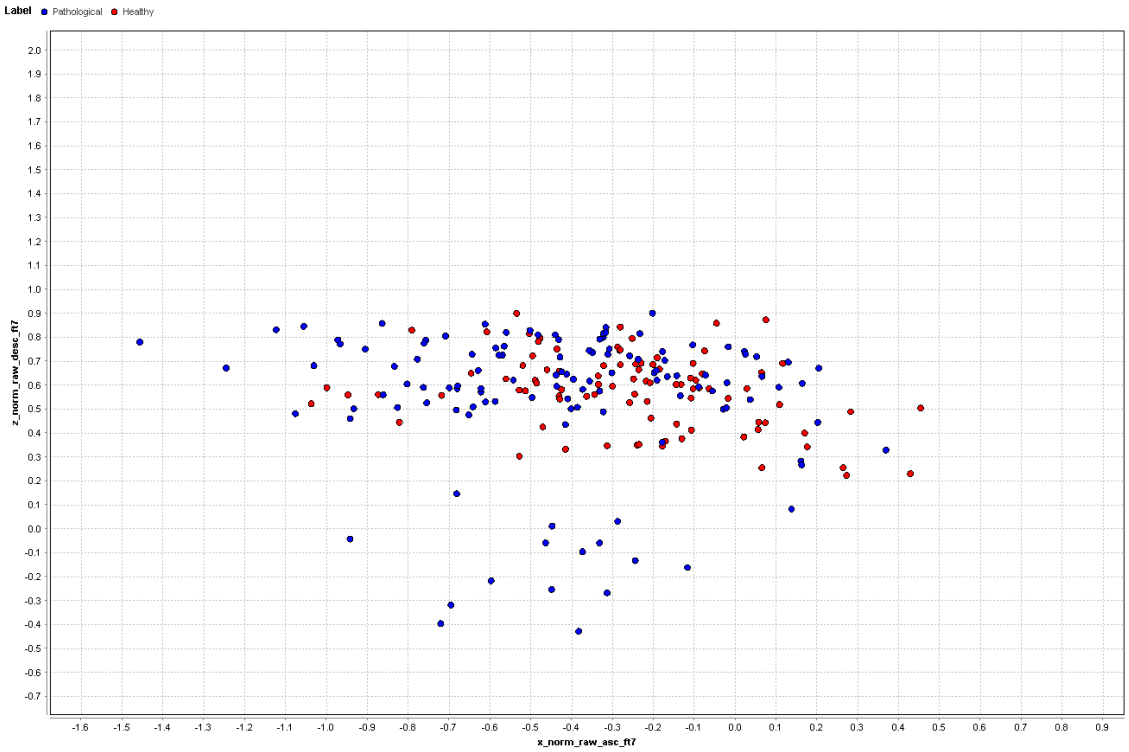

(c)

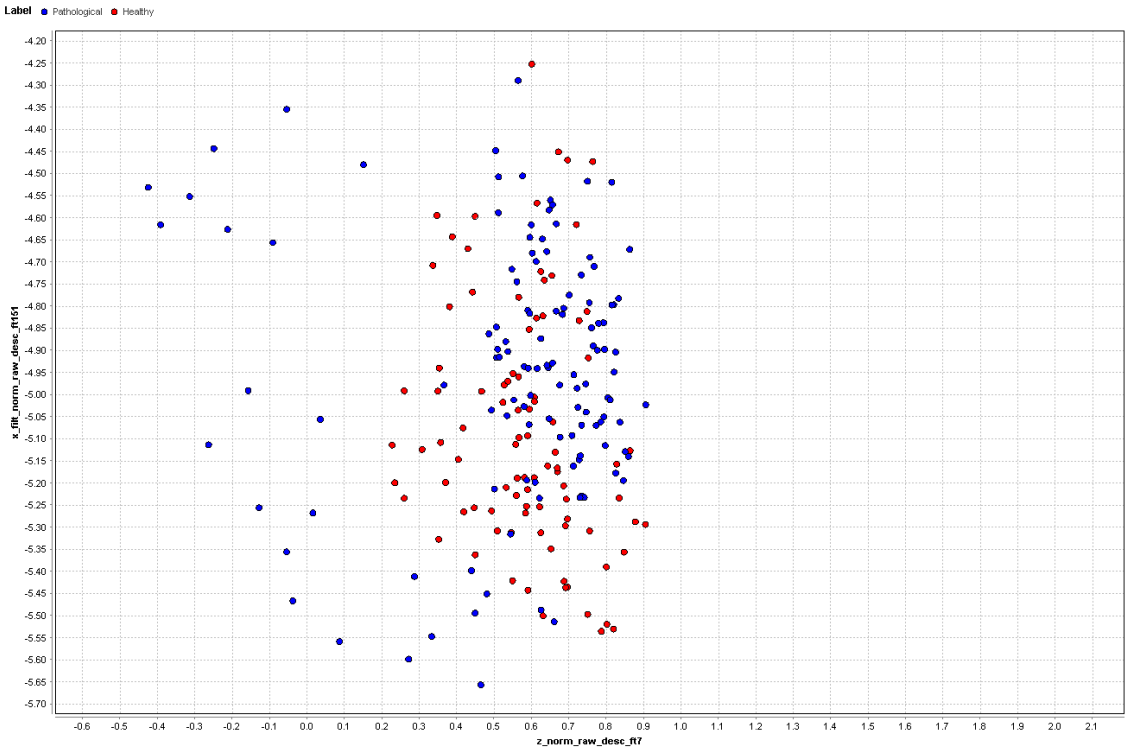

(d)

Figure A.2: Scatter plot images of the combination two features for inter-class evaluation (blue dots - Pathological; red dots - Healthy). Discriminative power of the selected features with k-NN classifier, can be visually inspected for different sets of two features: (a) TF_ft1_x_norm_raw vs TF_ft6_x_filt_norm, (b) TF_ft1_x_norm_raw vs TF_ft1_y_norm_raw, (c) TF_ft1_x_norm_raw vs TF_ft1_z_norm_raw and (d) TF_ft1_z_norm_raw vs TF_ft6_x_filt_norm.